DETERMINATION OF THE EQUIVALENT SATURATED HYDRAULIC CONDUCTIVITY OF FRACTURED ROCK LOCATED IN THE VADOSE ZONE

by

Vincent Carroll Tidwell

A Thesis Submitted to the Faculty of the

DEPARTMENT OF HYDROLOGY AND WATER RESOURCES

In Partial Fulfillment of the Requirements
For the Degree of

MASTER OF SCIENCE
WITH A MAJOR IN HYDROLOGY

In the Graduate College

THE UNIVERSITY OF ARIZONA

1 9 8 8

STATEMENT BY AUTHOR

This thesis has been submitted in partial fulfillment of requirements for an advanced degree at The University of Arizona and is deposited in the University Library to be made available to borrowers under rules of the Library.

Brief quotations from this thesis are allowable without special permission, provided that accurate acknowledgement of source is made. Request for permission for extended quotation from or reproduction of this manuscript in whole or in part may be granted by the head of the major department or the Dean of the Graduate College when in his or her judgment the proposed use of the material is in the interests of scholarship. In all other instances, however, permission must be obtained from the author.

SIGNED: Vinnie Tidwell

APPROVAL BY THESIS DIRECTOR

This thesis has been approved on the date shown below:

D. D. Evans — April 28, 1988

D. D. Evans
Professor of Hydrology and Water Resources

Date

This thesis, as well as the
purpose and intent of all
that I do, is dedicated to
the Lord

ACKNOWLEDGMENTS

This research was preformed at the University of Arizona under the guidance of Dr. Daniel Evans. Support for this work was obtained from the Nuclear Regulatory Commission.

I would like to express my deepest appreciation to Dr. Daniel Evans for his continual support and advice in this endeavor, as well as his good humor and incessant willingness to help. I would also like to thank Dr. Author Warrick and Dr. Jim Yeh for their advice and review of this manuscript.

I am also indebted to Todd Rasmussen for the insight and advice which he so willing gave. Priscilla Sheets provided invaluable assistance by drafting the figures contained in this manuscript while Jim Blanford extended much appreciated assistance in the field and laboratory. I would also like to acknowledge Dennis Hall, Yueh Chuang, Bill Haldeman, Gerald Vogt and Jim Mathieu who lent their knowledge and support to my efforts.

A special thanks is due my wife who has made the last three years among the most enjoyable of my life and who has given me the strength to overcome the frustrations associated with obtaining my degree.

Finally but by no means least, I would like to thank my parents and sister for their continual support and encouragement.

TABLE OF CONTENTS

TABLE OF CONTENTS -- continued

LIST OF ILLUSTRATIONS

LIST OF ILLUSTRATIONS -- continued

LIST OF ILLUSTRATIONS--continued

page

LIST OF TABLES

ABSTRACT

A method with which to estimate the equivalent saturated hydraulic conductivity and its associated spatial distribution in fractured rock situated in the vadose zone has been developed. Conductivity is estimated in part from outflow rates, induced by a constant hydraulic head, monitored over three meter intervals in boreholes which are oriented in a manner so as to intersect the major fracture sets of a field site. Outflow rates are monitored by means of a falling-head flowmeter while borehole intervals are isolated with a single inflatable packer. Upon collection of the field data, hydraulic conductivity values are estimated by means of two analytical solutions. The solutions are adapted to meet the special conditions posed by variable borehole orientations and multiple test intervals from existing solutions associated with borehole permeability tests. The developed methodology is subsequently utilized to determine the saturated hydraulic conductivity and the associated spatial variability of fractured tuff located near Superior, Arizona.

CHAPTER ONE

INTRODUCTION

The subject of fluid flow and transport through fractured rocks of low permeability has recently gained considerable interest due to the probable siting of a high level nuclear waste repository under such conditions. The main objective of such studies is the determination of the likelihood of leaking hazardous waste reaching the accessible environment. However, the flow behavior in fractured systems is very complex and warrants considerable investigation before the potential danger posed by such sites can be adequately assessed.

Of primary interest is the behavior of fluid flow and transport in the fractures themselves because they generally act as the major conduits for water movement within rock masses of low permeability. Fractures generally have hydraulic conductivities which are several orders of magnitude greater than that of the surrounding rock matrix, and thus dictate the direction of primary conductivity. In other words, the fractures influence the flow direction and flow velocities through rock of low permeability.

As a result of such interest, the University of Arizona has been contracted by the Nuclear Regulatory Commission to provide technical assistance in researching the phenomena of fracture and matrix flow in low permeability rock. The major purpose of the contract being the

characterization of partially-welded, fractured tuff, similar to that being investigated as a possible waste repository located at the Yucca Mountain, Nevada test site. A tuff exhibiting similar characteristics to that of the Yucca Mountain Formation has been identified near Superior, Arizona, in which the primary field site, known as the Apache Leap test site, for this project has been developed.

1.1 STATEMENT OF PROBLEM

One of the most critical properties required by most any hydrological investigation is an accurate estimate of the saturated hydraulic conductivity of the media of interest. The saturated hydraulic conductivity being the most basic of parameters which characterizes the ability of a media to transmit fluid. Thus the validity of any flow or transport model is intimately dependent on the accurate estimation of this parameter. Even for cases in which unsaturated conditions predominate, knowledge of the saturated conductivity is necessary for proper development of any conductivity verse water content relationship.

Unfortunately, conductivity is generally a very complex function due to the heterogeneous, anisotropic nature of most geologic materials. This is especially the case in fractured, low permeability rock owing to the complex geometry of the fracture network which is generally encountered in the field. In addition to its heterogeneous character, the hydraulic conductivity is also a function of the scale of the problem considered.

In the past, little concern has been paid to methods for estimating the hydraulic conductivity in fractured, low permeability rock due to the inability of such aquifers to supply sufficient quantities of water to be economically feasible. However, interest has shifted recently to fractured media due to its enticing qualities for storing hazardous wastes. It follows that a need exists for a reliable method with which to estimate the saturated hydraulic conductivity from field tests, and to develop a pool of field data for the expressed purpose of calibrating and validating flow and transport models. The saturated conductivity values will also provide an upper limit for curves representing relationships between the unsaturated conductivity and water content.

1.2 BACKGROUND

1.2.1 FRACTURE CONDUCTIVITY

On a basic level the ability of a fracture to transmit water depends primarily on the size of the opening, or the fracture aperture. Many workers (Huitt, 1956; Snow, 1970; Witherspoon et al.,1979b) have used flow between smooth parallel plates to model flow in fractures. An equation based on physical laws governing the conservation of momentum, and derived from shear stress considerations, as expressed in the Navier-Stokes equation, has been derived to describe flow through parallel plates. The equation known as the cubic law is

$$(1.1) \quad Q = C \frac{\rho g}{\mu} b^3 \nabla h$$

where Q is the total flow rate through the fracture, C is a proportionality constant containing information on the flow field dimensions, ρ is the fluid density, g is the gravitational acceleration, μ is the viscosity of the fluid, b is the fracture aperture, and ∇h is the hydraulic gradient. Basically the equation states that the rate of fluid flow per unit total head difference is proportional to the cube of the parallel plate separation. Application of the model requires laminar flow, and a homogeneous, incompressible fluid under isothermal conditions.

In treating fractures as a collection of parallel plates, one is assuming a constant aperture over the plane of the fracture. However, natural rock fractures are much more complex than simplified parallel plates. Natural fractures generally have rough surfaces, thus the fracture aperture varies erratically over the plane of the fracture. In fact, flow in a fracture under compressive stress is possible only because the fracture is not composed of parallel plates, and the roughness of the walls prevent the total closure of the fracture.

In order to neglect the complexity of the spatial aperture distribution, the fracture may be characterized by the apparent hydraulic aperture which considers only the average effect of the fracture aperture. The apparent hydraulic aperture is measured by applying a constant pressure gradient across a single fracture while monitoring the induced outflow rate. The apparent hydraulic aperture is subsequently determined by solving equation 1.1 subject to the results obtained from the test. Basically, the apparent hydraulic aperture

describes a true fracture in terms of a set of parallel plates with constant spacing.

Several studies investigating the applicability of the cubic law to flow through fractures has been conducted both in the field and in the laboratory. Schrauf and Evans (1986) investigated the relationship between the measured conductivity and the average aperture of a natural fracture. Tests were conducted on a block of granodiorite, cut by a single natural fracture. The fracture aperture was determined directly by dividing the fracture volume and fracture area which were monitored during the test. Fracture conductivity on the other hand was estimated from the fracture flow rate measured as a function of injection pressure for apertures ranging from 200 to 600 μm. Nitrogen gas was used throughout the experiment as the testing fluid. The results indicated that the fracture conductivity was well below that predicted by the cubic law when using the average fracture aperture.

Several other authors have obtained results which also imply that the cubic law is inadequate to model fracture flow in many instances (Sharp, 1970; Kranz et al., 1979; Abelin et al.,1983). In fact, existing laboratory data support the use of the cubic law, with appropriate corrections for roughness, only for fractures whose adjoining surfaces are not in contact. Because of the inability of the cubic law to model fracture flow accurately, many authors have proposed corrections to the model to make it more applicable to natural cases.

Since real fractures have rough walled surfaces, unlike parallel plates, models have been proposed which take the variability of aperture into account. Figure 1.1 is a profile of a natural fracture which cuts

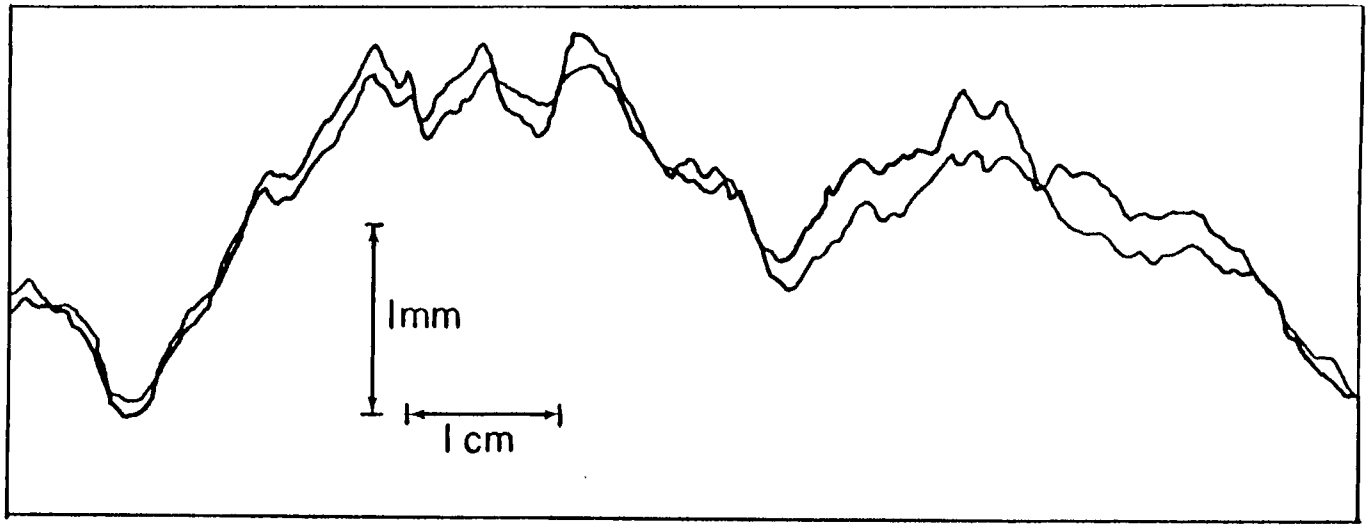

Figure 1.1. Surface roughness profile of a granite fracture (after Billaux et al., 1984).

a block of granite. The profile gives some idea of the variability of the fracture aperture and the tortuous nature of the fracture trace which is governed to a large extent by the stress acting on the fracture. It follows that by increasing the stress on the fracture the fluid flow through the fracture decreases owing to two primary factors: 1) the smaller fracture apertures, as a result of fracture closure with stress and 2) the increase in tortuosity and decrease in connectivity of the fluid flow paths as a result of more wall contact area.

Neuzil and Tracy (1981) were the first to consider the effects of aperture variation on fracture flow by developing a model which allowed fracture apertures to vary in a direction normal to flow while assuming a constant spacing in the direction parallel to flow. The parallel plate equation was modified to

$$(1.2) \quad Q = C\, \nabla h\, \frac{\rho\, g}{\mu} \int_0^\infty b^3\, f(b)\, db$$

where f(b) is the normalized aperture frequency distribution. Since fracture roughness is considered, the aperture density takes on shapes other than that of a delta function, as in the case of the cubic law. The actual shape of the distribution is governed by the roughness characteristics of the fracture in question. Available data concerning fracture aperture variation suggests that most fractures exhibit a log normal aperture distribution. Therefore, an accurate description of the relation between flux and mean aperture requires the consideration of both the mean aperture and the its standard deviation about the mean. This implies that fractures with the same mean aperture, but with

aperture distributions of various shape, will give rise to different flow rates. Distributions which are skewed to smaller aperture sizes will conduct considerably less water than a fracture of equal mean aperture but with a distribution that is skewed toward larger apertures. Therefore, the apparent aperture, determined from the cubic law for measured flux and hydraulic head values, has little or no physical meaning or relationship with the true aperture.

However, fracture apertures do in fact vary in the direction normal to the imposed hydraulic head. Tsang (1984) considered the effect of variation in aperture in the direction of flow, which he termed tortuosity. Tsang modeled the effects of tortuosity by representing flow paths by electrical resistors placed in a two dimensional grid. The resistance was varied as the inverse of the fracture aperture cubed. Results indicate that the aperture distribution plays a critical role in the degree with which tortuosity controls fracture permeability. Tortuosity exerts the greatest degree of influence when the fracture distribution is skewed toward smaller fractures. On the other hand when the aperture distribution is peaked toward large apertures, the effects of tortuosity is minimized for most applied stresses. It is also noted that when the fraction of contact area between the fracture surfaces rises above 30% the effects due to tortuosity become appreciable. Under these conditions the parallel plate representation of a fracture tends to overestimate flow rates by three or more orders of magnitude. Therefore, when fractures have tortuous flow paths, one must have some idea as to the fully two dimensional spatial aperture distribution in order to model fracture flow accurately.

Tsang and Witherspoon (1985) extended Tsang's previous work by relating the geometrical characteristics of a fracture to its mechanical properties. They found that the aperture density distribution for a fracture may be derived from the stress-strain relationship along the fracture. This method provides a practical way to estimate fracture tortuosity in the laboratory, however it would be extremely difficult to apply under field conditions.

In some cases the conductivity of a single fracture can be measured in situ such as outlined by Trautz (1984). The method requires the locating of a single fracture which is intersected by two separate boreholes. The fracture is then isolated by packing off the interval of each borehole containing the fracture. Nitrogen gas is forced through the fracture and the associated flow rate monitored. The pressure is measured in each borehole and the resulting gradient between the boreholes is plotted against the flow rate. The slope of the curve is then used in determining the fracture conductivity. The saturated gas conductivity may be subsequently converted to the hydraulic conductivity by altering the values of the fluid viscosity and density. One drawback to this method of determining fracture conductivity in situ is that one can never be certain that the fracture of interest is totally isolated from fractures which may intersect along the investigated interval.

1.2.2 FRACTURE NETWORK CONDUCTIVITY

In reality fractures do not exist as separate entities, but as a part of a complex fracture network. Likewise, water is generally transported through fractured media via many intersecting fractures as

opposed to only a single fracture. For this reason the conductivity of a fracture network is generally reported in terms of an equivalent porous medium conductivity which considers the interaction between the fractures within the network.

The parallel plate theory has also been extended to approximate flow in three dimensional fracture systems. Snow (1965, 1970) introduced a method to estimate the equivalent porous medium permeability tensor for a fracture system. The method relates the orientation, density, and aperture of each fracture to the orientation of the hydraulic head to determine the hydraulic conductivity of each fracture. In turn, the permeability tensor for the overall fracture system is obtained simply by superimposing the permeability contributions due to each individual fracture. However, a drawback to this method is that all fractures are assumed to be infinite in lateral extent. Assuming infinite length will tend to overestimate network permeability since: 1) some fractures may be isolated from the conducting network, 2) some fractures may be connect with other fractures only on one end thus not conducting flow or contributing to the permeability of the system and 3) the contribution of a conducting fracture depends on how it is connected to the rest of the system, as in the case of flow being restricted through a fracture which is connected to the fracture network through a conduit with a smaller aperture. Therefore, the determination of fracture permeability for a system of finite fractures is highly dependent on the degree of interconnection between the fractures.

The interconnection between a set of fractures is known to be a function of both fracture density and fracture length. Long and Witherspoon (1985) investigated the effect that these two parameters have on the interconnectiveness of a fracture system and the implications of connectivity on the anisotropic permeability tensor. Interconnection was investigated by numerically simulating flow in two dimensional fracture networks in which all fractures were treated as parallel plates with a constant aperture. The numerical simulation involved generating sample fracture systems from a given set of parameters. In the case of the fracture length and density, the parameters were allowed to vary inversely, while the product of the parameters was held constant. Once the fracture systems were generated, they were subjected to the boundary conditions shown in Figure 1.2. The directional permeability were then determined in several orientations and a subsequent anisotropic permeability ellipsoid developed. The results obtained indicate that as fracture length increases and density is proportionally decreased, the permeability of the system increases. It was also found that longer, less dense fracturing behaves more like a continuum than does shorter, more densely fractured rock masses. Basically this means that longer fractures tend to have a greater propensity to intersect, thus increasing fracture network connectivity. As connectivity increases conductivity likewise increases and a larger number of connected flow paths occur which cause the medium to function more like a continuum. Long and Witherspoon supported their results by predicting the outcome of the solution by using techniques related to the percolation theory (Englman et al., 1983). Most importantly, this

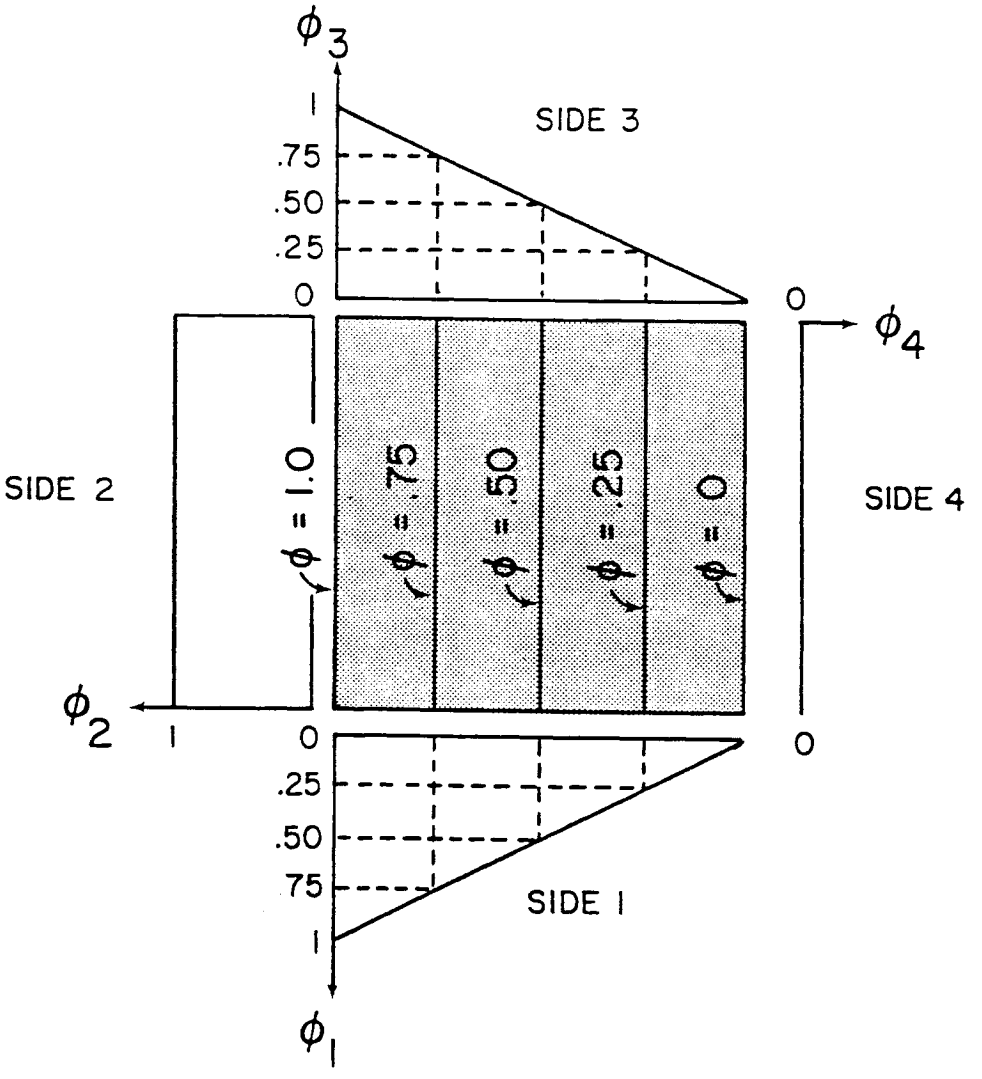

Figure 1.2. Boundary conditions applied to fracture models during directional permeability measurements as developed by Long and Witherspoon (1985).

article indicates that knowledge of fracture frequency and orientation, data which is readily available in field situations, is not sufficient in most cases to accurately predict the anisotropic conductivity tensor for fractured rock masses, but that it is the fracture length which is most critical in estimating the conductivity of a fracture system.

Long et al. (1985a) extended their previous analysis to include fracture heterogeneity. Fracture heterogeneity being a measurement of the variability in aperture size between different fractures in a fracture network. The same numerical simulation was preformed by Long and Witherspoon (1985), however fractures of various apertures were used. Using a well connected system, the coefficient of variation of aperture was varied while the mean aperture of the system was held constant. The results of the simulation indicated that heterogeneity caused a decrease in flow rate. For the case investigated, the permeability was only half that predicted when fractures of constant aperture were used. The lower flow rates were determined to be a direct result of the smaller fractures governing the flow through the fracture system. Results also indicate that it is more difficult to assign an anisotropic permeability ellipsoid for a given fractured rock mass when heterogeneity increases due to the concentrating of flow along the fractures with the largest apertures.

The authors also simulated the case where fracture length and aperture size were correlated. By correlating the two parameters, it was found that the permeability was twice as great as that predicted when aperture size was held constant. The apparent reason for the increase in permeability is simply due to an increase in the number of

"super" conducting fractures, long very permeable fractures, within the rock mass.

Up until now, only models which treat fractures and fracture networks discretely or stochastically have been investigated. It is evident that the application of such models to predict fluid flow and transport through fractures is a formidable task. The task is further complicated by the need for detailed deterministic and/or statistical information about the geometry of the fractures for use in these models. Parameters such as fracture length, fracture density, fracture orientation, fracture system heterogeneity and the spatial aperture distribution make up the list of critical information. However, most of these parameters are virtually impossible to obtain whether for use in purely deterministic or stochastic models.

It follows that an alternative approach to discrete modeling of fracture systems is necessary. An alternative which is commonly employed is the treatment of the fracture system as an equivalent porous medium. Such treatment allows one to neglect the complexities of the network and concentrate on the average phenomenon.

The reason for treating fractured media as a continuum is to allow the passage from the microscopic level at which we consider what happens at each point within each pore to the macroscopic level at which only average phenomena are considered. Measurement of hydraulic conductivity in a porous medium, for instance, represents an averaging over many pores. As long as such measurements are insensitive to small variations in the volume of the porous medium, the hydraulic conductivity of the porous medium can be treated as a continuous function of space which

varies smoothly enough to be analyzed by standard methods of differential calculus. Therefore the hydraulic conductivity is understood to represent an average over a finite volume surrounding the point at which the value is defined. This finite volume is known as the Representative Elementary Volume, or REV (Bear 1979).

The continuum concept can likewise be extended to cases involving fractured media. Measurements of hydraulic conductivity in fractured media tend to be erratic due to the sensitivity of the measurement relative to the number of fractures intersected in the test interval. Likewise, REV measurements must be made on a sufficient scale so that the conductivity values will be insensitive to small variations in the fracture network. Due to the nature of fracture networks, the scale at which an REV may be defined, if such an REV can be defined at all, is generally large as compared to a porous medium REV scale. If an REV can at least be defined, many times information may be required about the inner structure of the REV which will be lost due to the continuum approach.

Neuman (1987) describes a technique from which REV scale parameters may be estimated from sub-REV scale tests. The method involves emphasis being placed on the analysis of field data measured on a practical scale. Neuman demonstrates that hydraulic test data taken on the sub-REV scale may be analyzed quantitatively by "treating them as the realization of a stochastic process defined over a continuum. The nature of this stochastic process on scales smaller and/or larger than the scale of measurement can be studied by means of convolution and/or spatial averaging techniques."

Investigations applying this method were preformed in fractured granite near Oracle, Arizona by Hseih (1985). Both cross-hole packer tests and single-hole packer tests were used to obtain data for the investigation. In the case of the single-hole packer tests, a measuring interval of 3.8 meters was adopted. At this length a large sample of hydraulic conductivities were found to be non-zero. Hseih contended that one would expect that similar sized volumes centered about arbitrary points within the rock would also register non-zero hydraulic conductivity values if subjected to the same type of packer test. Thus, by assigning hydraulic conductivity values to the centroid of each volume, one ends up having a hydraulic conductivity associated with each point in the rock mass. In other words a hydraulic conductivity field defined over a continuum was developed. From the data obtained from sub-REV scale measurements, geostatistical analysis was preformed on the data to determine the size of the REV and the associated anisotropic hydraulic conductivity ellipsoid.

1.3 SCOPE AND PURPOSE OF INVESTIGATION

The primary purpose of this particular study is the development of a methodology with which to estimate the spatial variability of the equivalent saturated hydraulic conductivity of fractured media which resides within the vadose zone. Application of this field technique is subsequently used to estimate the equivalent saturated hydraulic conductivity and its associated variability at the Apache Leap test site. These estimates should prove to be quite valuable in following

investigations concerning fluid flow and transport through fractured media.

The methodology is based primarily on falling-head borehole permeability tests as described by the U.S. Bureau of Reclamation (1977, pp.283-285) which are especially well suited for permeability tests conducted in the vadose zone. These tests are designed to measure outflow rates emanating from uncased, flooded boreholes under the influence of a constant hydraulic head. Several modifications to the basic test procedure have been made in addition to developing a scheme with which to measure the spatial variability of the conductivity. Modifications include the development of a falling-head flowmeter which allows the monitoring of a large range of outflow rates, prevents a significant drop in head during testing, and maintains a high degree of accuracy when measuring small outflow rates. A down-hole packer was also developed with which to isolate test intervals in the boreholes to allow the measurement of the spatial distribution of the conductivity with depth. The spatial variability in the other principal directions is measured by conducting tests in nine boreholes which comprise a 10 m x 20 m grid.

Borehole orientation adopted in this investigation is predicated on the structural geologic properties of the test site. For this reason, slanting boreholes have been adopted in this investigation for the expressed purpose of intersecting vertical fractures which predominate at the test site.

Because borehole permeability tests do not measure the hydraulic conductivity directly, a numerical solution or analytical solution is

necessary. However, for the purpose of this paper only an analytical solution will be investigated. Classical analytical solutions which have been developed for permeability tests assume a vertical borehole orientation and that the entire borehole represents a single test interval. Therefore, an alternate solution is required with which to estimate the hydraulic conductivity from the borehole permeability test data. To address this problem, several classical analytical solutions were investigated to determine the feasibility of adapting them to meet the needs presented by this investigation.

CHAPTER TWO

APACHE LEAP TEST SITE

The field data which are presented throughout this investigation were collected at the Apache Leap test site located approximately 8 km (5 mi.) east of Superior, Arizona (Figure 2.1). The Apache Leap test site was developed by the University of Arizona for the purpose of characterizing the hydrologic properties, pertaining to fluid flow and contaminant transport, in fractured partially-welded tuff. The suitability of the test site for such an investigation is predicated primarily on the similarity between the Apache Leap tuff and that of the Yucca Mountain tuff in Nevada, which is currently under investigation as a probable high-level nuclear waste repository.

2.1 SITE LOCATION

The Superior study area is located at the western edge of the mountains of central Arizona between the Superstition Mountains to the northwest and the Pinal Mountains to the east. The topography of the region is dominated by steep, rocky mountains which have an average elevation of 1400 meters (4600 ft.). Vegetation in the region consists mainly of mesquite, chaparral, creosote, and oak woodland.

The town of Superior, at an elevation of 910 m (2985 ft.), lies at the foot of a steep west-facing escarpment of ash-flow tuff known as

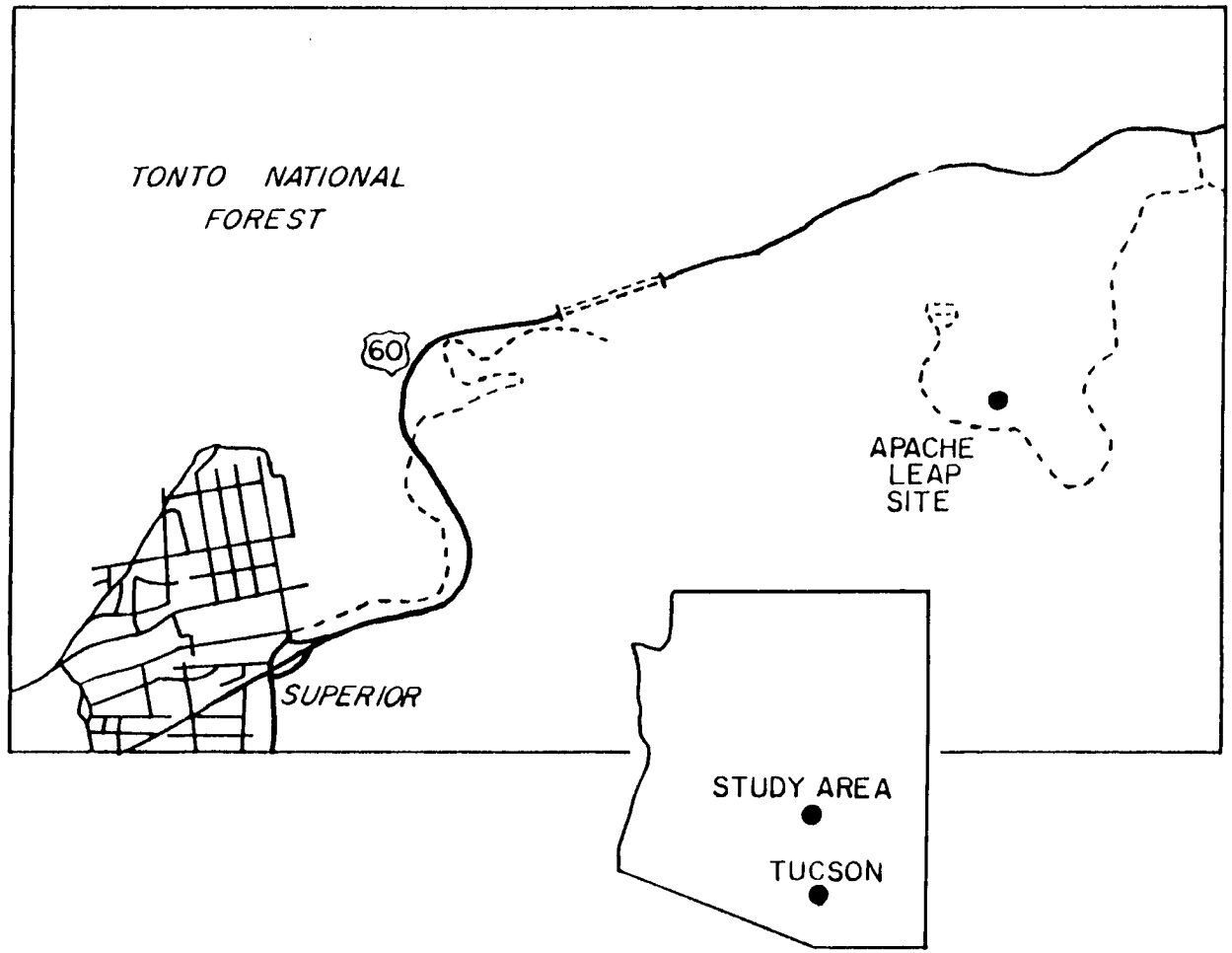

Figure 2.1. Location of the Apache Leap test site.

Apache Leap. Apache Leap rises to an elevation of 1433 meters (4700 ft.) and is part of the massive dacitic ash-flow tuff which acts as the major relief forming agent in the Superior region. The ash-flow sheet is of particular local interest because it covers potential mineral exploration targets in a region that has many ore deposits.

The region around Superior is drained primarily by Queen Creek and its tributaries. Queen Creek, in turn, is a tributary of the Gila River which is one of the major drainage systems in Arizona. As might be expected, stream flow is ephemeral throughout the Superior region.

2.2 CLIMATE

Because the Apache Leap test site is located at an elevation of approximately 1275 meters (4180 ft.), it experiences a slightly milder climate than that of the central Arizona deserts. Generally temperature extremes do not exceed 40 C° in the summer or drop below -5 C° in the winter. In addition, high temperatures are usually accompanied by low relative humidities. As with the majority of south-central Arizona, the Superior region is subject to a semi-arid climate.

Rainfall patterns at the site are comparable to those of the neighboring desert in that approximately one-third of the total annual precipitation falls during the summer months (July to September) by way of localized high intensity thunderstorms. These summer storms are primarily of a convective nature, deriving their moisture from the Gulf of Mexico. In contrast, frontal storms producing low intensity precipitation are characteristic of the rainy winter months (December to

February) with only a small part of the winter precipitation falling as snow.

For the town of Superior, records of precipitation dating from 1914 to 1970 indicate that the average annual precipitation was 453 mm (17.8 in). Precipitation has also been monitored at the Magma Copper Company's number 9 shaft from 1974 to 1984. The number 9 shaft is at an elevation of 1270 m (4166 ft) and is within a kilometer of the field site. These records indicate an average annual precipitation of 639 mm (25.2 in). For the same time period, the average annual precipitation for the town of Superior was 538 mm (21.2 in) which is noticeably higher than that given by the more extensive precipitation record (Weber, 1986).

2.3 GEOLOGY OF TEST SITE

Peterson (1961, 1968) made an exhaustive study of the units and structure of the Apache Leap tuff in the region around Superior. This section, unless otherwise noted, is a summary of his comprehensive work.

Remnants of a thick Tertiary (mid-Miocene) ash-flow sheet, termed the Apache Leap Formation, covers much of Gila, Pinal and Maricopa counties. Ash-flow sheets being a characteristic tuffaceous deposit derived from highly explosive volcanic events which eject immense clouds of intensely heated minute fragments. The Apache Leap Formation is composed of numerous individual ash-flows each produced by a separate eruptive event in rapid enough succession to form an ash-flow sheet representing a single cooling unit. Accumulation of the ash-flows led to the deposition of a sheet over 600 m thick in some areas. The ash-

flow sheet is composed of densely-welded to non-welded tuff which can be divided into five different units based on the degree of welding and flatting of pumice lapilli (Figure 2.2).

The Apache Leap test site is characterized by partially-welded tuff, typical of the upper partially-welded unit of the ash-flow sheet. The chemical composition of the tuff near the test site, as well as throughout the Apache Leap Formation is characteristic of a quartz latite, however the tuff is more commonly called a dacite due to the numerous quartz and plagioclase phenocrysts. The tuff of the upper partially-welded unit is generally composed of 35% to 45% phenocrysts and 1% to 2% lithics. The majority of phenocrysts are plagioclase crystals (55% to 80%) while quartz (5% to 14%), biotite (5% to 13%), and sanidine (0.5% to 5%) compose the other primary minerals. Generally the phenocrysts range in size from barely discernable with the aid of a hand lens to 3 mm. Pumice fragments, which usually range in size from 25.4 mm to 100 mm, are also common throughout the tuff. Overall, the tuff is relatively dense and competent, mainly due to intense vapor-phase crystallization which permeated pores during the cooling of the unit.

An angular unconformity occurs at the base of the Apache Leap Formation as a result of upper Precambrian and Paleozoic rocks of moderate to steep relief underlying gently dipping tuffaceous deposits of mid-Tertiary origin. These underlying rocks dip eastward at angles from 30° to 45° while the overlying tuff dips eastward at smaller angles, generally from 15° to 25°. Analysis of the relationships between the tuff and underlying beds indicate that the structural block of the area began to be tilted before the tuff was laid down and that

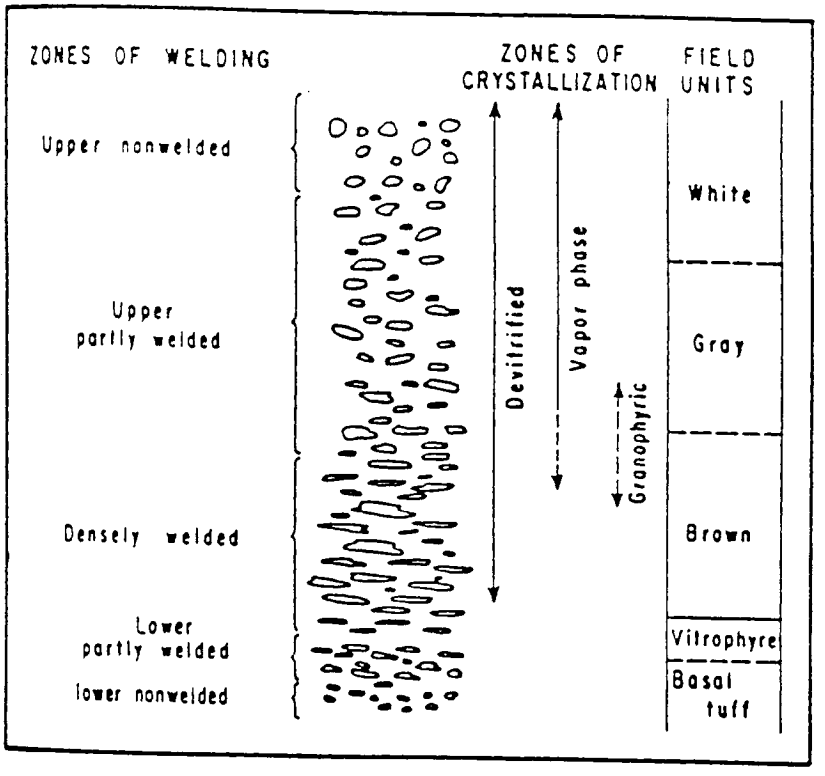

Figure 2.2. Physical characteristics of the Apache Leap tuff.

tilting continued after the tuff had solidified.

Two principal sets of faults have been identified in the Superior region. The oldest set trends principally east and is mineralized while the younger set trends generally north to northwest. Faults were identified by Peterson upon the recognition of, 1) striations and slickensides on fracture planes, 2) brechiated core, and 3) zones of granulation and low core recovery.

The Apache Leap tuff is also cut extensively by joints in all of the zones of welding. In many areas there are two primary joint sets which intersect at angles from 60° to 90°. The joints are also generally more closely spaced in the densely-welded units than in the less welded units. Commonly the joint systems in outcrop are distinct, and parallel joints in some instances extend continuously for hundreds of meters. The continuity of the joints indicate that they are of a tectonic origin, rather than a cooling feature of the tuff.

Core from the nine boreholes located at the Apache Leap test site have been analyzed to determine the relative and absolute strike and dip of the fractures intersecting the boreholes. The data indicate the predominance of steeply dipping fractures which are generally directed toward the southwest and northwest (Figure 2.3). The fracture orientations obtained from the borehole cores show good agreement with surface exposures in surrounding outcrops of the study area.

2.4 TEST SITE DESCRIPTION

Three sets of three 100 mm (4 in.) diameter boreholes are located at the Apache Leap test site, designated as sets X, Y and Z

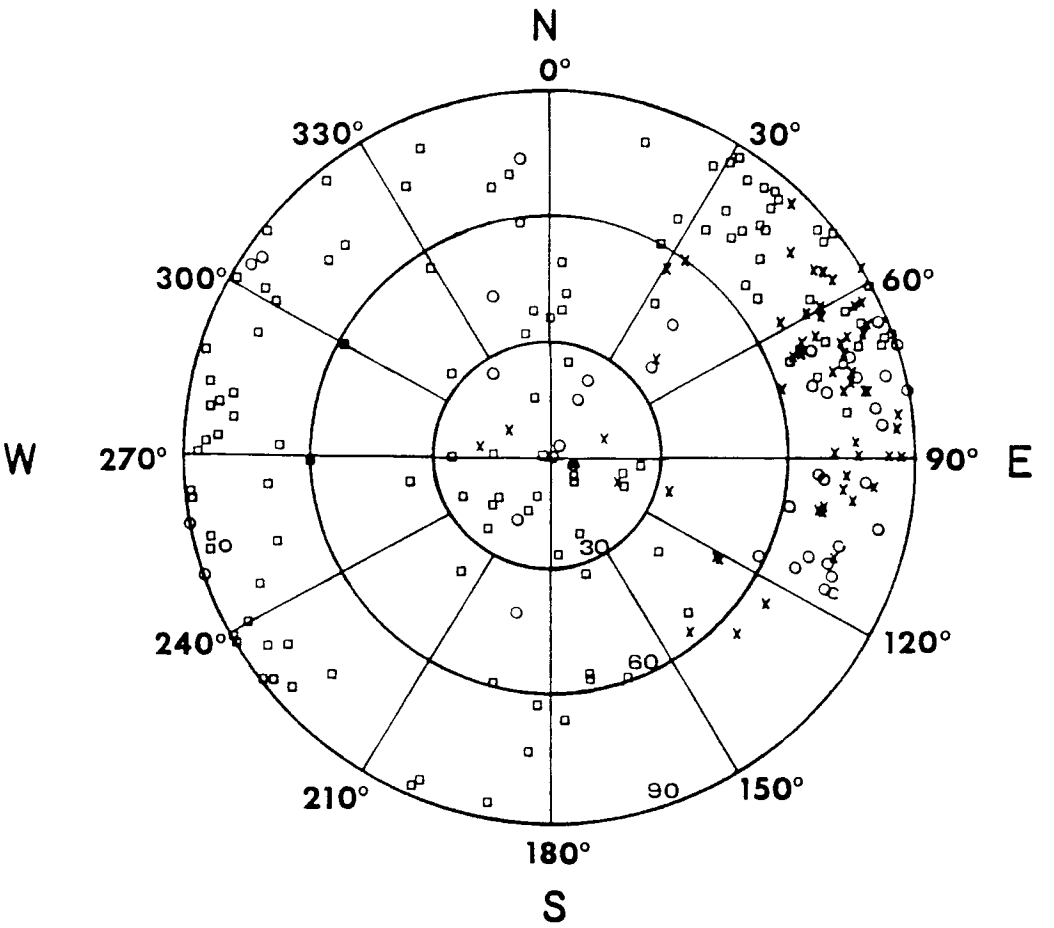

Figure 2.3. Lower stereonet projection of fracture orientations observed at the Apache Leap test site, from X series boreholes (crosses), Y series boreholes (circles) and Z series boreholes (squares) (after Yeh et al., 1988).

(Figure 2.4). Set X was drilled in September, 1985, while sets Y and Z were drilled in the month of November, 1986. All nine boreholes were drilled at a 45° angle to the horizontal. Sets X and Y are oriented with the bottom of the borehole nearly due west relative to the top of the borehole, while set Z is oriented in exactly the opposite manner. The boreholes in each set are spaced 10 m apart and each set is separated by a 5 m interval. Each set contains boreholes that are approximately 15 m, 30 m, and 45 m in length. Set X is cased to a depth of 1.34 m while sets Y and Z are cased to a depth of 1.58 m.

This particular borehole configuration makes monitoring of fluid flow in three dimensions possible. Also the 45° angle of the boreholes increases the probability of intercepting the vertical and near vertical joints which dominate the test site.

Cores were logged during the drilling of the boreholes, with an orientation mark every 3.05 m. The cores were studied in order to provide information about the location and orientation of fractures, and the occurrence and composition of mineralization along fracture surfaces. Relative permeabilities of the fractures, based on the degree of mineralization observed in the well logs, were also estimated (Figures 2.5 - 2.7).

All nine boreholes are developed well above the local water table. The true depth to the water table in the area of the test site is unknown, however it is of a sufficient depth that its presence may be neglected. The test site also lacks the presence of any significant

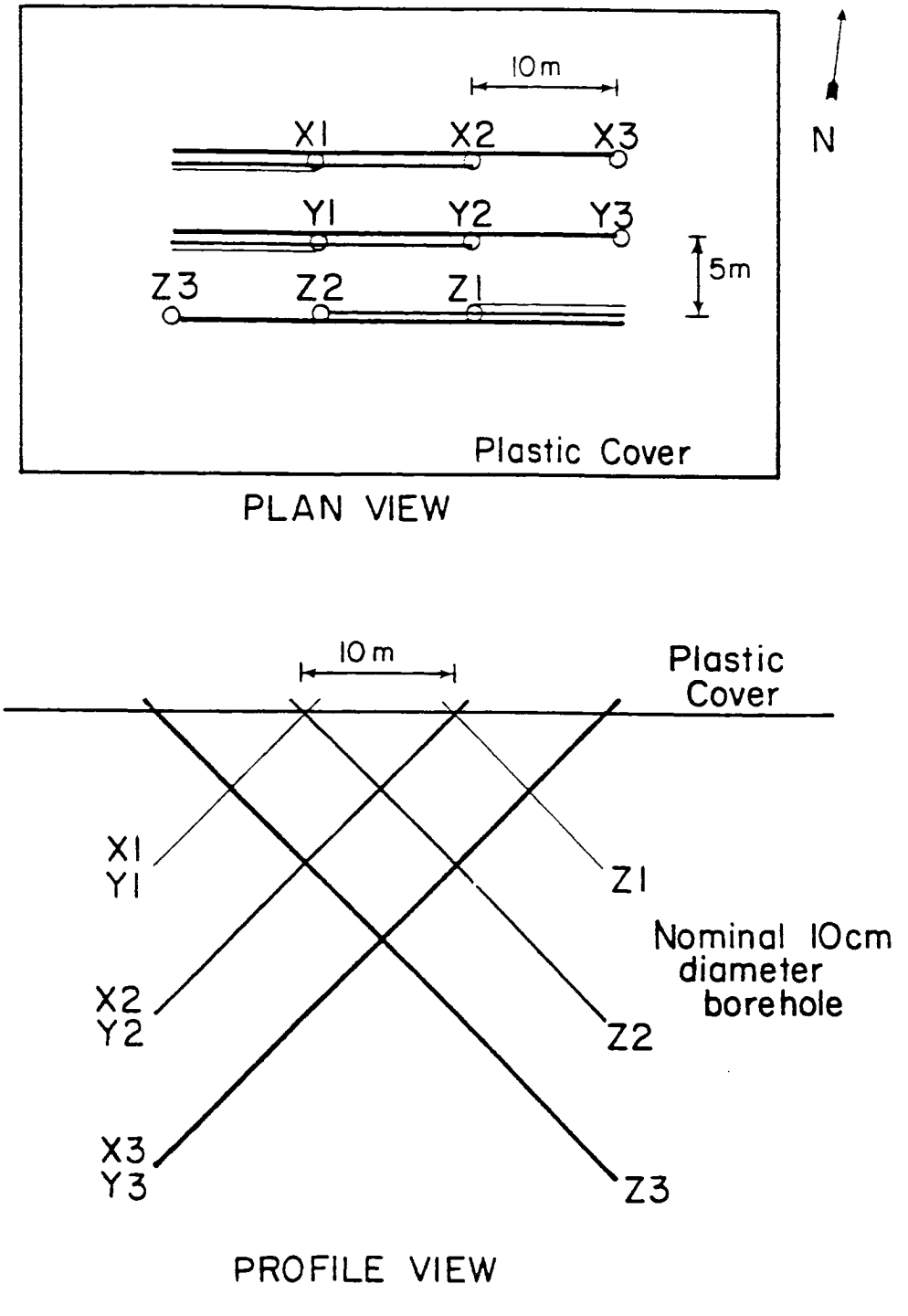

Figure 2.4. Borehole configuration at the Apache Leap test site.

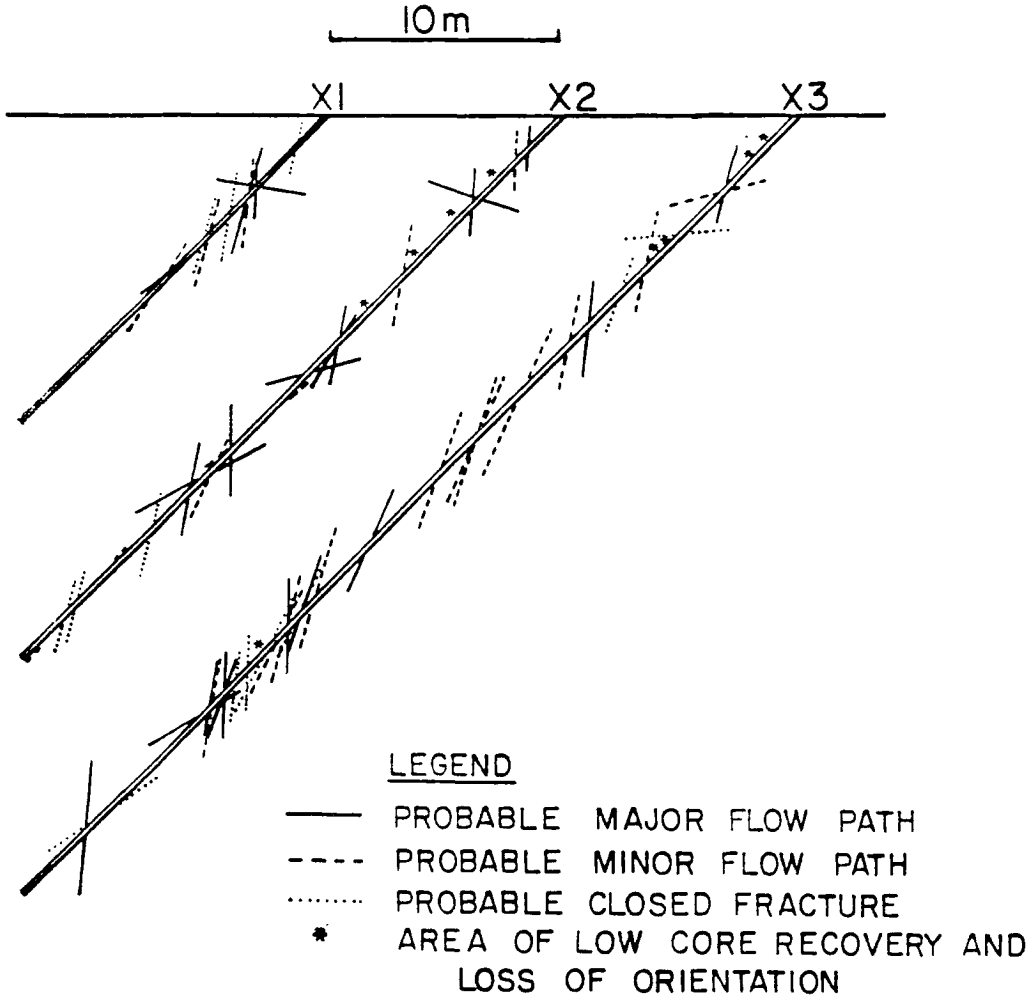

Figure 2.5. Fracture distribution along the length of the X-series boreholes at the Apache Leap test site (after Weber, 1986).

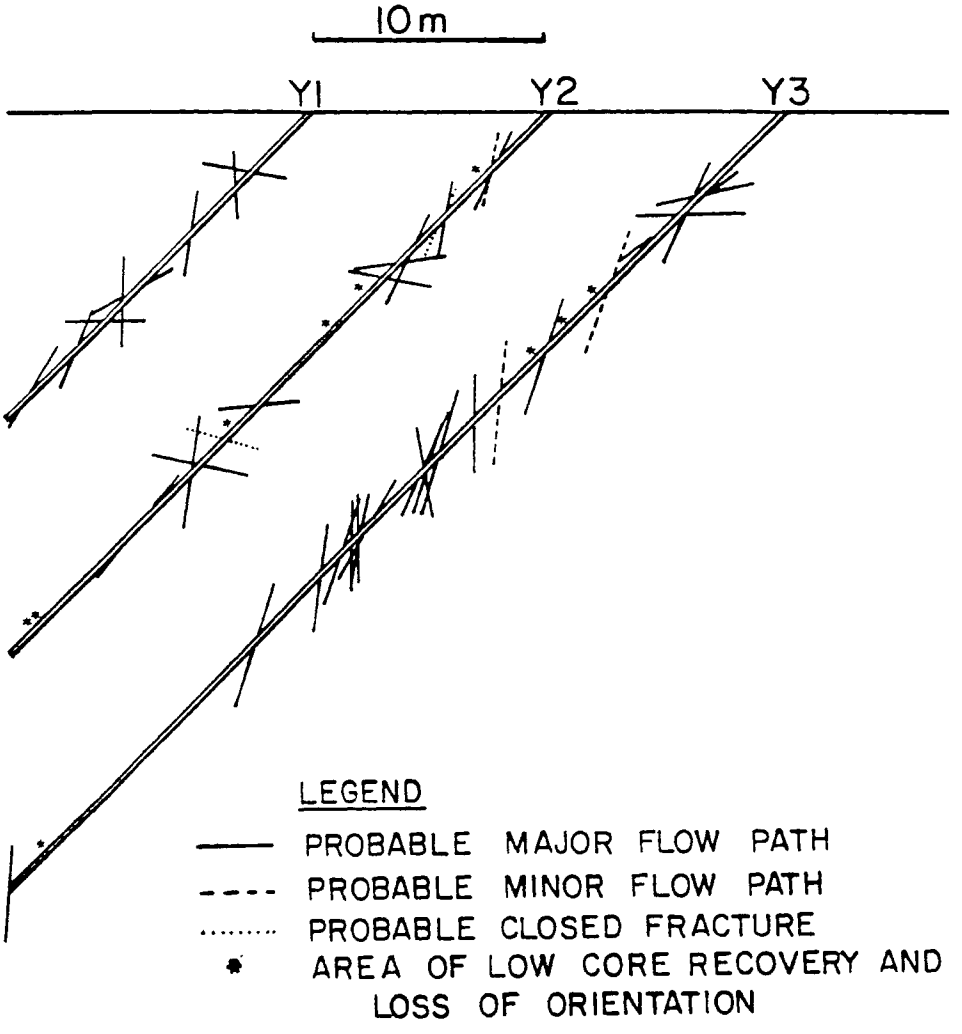

Figure 2.6. Fracture distribution along the length of the Y-series boreholes at the Apache Leap test site.

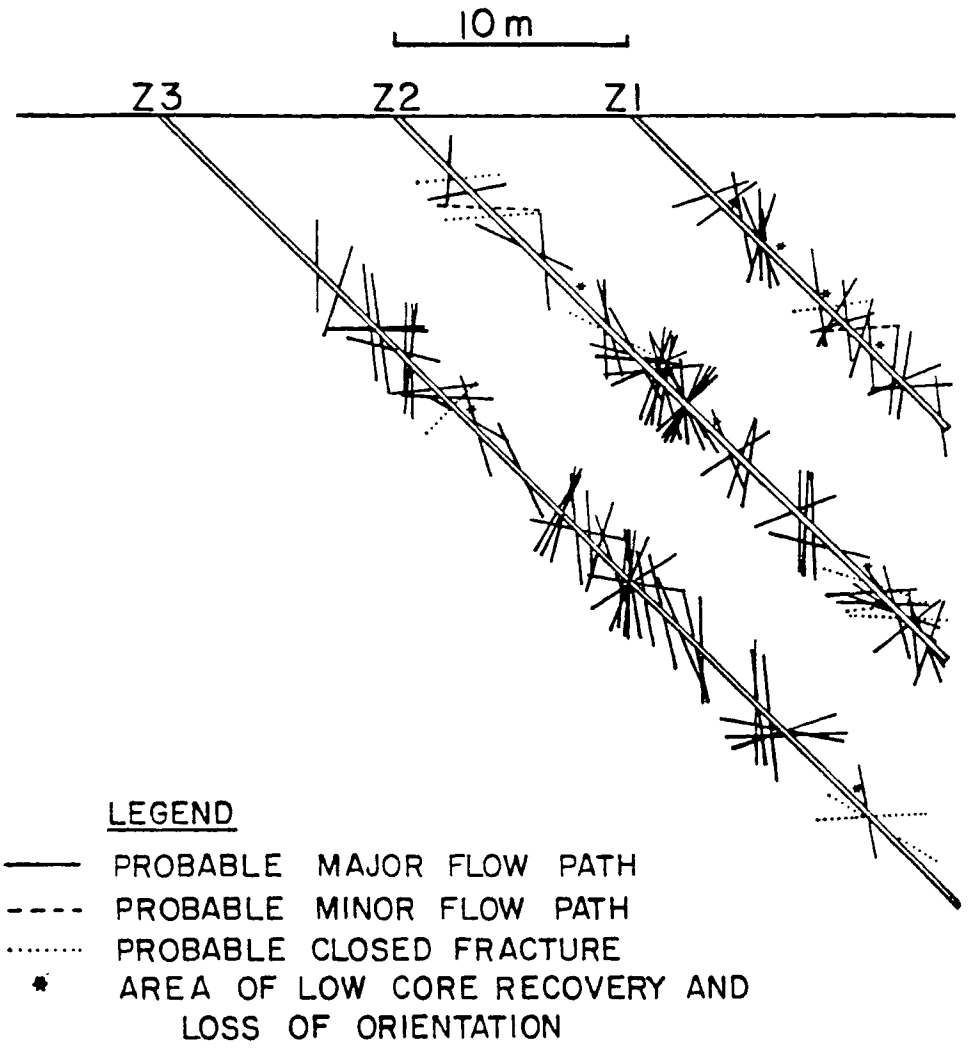

Figure 2.7. Fracture distribution along the Z series boreholes at the Apache Leap test site.

storm water runoff arteries. Futhermore, a 30 m x 30 m plastic tarp has been installed to prevent the infiltration of precipitation in the vicinity of the nine boreholes.

CHAPTER THREE

DEVELOPMENT OF INSTRUMENTATION AND PROCEDURE FOR COLLECTING FIELD DATA

In order to estimate the equivalent saturated hydraulic conductivity in situ, a practical method for collecting field data must be developed. Generally borehole permeability tests, tests which measure the outflow emanating from an uncased borehole subject to a constant hydraulic head, are conducted to obtain the required data. In situations involving deep water table conditions, it is obviously necessary to flood the boreholes in order to conduct this type of test. It is the intention of this investigation to adapt such an approach to fit the particular problem at hand.

3.1 BOREHOLE CONFIGURATION

Borehole permeability tests are primarily conducted in boreholes which are oriented vertically, however vertical orientations do not always provide a sampling method which is representative of the media of interest. Of primary concern is the fact that vertical boreholes tend to neglect the influence of structures which are steeply dipping. It follows that by neglecting vertical structure, grave error in estimating the hydraulic conductivity is possible. For this reason, consideration of the structural and stratigraphic geologic properties of a field site is of great importance when developing a sampling scheme for a

particular field site. Therefore, the development of the borehole configuration over which sampling will be conducted must be predicated on the geology of the field site.

The dominate structural geologic property of the Apache Leap test site is the fracture network which permeates the tuff. Observation of fracture outcrops at the test site indicate the predominance of steeply dipping fractures oriented toward the southwest and northwest. As a result, boreholes located at the field site are drilled at a 45° angle in order to intersect the steeply dipping fractures; furthermore, the boreholes are oriented with the northwest and southwest trend of the fractures in mind.

3.2 SCALE OF MEASUREMENT

When dealing with the hydraulic conductivity, the scale over which the measurement is conducted will have a profound effect on the results obtained, as previously discussed in Section 1.2.2. For this investigation, a measurement interval of approximately three meters in length has been adopted. Three meter intervals are utilized because most borehole segments of this length, analyzed at the test site, are cut by at least one fracture. Also, at this scale all intervals exhibit outflow rates which are within the range of sensitivity of the developed field technique. Finally, this sampling scheme will allow comparison between the hydraulic conductivity and other rock properties measured at the same scale in the field.

Measurements of this scale will give rise to estimates of the equivalent saturated hydraulic conductivity which may be associated with

only a small cylinder of rock in close proximity to the borehole. However, greater detail concerning the heterogeneity of the material will be obtained than would be if REV scale measurements were made.

On the other hand, if conductivity values of an REV scale are desired, methods such as that described by Neuman (1987) may be used to analyze the data.

3.3 DEVELOPMENT OF THE FALLING-HEAD FLOWMETER

Initially outflow rates were measured by means of the heat-pulse flowmeter (Figure 3.1) developed by Messer (1986). The heat-pulse flowmeter consists of a 25.4 mm (1 in.) pipe centered inside a 75 mm (3 in.) steel casing. Around the steel casing a 600 mm (2 ft.) natural rubber tube is fitted which acts as a packer when inflated. A heating grid is secured in the center of the 25.4 mm pipe with thermistors placed at a distance of 50 mm (2 in.) on either side of the heating element. The thermistors are wired in a bridge such that they record only differences in temperature relative to one another. Flow rate is measured by inflating the packer at the desired location and applying a 0.05 second, 120 V AC pulse across the heating grid. The thermistors, in turn measure, the convection/conduction of the heat pulse away from the heating grid. The time to peak resistance (resistance to electric current passing through the thermistor is increased by increasing temperature) is measured, and the associated flow rate is obtained from the calibration curve. This procedure is repeated at 3 m (9.84 ft.) intervals down the borehole. The subsequent flow rate over a given three meter interval is determined by subtracting the outflow rates

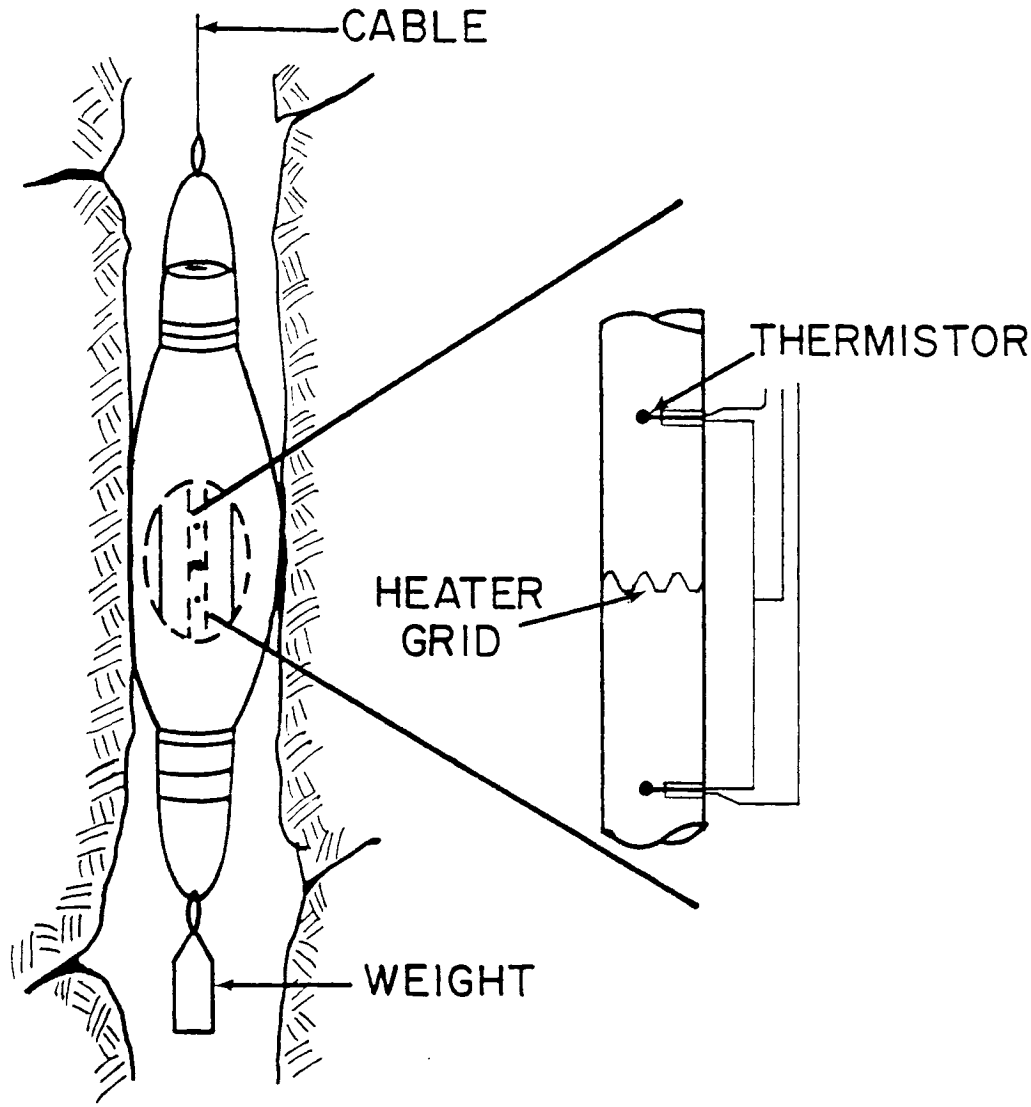

Figure 3.1. Description of heat-pulse flowmeter and packer assembly. Wall roughness exaggerated (after Rasmussen and Evans, 1987).

measured at either end of the test interval.

Upon application of this technique at the Apache Leap test site, it became evident that the heat-pulse flowmeter was not able to reproduce data accurately. The reason for the lack of repeatability was never determined, however it was believed to be the result of several factors. The lack of repeatability, in turn, produced a high degree of error in the results which made the data practically useless for determining the hydraulic properties of the tuff. Therefore, it was concluded that the lack of precision associated with the heat-pulse flowmeter would prevent the collection of reliable data from which the hydraulic conductivity could be determined.

As a result of the lack of precision of the heat-pulse flowmeter, an alternative method which will provide reliable data is sought. Generally, measurements of saturated hydraulic conductivity measured above the water table are made by gravity permeability tests or by falling-head tests (USBR, 1977, pp.266 - 285). Gravity permeability tests include several methods which are intended primarily for use in unconsolidated or unstable materials. The tests are usually preformed in shallow holes with relatively large diameters. The basic method involves monitoring the flow of water into the hole necessary to maintain a constant head. The borehole geometry, flow rate, hydraulic head, and depth to the water table are subsequently used in calculating the saturated hydraulic conductivity. Falling-head tests, on the other hand, are used primarily in open holes in consolidated rock. Packers are used to isolate a desired interval of borehole while water is transmitted between the packers via a "drop" pipe. During testing only

the interval between the packers is maintained at a positive hydrostatic pressure. Outflow rates are monitored by noting the head drop which occurs within the "drop" pipe over a specific length of time. Outflow rate, geometry of the borehole and the location and length of the test interval are subsequently used to determine the hydraulic conductivity by means of an analytical solution.

Based on the presented facts, the falling-head method is adopted for measuring the outflow rates associated with the nine boreholes at the test site. Several modifications to the falling-head method are made before implementing it in the field. One modification includes using a single packer as opposed to the straddle-packer system suggested by the U.S. Bureau of Reclamation. Also, a flowmeter was developed to monitor outflow rates, as opposed to a "drop" pipe, which allows monitoring of a large range of outflow rates, prevents a significant drop in head during testing, and maintains a high degree of accuracy when measuring small outflow rates. A more lengthy discussion of the technique and equipment used in measuring outflow characteristics at the test site is given in the following section.

3.4 DESCRIPTION OF THE FALLING-HEAD FLOWMETER AND ASSOCIATED PACKER

In order to gather the needed data, both a down-hole packer configuration and a monitoring system are needed. The purpose of the down-hole packer being to isolate intervals of the borehole (intervals extend from the packer to the bottom of the borehole) so as to allow water to enter the interval of interest only through the packer. In

turn, a means with which to monitor the water passing through the packer is accommodated by the development of a falling-head flowmeter.

The packer developed to meet these needs consists of a 19 mm (3/4 in.) pipe centered inside a 76 mm (3 in.) steel casing (Figure 3.2). A cap is welded to the down-hole end of the casing through which the 19 mm pipe passes and is supported. The 19 mm pipe is, in turn, attached to 48 m (160 ft) of 15.8 mm (5/8 in.) flexible tubing which spans the length between the packer and the falling-head flowmeter located outside the borehole. The outer steel casing provides weight for the instrument as well as serving as a mount for the packer. Two 300 mm (1 ft.)long tubes made of 3.2 mm (1/8 in.) thick pure gum rubber, obtained from Goodyear Rubber Company, are clamped, one inside the other, onto the outer casing. The rubber tubes function as a packer when inflated with air. The air used to inflate the packer is supplied by 9.5 mm (5/8 in.) plastic tubing which is connected to a source of compressed gas at the surface. Once inflated, water can only enter the section of borehole below the packer via the 19 mm pipe.

Several packer arrangements were tested before settling on a single, 300 mm (1 ft.) long packer assemblage. Initially a straddle-packer system, using 1.5 m (5 ft.) long packers, was tried, however pressure build-up, which required several hours to dissipate, was encountered. The pressure build-up was blamed primarily on water, which is displaced by the inflating packers, being trapped within the test interval. The same problem was also encountered when using a single, 1.5 m long packer. Subsequently the packer length was reduced to 300 mm in order to lessen the volume of water displaced by the inflating

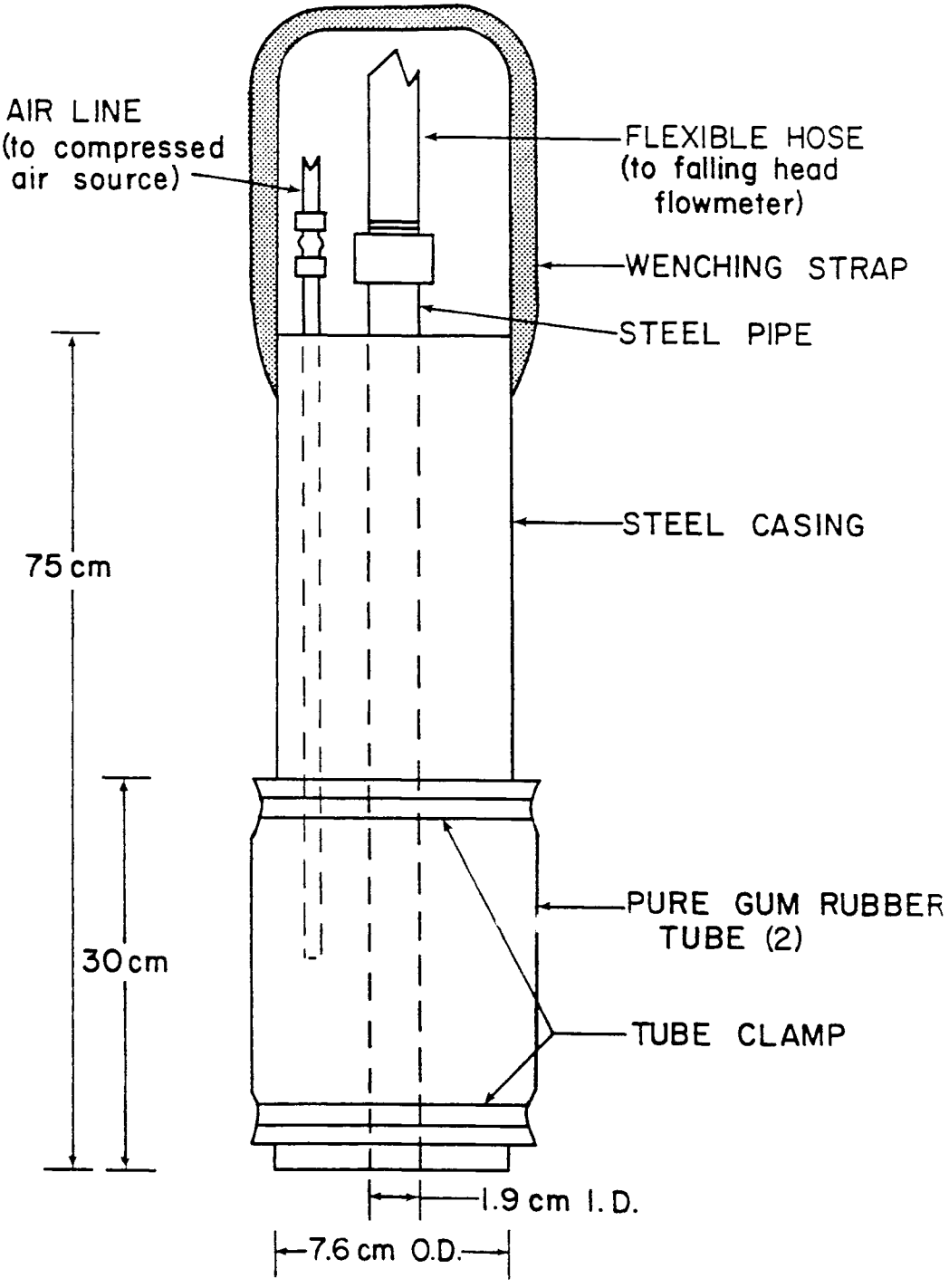

Figure 3.2. Down-hole packer utilized in isolating intervals of borehole.

packer. As hoped, the shorter packer produced no detectable pressure build-up during inflation. However, whether a long or a short packer is used, leakage around the packer is assumed to be insignificant since the pressure gradient across the packer is small. The pressure gradient across the packer is maintained at an insignificant level by keeping the interval of borehole above the packer full of water.

Water passing through the packer assemblage is monitored outside of the borehole by the falling-head flowmeter. The flowmeter monitors outflow by means of a collection of plexiglass cylinders of various sizes, mounted to a piece of plywood (Figure 3.3). Thick walled plexiglass is used because of its durability and resistance to expansion due to heat. In addition to the plexiglass cylinders, a constant head reservoir is implemented to maintain a constant hydraulic head on the system between tests. The constant head reservoir consists of a 1000 ml flask with a 9.5 mm (3/8 in.) overflow outlet, drilled 25.4 mm (1 in.) below the lip of the flask. Valves are located at the outlets of the reservoir and each of the cylinders to regulate outflow. The reservoir and plexiglass cylinders are linked by 9.5 mm (3/8 in.) plastic tubing, which in turn is connected to the flexible hose linking the flowmeter and the down-hole packer.

A great deal of care was given to the proper sizing of the cylinders for the falling-head flowmeter. The cylinders had to be sized so as to handle the various flow rates encountered during testing, as well as, reduce the amount of head loss during a test. In order to monitor a given outflow rate, the total drop in head during a test must be maintained within the cylinder used for testing. Therefore, small

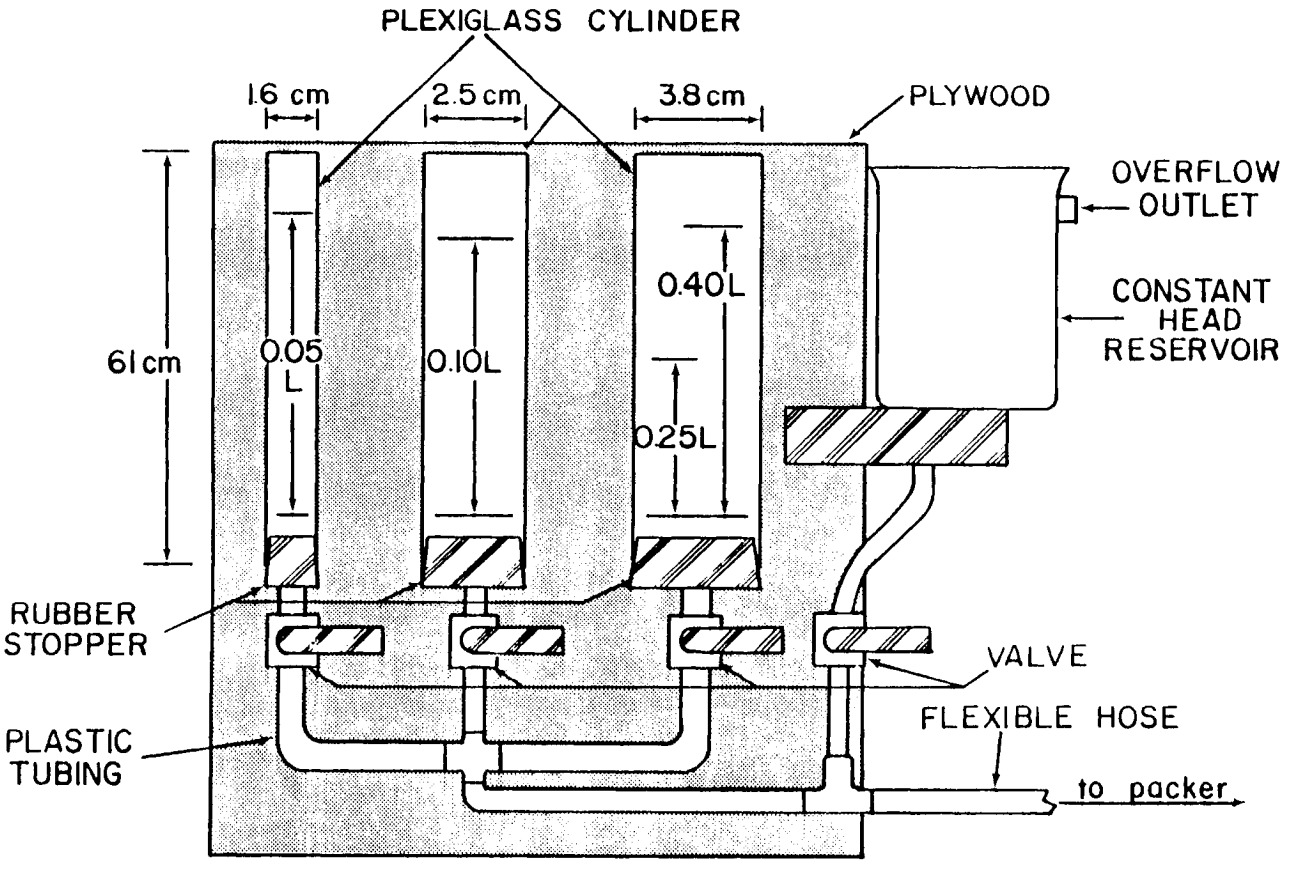

Figure 3.3. Falling-head flowmeter utilized in monitoring borehole outflow.

cylinders are need to accelerate the drop in head due to low outflow rates while large diameter cylinders are needed to slow the falling head attributed to higher outflow rates. Cylinders with diameters of 38.1 mm (1.5 in.), 25.4 mm (1 in.) and 15.8 mm (5/8 in.) were found to meet these criteria. The cylinders, in turn, were graduated for volumes of 0.4 liters and 0.25 liters in the large cylinder and 0.1 liters and 0.05 liters, respectively, for the two smaller cylinders. With this combination of volume and cylinder size, a maximum head drop of only 250 mm (10 in.) was encountered. The 250 mm head drop only accounts for 8% of the total head on the system when the packer is positioned at the top of the well, and is even less significant as the packer is moved down the borehole. Obviously, allowing a head drop of this magnitude during testing has little effect on the outflow rate from the boreholes. On the other hand, the cylinder size to volume ratio also improves the accuracy of the measurement technique at lower outflow rates. Utilization of variously sized cylinders provide a means with which to monitor relatively large outflow rates with larger cylinders while small cylinders yield an appreciable head drop during measurement of low outflow rates.

3.5 PROCEDURE FOR MONITORING BOREHOLE OUTFLOW RATES

3.5.1 NORMAL MEASUREMENT PROCEDURE

The quality of water used in permeability tests of this type is of primary importance. The presence of only a few parts per million of turbidity in water can plug fractures and cause serious errors in test

results. To assure high quality water, potable water from a nearby mine is used only after being filtered by a diatomaceous earth pool filter.

Since the boreholes at the test site are located in unsaturated fractured tuff, each borehole must be flooded before testing can take place. Only one borehole is flooded at a time to prevent the outflow of one borehole from interfering with the outflow of the other. Once flooding of the borehole is accomplished, steady-state flow conditions must be achieved before measurements can be taken. However, the head maintained by the flowmeter is generally about 760 mm (2.5 ft.) above the top of the casing. Therefore, in order to allow the borehole outflow rate to equilibrate with the head maintained by the flowmeter, the packer must be positioned and inflated immediately after flooding.

To determine the amount of time necessary for steady-state flow conditions to develop, measurement of the outflow rate as a function of time were made at the upper packer location in well Z-2 (Figure 3.4). The results obtained indicate that approximately two hours were necessary for flow conditions to stabilize. Subsequently, the two hour period was adopted as the length of time necessary to allow equilibration of outflow which, in turn, dictates the time allowed between the flooding of the borehole and the taking of the first measurement.

Prior to dropping the packer down the borehole, careful attention must be given to purging the water line, leading to the packer, of air. The best method for preforming this task is to move the packer assemblage down a hill in order to increase the head between the falling-head flowmeter and the packer. Water is then allowed to flow

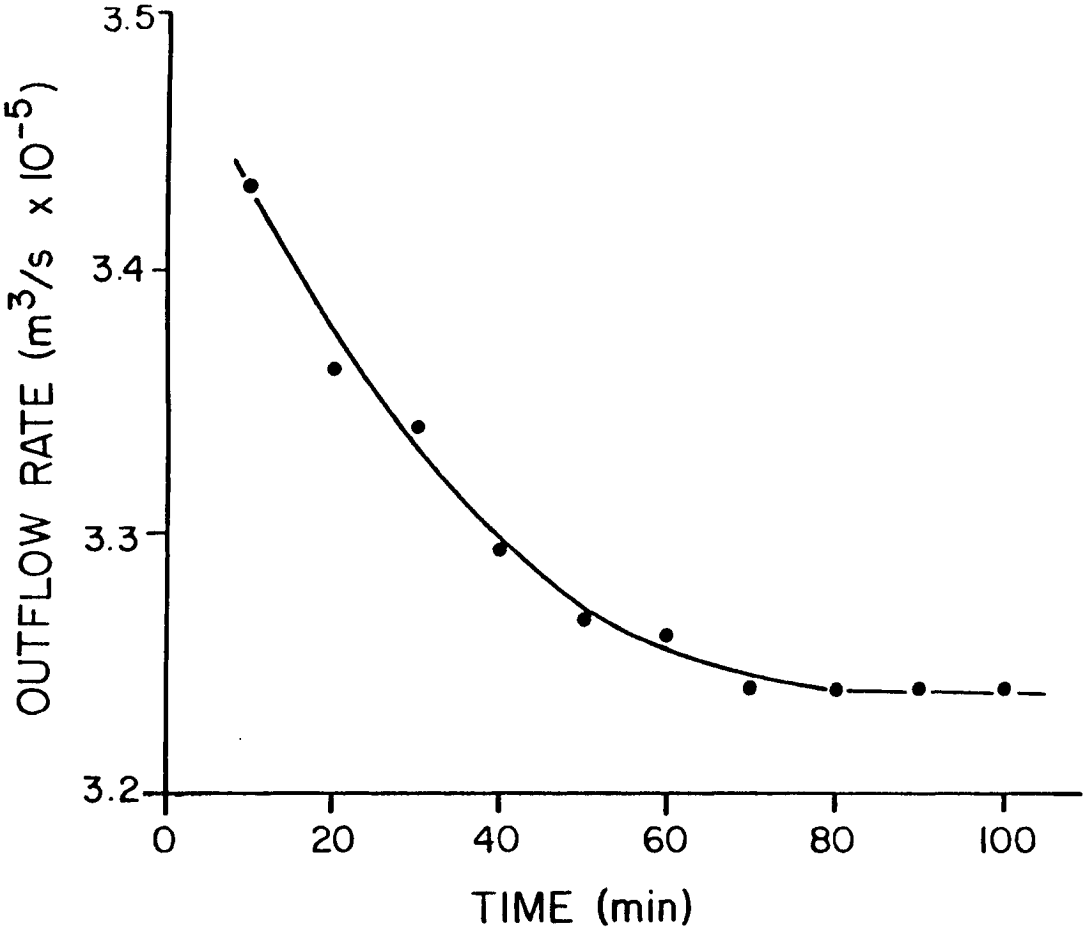

Figure 3.4. Outflow rate against time as measured in borehole Z-2 at the upper packer location.

through the system for several minutes. The packer is then carefully moved back to the borehole while making sure that water continues to flow through the system.

Once the system is purged of air and an equilibrium outflow rate is achieved, testing is initiated. Six measurements at each packer location are made and averaged together. To take a reading, the valve to one of the plexiglass cylinders is opened while the valve to the reservoir is closed. Immediately after closing the reservoir valve, the head in the cylinder will begin to drop. By timing the falling head, one may calculate the outflow rate. The outflow rate is calculated by dividing the graduated volume of the plexiglass cylinder by the time necessary for the head to fall through the graduated portion of cylinder. Once a measurement is taken the valve to the constant head reservoir is reopened so as to fill the drained cylinder and re-institute a constant head.

Generally, test intervals are kept in the range of 30 seconds to one minute. Test intervals are preferred in this range because the error associated with response time is minimized while also keeping testing time to a reasonable length.

Once measurements are finished at a given location, the packer is deflated and moved. After positioning, the packer is re-inflated, generally 10 - 15 psi above local hydrostatic pressure, and a 5 - 10 minute period is allowed before the next measurements are made. The 5-10 minute period simply permits the outflow rate to stabilize.

Positioning of the packer, for the most part, is based on a horizontal datum arbitrarily positioned at the upper lip of the casing

in borehole X-1. The initial reading in each borehole is centered 1.5 m below the casing of the borehole, while the second reading is taken 4.5 m, plus the length of the casing, below the datum with the following readings being taken at 3 m intervals down the borehole. Since the packer is located relative to the top of the casing, corrections for casing length and the elevation of the borehole relative to X-1 must be considered.

Since field data were collected during June and July, efforts to prevent excessive swings in water temperature were made. One method of prevention was to shade, as best as possible, all water reservoirs, tubes, hoses and cylinders. Water added to the constant head reservoir was kept at relatively stable temperature by storing the water in a 100 gallon trough prior to its use. By taking these precautions, the maximum water temperature variation experienced during the testing of any of the nine boreholes at the Apache Leap test site was only 5 C°.

3.5.2 PROCEDURE FOR MONITORING SUPER CONDUCTING FRACTURES

Unexpected problems were encountered during the testing of boreholes Z-1 and Z-3. It was found that both boreholes were cut by highly permeable fractures which prevented the filling of the boreholes with water. Therefore, the fractures had to be packed-off with a secondary packer in order to fill the boreholes and monitor the outflow rates over the interval above the "super" conducting fractures. The secondary packer would simply be positioned over the "super" conducting fracture and inflated. A fitting on the bottom of the packer associated with the falling-head flowmeter allowed a 9.5 mm air tube to pass from the

secondary packer to a source of compressed air on the surface. The chain used to move the secondary packer was allowed to drop into the well and would be fished out after measurements were finished. Unfortunately a small interval in borehole Z-3 could not be measured due to the positioning of the secondary packer.

The outflow rate passing out of the borehole through the "super" conducting fractures was difficult to measure with the limited supply of water at the test site. However, an estimate of the outflow rate was measured by pumping water into the borehole, aided by a single stroke gasoline powered pump, until a constant head was maintained. Once a constant head was achieved, the outflow rate necessary to maintain the constant head was monitored with a 5/8" Rockwell International flowmeter. Although the technique measures the outflow rate through the entire borehole, the outflow through the minor flow paths is insignificant compared to that of "super" conductors.

CHAPTER FOUR

ANALYTICAL SOLUTIONS FOR ESTIMATING THE EQUIVALENT SATURATED HYDRAULIC CONDUCTIVITY

Since borehole permeability tests do not measure the hydraulic conductivity directly, a method for estimating this parameter from collected field data is necessary. There are four such analytical solutions which are generally used in conjunction with borehole permeability tests, however none of these solutions are applicable to the problem at hand. Classical analytical solutions cannot be applied in their present form to the permeability tests developed in this investigation because of two main reasons, 1) the classical solutions cannot handle inclined borehole orientations, and 2) the classical solutions do not account for multiple test intervals along the length of a single borehole. For this reason a solution is sought which will account for the special needs required by this investigation.

4.1 MATHEMATICAL BASIS FOR ANALYTICAL SOLUTION

For borehole permeability tests conducted above the water table, a saturated region surrounding the borehole is formed as a result of infiltrating water. Steady-state flow within the saturated region is governed by the equation

$$(4.1) \qquad \frac{\partial}{\partial x}K_x \frac{\partial h}{\partial x} + \frac{\partial}{\partial y}K_y \frac{\partial h}{\partial y} + \frac{\partial}{\partial z}K_z \frac{\partial h}{\partial z} = 0$$

However, to make this equation more manageable, the hydraulic conductivity is assumed to be homogeneous and isotropic. This assumption allows the transformation of equation 4.1 to the well known Laplace equation

$$(4.2) \qquad \nabla^2 h = 0$$

For the case of borehole permeability tests preformed under a constant hydraulic head, equation 4.2 is subject to the following boundary conditions

$$(4.3) \qquad 0 \leq z \leq H \qquad r = r_w \qquad h = H$$

$$(4.4) \qquad z = H \qquad 0 \leq r \leq r_w \qquad h = H$$

where r_w is the radius of the borehole and H is the saturated length of the borehole. In addition to these is the boundary condition at the free surface which encompasses the saturated region. At this boundary water pressures are atmospheric and the gradient normal to the free surface is zero (Figure 4.1).

The classical conceptual model is one in which Laplace's equation and its associated boundary conditions are restricted to the soil region between the borehole and the free surface. The movement of the water within this region being due to two forces, that of gravity and the hydrostatic weight of the column of water in the borehole. The hydrostatic forces act equally in all directions, while the strength of

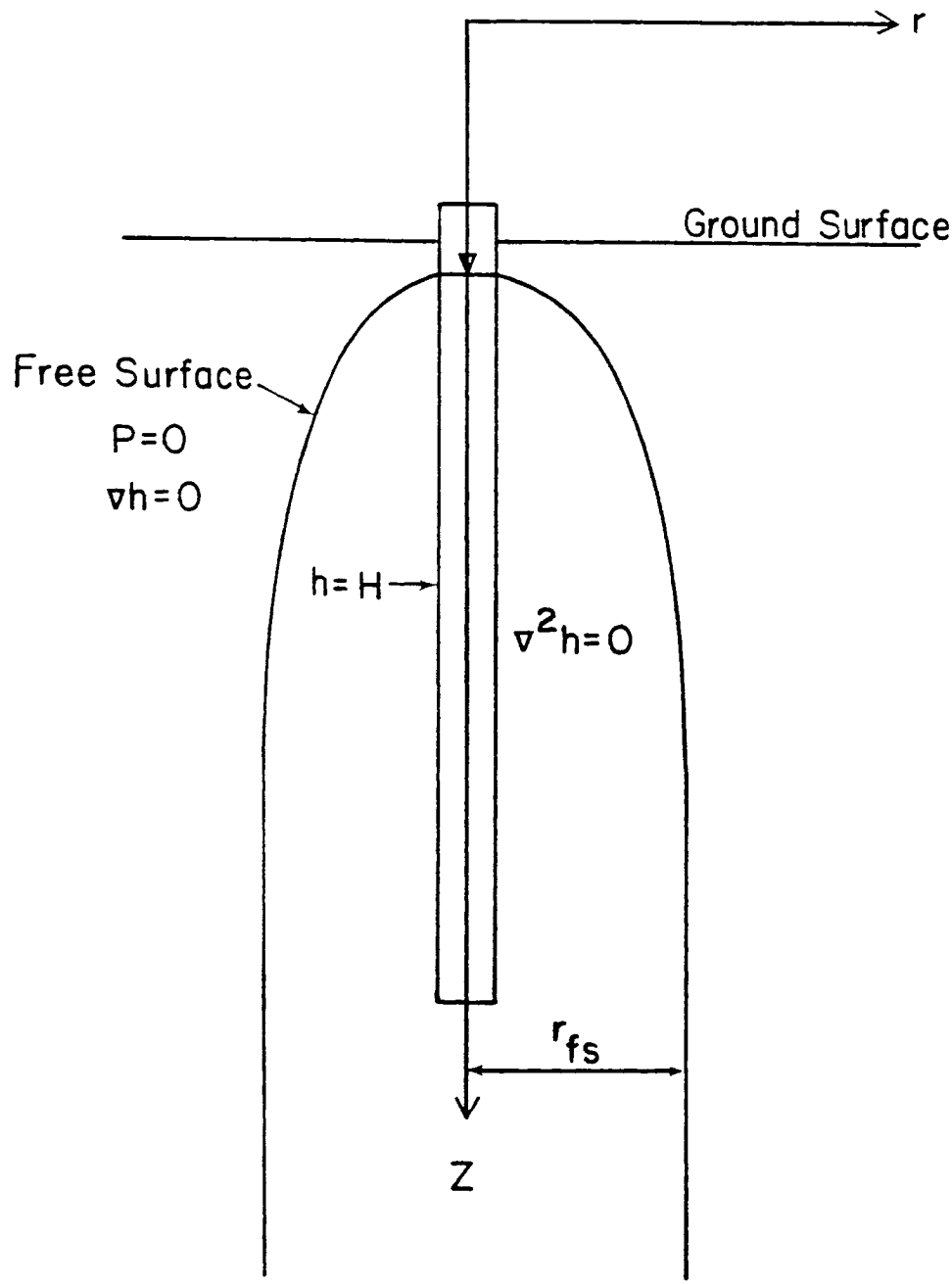

Figure 4.1. Conceptual model of free surface developed during vertical borehole infiltration tests.

this force increases linearly with depth. The gravity force, in turn, is responsible for the vertical flow component which increases in influence with distance from the source. At some distance from the borehole, where the pressure head owing to the source is nearly dissipated, water flows vertically as a result of the force of gravity only. Likewise, with depth below the borehole the gradient driving the flow is due only to gravitational forces. At such a depth the quantity of water flowing across any horizontal plane can be computed from Darcy's law as

$$(4.5) \quad Q = \pi r_{fs}^2 K$$

where r_{fs} is the horizontal distance from the axis of the borehole to the free surface (Figure 4.1).

4.2 CLASSICAL ANALYTICAL SOLUTIONS

Cornwell (1953) was probably the first to develop a solution for borehole permeability tests. Actually this solution was initially designed for cases below the water table, however the U.S. Bureau of Reclamation (1974, p.576) states "this test can be made both above and below the water table provided the hole will remain open" (remain open meaning the sides of the borehole are not prone to caving). The derivation begins with a point source of strength Q located a distance z below the water table. The water table is treated as an impermeable boundary by placing an imaginary point sink of strength Q at a distance z above the water table. It follows from the principle of superposition

that the total pressure field is just the sum of the individual fields created by the source and sink. The point source and sink are extended to a line source and sink by integrating along the open length of borehole, while assuming that their strength remains unchanged with elevation. The cylindrical nature of the source is approximated by setting the pressure head at the borehole radius equal to the total pressure head at the center of the open interval of borehole. His final solution takes on the following form

$$K = \frac{Q \ln (L/r_w)}{2\pi HL} \tag{4.6}$$

where L is the open length of borehole. Cornwell tested the validity of his solution by means of four electric analog tests. He reports that especially good results were obtained for cases in which $H/r \geq 20$. No other details concerning model validation are given.

Glover (1953) developed a solution which was adopted by the U.S. Bureau of Reclamation for borehole permeability tests associated with deep water table conditions, as well as cases below the water table. Initially Glover considers a point source at the base of the borehole. The principle of superposition is used to separate the gravity field from that of the pressure field created by the source. The point source is extended to a line source by integrating over the length of the borehole assuming that the source strength increases linearly with depth. The line source is subsequently approximated as a cylindrical source by assigning a constant pressure at the base and periphery of the

borehole which is equal to the height of water in the borehole. Given these assumptions, Glover arrives at the following solution

$$(4.7) \qquad K = \frac{Q}{2\pi H^2} \left(\sinh^{-1}(H/r_w) - 1\right)$$

Glover also compared his analytical solution to electric analog tests and found that the analytical solution generally provided values which deviated from the simulated results by less than 8 percent when $H/r \geq 20$. Once again this is the only description given to validation of the model.

Zanger (1953) extended the Glover solution to include situations in which the water filled length of borehole is greater than the uncased length of borehole. For such cases, Glover's solution becomes

$$(4.7) \qquad K = \frac{Q}{2\pi(2HL - L^2)} \left[\sinh^{-1}(L/r_w) - (L/H)\right]$$

Due to the work of both Nasberg (1951) and Terletskaya (1954), a solution of a more complex nature was developed. Nasberg derived an analytical solution which considers the existence of a free surface boundary for steady-state flow from a point source above the water table. As with the other solutions, the flow field is represented by the superposition of the gravity field, a pressure head field due to a point source of strength Q, and due to an image source of strength Q. The image point is used to satisfy the free surface boundary condition and account for a stagnation point above the point source. Terletskaya

broadened Nasberg's work by extending the point source to a line source. The transformation was accomplished by integrating the point source along the length of the borehole assuming a constant source strength with depth. Once again a constant head boundary condition, in which the head is assumed to equal the height of water in the borehole, is assigned to the base and periphery of the borehole to approximate the cylindrical nature of the source. As a result the Nasberg-Terletskaya equation takes on the following form

$$(4.9) \qquad K = \frac{0.423\ Q}{H^2} \log_{10} \frac{2H}{r}$$

for any set of parameters with consistent units. This solution is reported by Kozminski (1973) to be valid in the range $50 \leq H/r \leq 200$. A complete derivation of the Nasberg-Terletskaya equation may be found in Appendix F of Stephens (1979).

More recently J.R. Philip (1985) developed an analytical solution for borehole permeability tests conducted in unsaturated soil. Unlike the other three solutions mentioned, Philip does not rely on the principle of superposition in his derivation. Philip utilizes an analytical solution from Carslaw and Jaeger (1959) for heat flow from an ellipsoid of conductivity K' situated within a media of conductivity K. Philip utilizes this heat flow analogy by replacing the borehole with the lower half of a prolate spheroid. Philip also developed a term that accounts for the effect of capillary forces on the saturated flow field. However, the term is neglected in this analysis. The resulting saturated flow equation, equation 44 in Philip (1985), is as follows

$$(4.10) \quad K = \frac{Q}{(3/2)^{2/3}\pi r^2} \quad \frac{H_D \ln [H_D + (H_D^2 - 1)^{1/2}] - [H_D^2 - 1]^{1/2}}{(H_D^2 - 1)^{3/2}}$$

where H_D is the saturated length of the borehole divided by the borehole radius. No particular restrictions are given by Philip regarding the validity of equation 4.10.

After careful consideration of each of the four analytical solutions, the Philip and Glover solutions were found to be the best suited for adapting to the specific needs of this investigation. The reason for rejecting the Nasberg-Terletskaya solution was due to its restriction to situations in which $50 \leq H/r \leq 200$. The Cornwell solution was neglected due to its similarity with the Glover solution which arises out of the analogous nature of the transcendental functions appearing in each equation. Recall that $\sinh^{-1}(x) = \ln(x + \sqrt{x^2 + 1})$. For this reason adapting both solutions to fit the needs of this investigation seemed redundant.

4.3 DERIVATION OF THE ADAPTED GLOVER SOLUTION

In a media where the velocity is proportional to the pressure gradient, the flow patterns are superimposable, or in other words, gravitational effects may be separated from the effects of the pressure induced by the source. For the case of the gravitational forces, consider a ground surface which is ponded with water to a very small depth, and saturated conditions exist everywhere below the ground surface. Under these conditions the pressure head is zero everywhere and the infiltrating water is moving vertically due only to the force of

gravity. This simplification neglects the presence of capillary forces since the entire region of investigation is assumed saturated. Superimposed on the gravity field is the pressure field as induced by the borehole source. The source gives rise to a boundary which contains the area of influence of the source (Figure 4.2). Assuming that the medium is homogeneous and isotropic, a boundary develops which may be approximated in part by considering a cylindrical surface with its axis parallel to the source. The radius of the cylinder being of a size large enough to contain all flow from the borehole, at a great depth, which is traveling at velocities maintained by gravitational forces. Since the cylinder contains the flow from the source, the surface of the cylinder at depth can be considered a streamline. Due to the fact that capillary effects are neglected, the streamline is also known to cut the borehole at the associated static water surface. By rotating the streamline about the axis, one creates an axisymmetric confining boundary which assumes the shape of a cylinder at depth. This boundary is a much simplified representation of the free surface which is expected to develop given unsaturated conditions surrounding a flooded borehole. The simplified boundary condition is approximated in this solution by taking into consideration that the pressure head along the surface of the borehole increases with depth. This increase in pressure with depth is accompanied by an increase in source strength which can be represented by a series of uniformly spaced sources, starting at zero strength at the top of the borehole and increases linearly in strength to a maximum at the bottom. The streamline produced by the line of

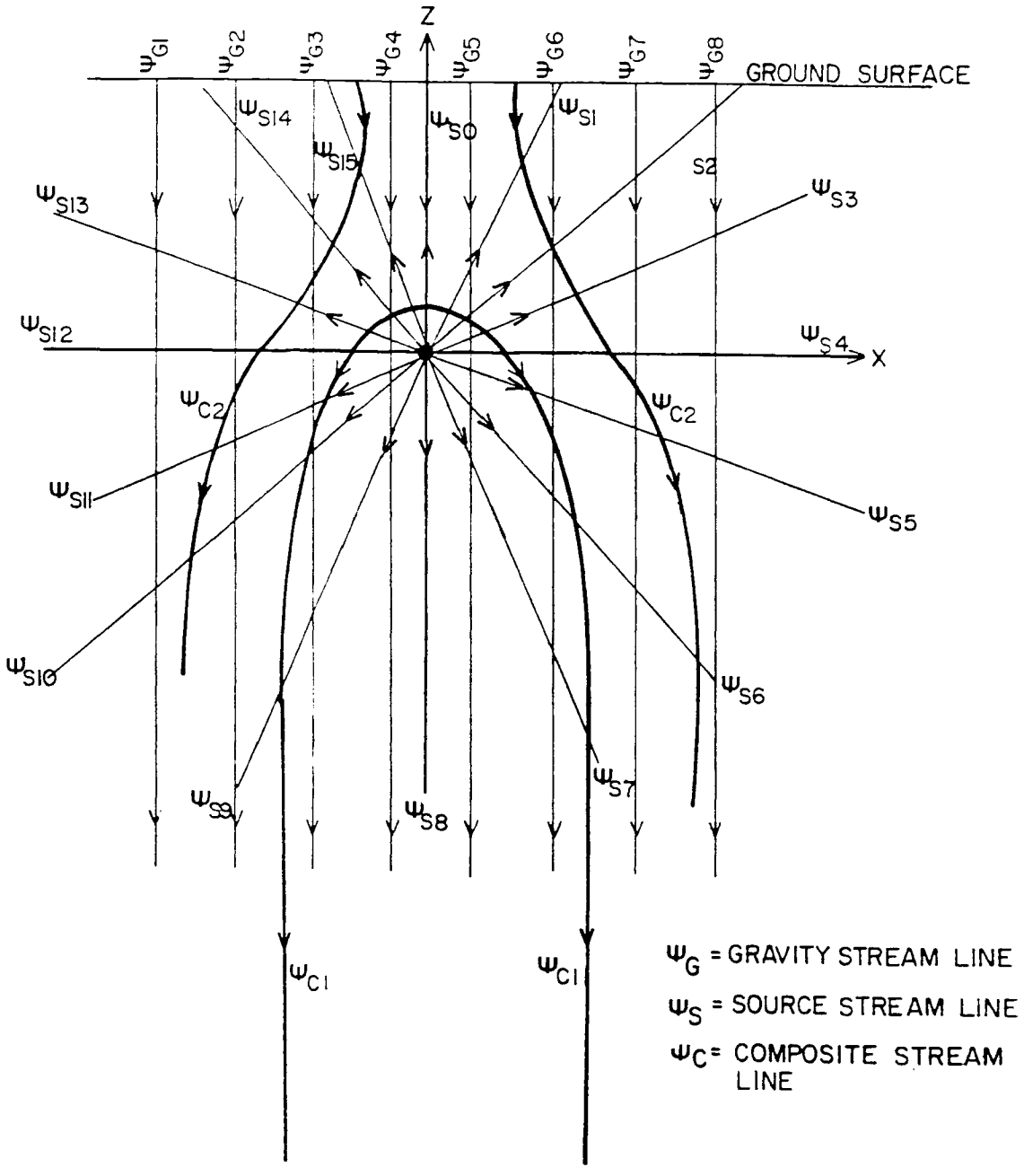

Figure 4.2. Graphical representation of superimposable flow fields resulting from a point source, and the gravitational field.

sources provides a reasonably close representation of the boundary condition required when rotated about its axis.

Recall that the total flow field consists of the superposition of the gravity field and the pressure field induced by the source. However, the gravity field is assumed to be uniform, capillary effects being neglected, thus variation in the total flow field is due only to the effects of the pressure field induced by the source. Therefore, effects of the gravitational flow field may be neglected without adverse consequences. By neglecting gravitational forces, flow emanating from the borehole will occur in a radial manner regardless of the orientation of the borehole. As a result, a cylindrical coordinate system, oriented parallel with the axis of the borehole, is adopted for the derivation of the solution (Figure 4.3).

We begin the derivation of the adapted Glover solution by considering a point source subject to Darcy's law

$$q = -K\, dP/dR$$

$$Q = q \cdot A \qquad \text{where } A = 4\pi R^2$$

$$Q = -4\pi R^2 K\, dP/dR \tag{4.11}$$

where A is the area normal to flow, or in this case the surface area of a spheroid, P is the pressure head, R is the radial distance from the point source and q is the specific flux vector. Assuming that the pressure is zero at $r = \infty$, the pressure head, P, at any point due to the point source is

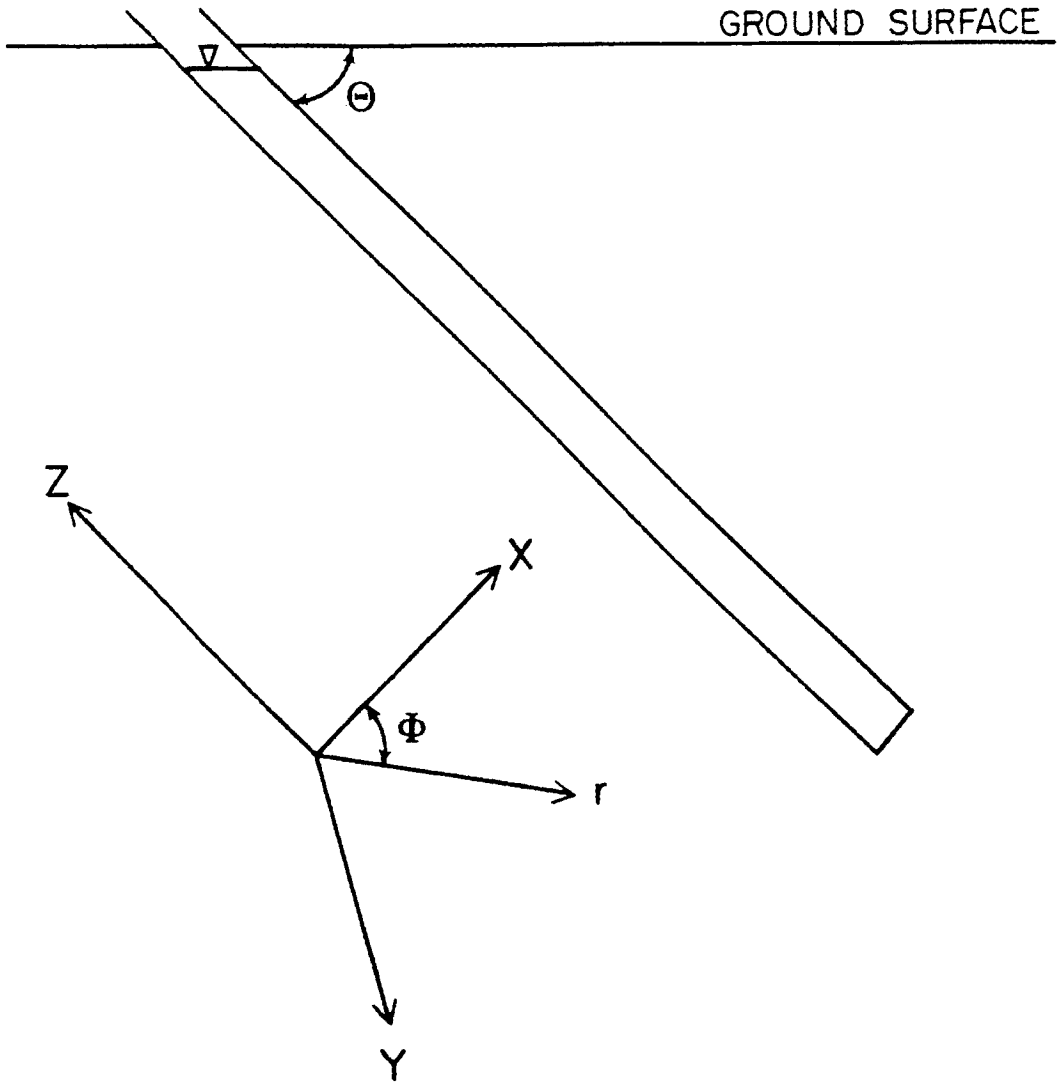

Figure 4.3. Orientation of the cylindrical coordinate system utilized in the derivation of the adapted Glover solution.

$$\int_0^P dP = -\frac{Q}{4\pi K}\int_\infty^R \frac{dR}{R^2}$$

$$P = \frac{Q}{4\pi K}\left(\frac{1}{R}\right)\Bigg|_\infty^R$$

$$(4.12) \qquad P = \frac{Q}{4\pi K}\left(\frac{1}{R}\right)$$

The pressure due to a source of strength Q at the point $r = 0$, $z = H^*$ along a cylindrical borehole of radius r is (Figure 4.4)

$$(4.13) \qquad P = \frac{Q}{4\pi K}\,\frac{1}{\sqrt{r^2 + (z - H^*)^2}}$$

Assume that the strength of the point source increases linearly with depth, so that the following represents the strength of an infinitesimal line segment

$$(4.14) \qquad dQ/dH^* = B(H - H^*)$$

where B is a constant of proportionality which will be defined later. Differentiating equation 4.13 with respect to Q and substituting equation 4.14 into the resulting expression results in

$$(4.15) \qquad dP = \frac{B(H - H^*)\, dH^*}{4\pi K\sqrt{r^2 + (z - H^*)^2}}$$

Equation 4.15 is integrated along the length of open borehole, L, so that

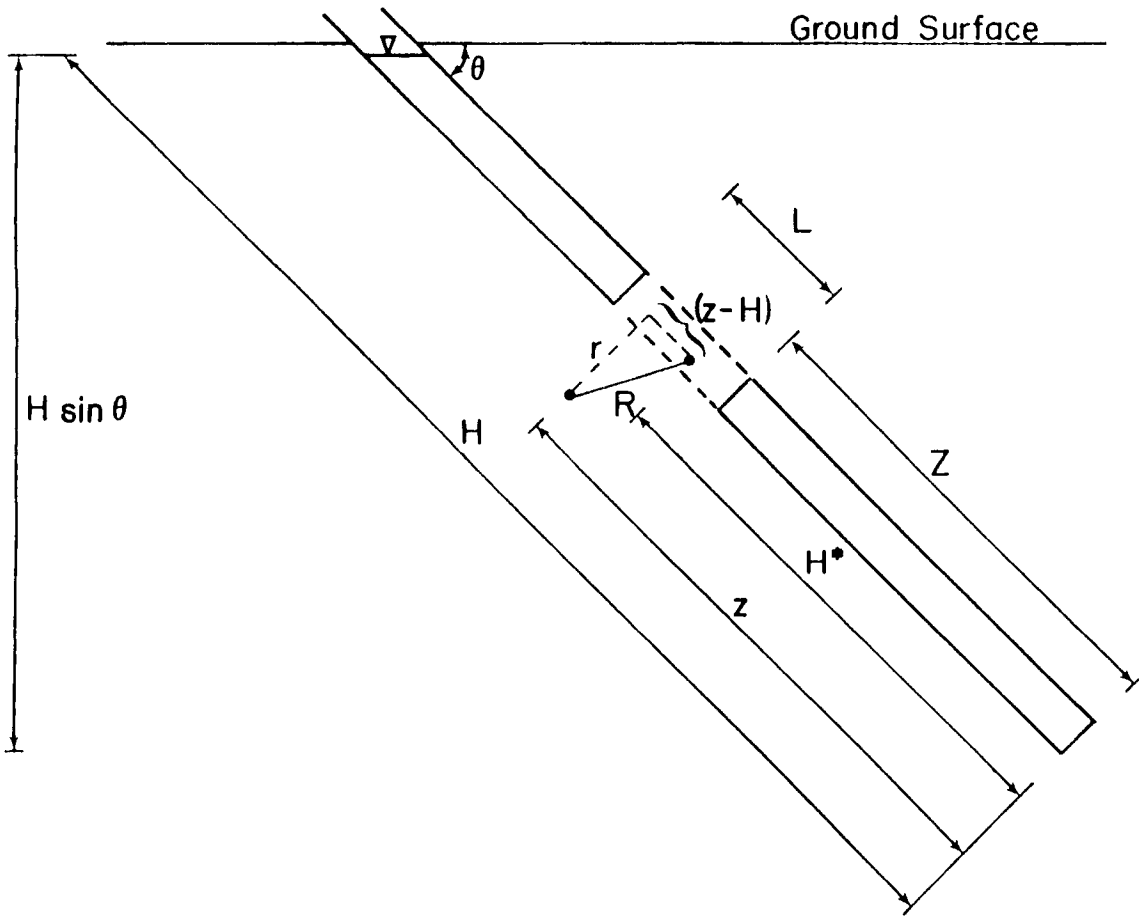

Figure 4.4. Schematic diagram of the borehole permeability test.

$$(4.16) \quad P = \frac{B}{4\pi K}\int_0^L \frac{(H - H^*)\, dH^*}{\sqrt{r^2 + (z - H^*)^2}}$$

If we allow $x = (H^* - z)$, then $H^* = (x + z)$ and $dH^* = dx$. Making the transformation of variables, equation 4.16 can be written as

$$P = \frac{B}{4\pi K}\left[H\int_{-z}^{L-z} \frac{dx}{\sqrt{r^2 + x^2}} - \int_{-z}^{L-z} \frac{(x + z)}{\sqrt{r^2 + x^2}}\, dx\right]$$

$$(4.17) \quad P = \frac{B}{4\pi K}\left[H\int_{-z}^{L-z} \frac{dx}{\sqrt{r^2 + x^2}} - \int_{-z}^{L-z} \frac{x\, dx}{\sqrt{r^2 + x^2}} - z\int_{-z}^{L-z} \frac{dx}{\sqrt{r^2 + x^2}}\right]$$

Integrating equation 4.17 gives

$$P = \frac{B}{4\pi K}\left[H \sinh^{-1}(x/r) - \sqrt{r^2 + x^2} - z \sinh^{-1}(x/r)\right]\Bigg|_{x = -z}^{x = L-z}$$

$$(4.18) \quad P = \frac{B}{4\pi K}\left[H \sinh^{-1}(L-z/r) - H \sinh^{-1}(-z/r) - \sqrt{(L - z)^2 + r^2} + \sqrt{z^2 + x^2} - z \sinh^{-1}(L-z/r) + z \sinh^{-1}(-z/r)\right]$$

Combining terms and recalling that $\sinh^{-1}(-x) = -\sinh^{-1}(x)$ results in equation 4.19

$$(4.19) \quad P = \frac{B}{4\pi K}\left[(H - z)\sinh^{-1}(L-z/r) + (H - z)\sinh^{-1}(z/r) - \sqrt{r^2 + (L - z)^2} + \sqrt{r^2 + x^2}\right]$$

Satisfying the constant head boundary condition at $r = r_w$, $z = 0$ where $P = H \sin \theta$

$$(4.20) \quad H \sin \theta = \frac{B}{4\pi K} \left[H \sinh^{-1}(L/r_w) - \sqrt{r_w^2 + L^2} + r_w\right]$$

If r_w is small, then equation 4.20 can be written approximately as

$$(4.21) \quad H \sin \theta = \frac{B}{4\pi K} \left[H \sinh^{-1}(L/r_w) - L\right]$$

Considering the total flow rate along the open length of the well bore, B can be solved as follows

$$(4.22) \quad Q = \int_{z}^{L+z} dQ$$

Where Z is the length measured from the bottom of the borehole to the bottom of the test interval. The limits of integration consider the location of the test interval relative to the bottom of the borehole because source strength increases with depth as a direct result of the increase in pressure head.

$$Q = \int_{Z}^{L+Z} B(H - H^*)dH^*$$

$$Q = BHH^*\Big|_{H^*=Z}^{H^*=L+Z} - \frac{BH^{*2}}{2}\Big|_{H^*=Z}^{H^*=L+Z}$$

$$Q = BHL - BZL - \frac{BL^2}{2}$$

$$(4.23) \quad B = \frac{2Q}{2HL - 2LZ - L^2}$$

Substituting B into equation 4.21 and dividing through by H yields:

$$(4.24) \quad \sin \theta = \frac{Q}{2\pi K(2HL - 2LZ - L^2)} \quad [\sinh^{-1}(L/r_w) - (L/H)]$$

Solving for Q, Equation 4.24 becomes

$$(4.25) \quad Q = \frac{2\pi K\ (2HL - 2LZ - L^2) \sin \theta}{\sinh^{-1}(L/r_w) - (L/H)}$$

Note that in equation 4.25 the total flow rate out of any particular section of borehole is dependent on the section's location and length, the total hydraulic head on the system and the inclination and geometry of the borehole. Finally, solving for K yields

$$(4.26) \quad K = \frac{Q\ \sinh^{-1}(L/r_w) - (L/H)}{2\pi\ (2HL - 2LZ - L^2) \sin \theta}$$

However, when the borehole is oriented in a horizontal position, the outflow as measured in equation 4.25 goes to zero, thus an alternative solution is necessary. Following the same basic derivation, on can easily adapt the Glover solution to cases involving horizontal boreholes by simply realizing that the source strength will not increase as one moves along the length of the borehole. For cases involving horizontal boreholes, equation 4.14 becomes

$$(4.27) \quad dQ/dH^* = B$$

Substituting this into equation 4.16 gives

$$(4.28) \quad dP = \frac{B}{4\pi K} \int_0^L \frac{dH^*}{\sqrt{r^2 + (z - H^*)^2}}$$

Making the transformation of variables as before results in

$$(4.29) \quad dP = \frac{B}{4\pi K} \int_{-z}^{L-z} \frac{dx}{\sqrt{r^2 + x^2}}$$

Integration of equation 4.29 yields

$$(4.30) \quad P = \frac{B}{4\pi K} [\sinh^{-1}(L-z/r) - \sinh^{-1}(L/r)]$$

Applying the boundary condition at $r = r_w$, $z = 0$, where $P = H$

$$(4.31) \quad H = \frac{B}{4\pi K} [\sinh^{-1}(L/r_w)]$$

Recalling that it is not necessary to consider the location of the open length of borehole in the limits of integration, the constant B can be solved as follows

$$Q = \int_0^L dQ$$

$$Q = \int_0^L B \, dH^*$$

$$(4.32) \quad B = Q / L$$

Substituting this expression into equation 4.31 and solving for K yields the solution for horizontal boreholes.

$$(4.33) \quad K = \frac{Q \sinh^{-1}(L/r_w)}{4\pi HL}$$

It is now possible to determine the equivalent saturated hydraulic conductivity from boreholes oriented in any fashion. The analytical solution in equation 4.33 is applicable to cases in which the borehole is oriented horizontally while the solution in equation 4.26 fits cases in which $0^\circ < \theta < 90^\circ$. A point worth mentioning is that equation 4.26 is prone to a small degree of error when θ gets very near 0°. The error is associated with the difference in the orientation of the water surface within the borehole relative to that assumed in the derivation of the solution (Figure 4.5). In the derivation of equation 4.26, the water surface is assumed to be oriented in a position normal to the axis of the borehole, where in actuality the water surface will position itself normal to the gravitational gradient. Because the orientation of the two surfaces differ, a portion of the borehole is left empty. The analytical solution does not take the void area into consideration and thus assumes a larger surface area over which outflow is to occur than that which exists in the true field test. However, error of this nature is avoided when using packers, because the packers maintain fully saturated conditions at all times within the test interval. Therefore, error of this nature will not effect the accuracy of the estimated conductivity values in this investigation.

4.4 DERIVATION OF THE ADAPTED PHILIP SOLUTION

In addition to the adapted Glover solution, an alternative solution for estimating the equivalent saturated hydraulic conductivity from permeability tests conducted in slanting boreholes is developed for the sake of comparison. The alternate solution is developed from the

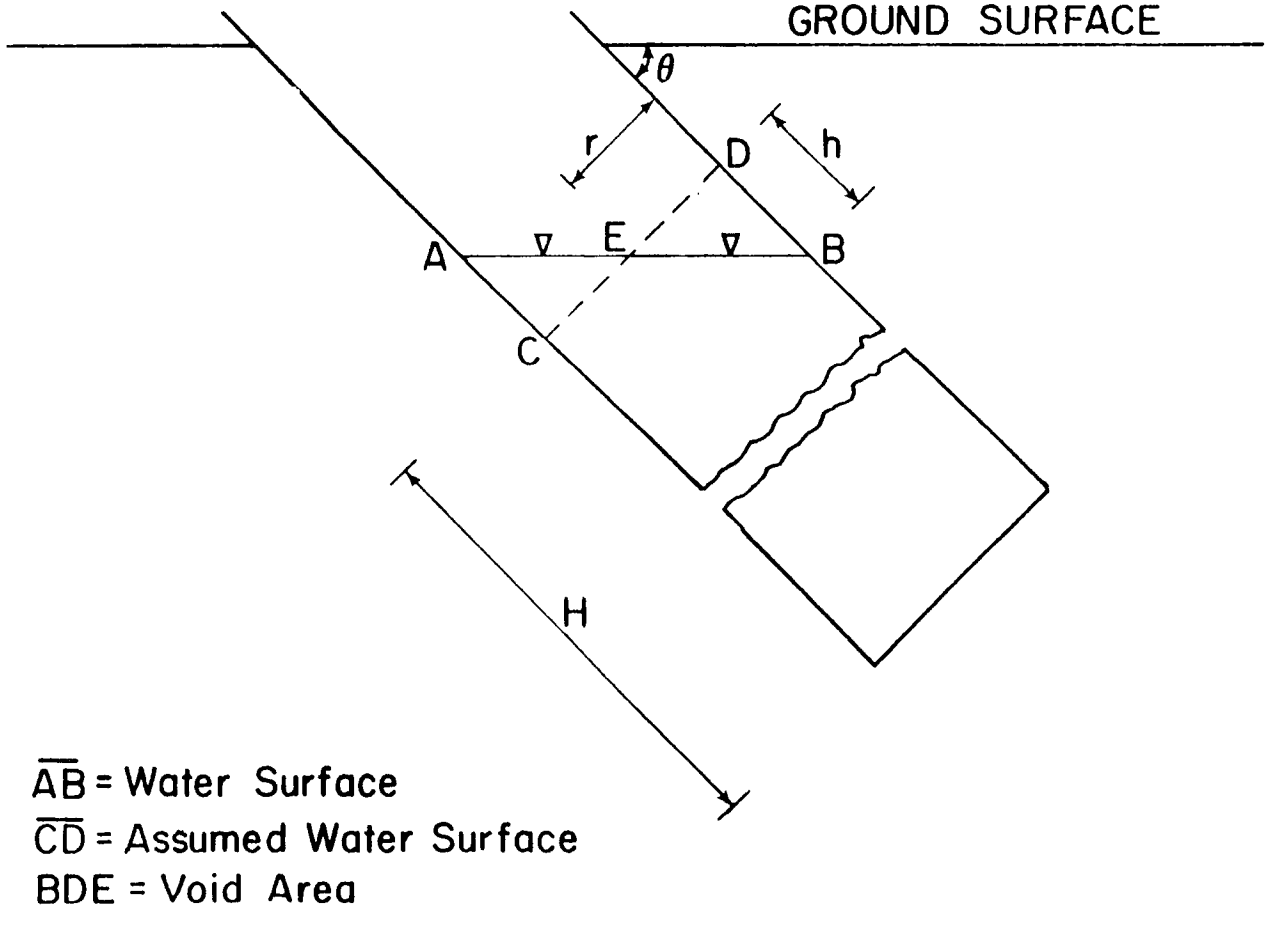

Figure 4.5. Sketch depicting the difference between the true water surface orientation and that assumed in the derivation of the adapted solutions.

analysis of Carslaw and Jaeger (1959 pg. 427) for heat flow from an ellipsoid of conductivity K', situated within a media of conductivity K. Philip (1985) recognized that the Carslaw and Jaeger solution was applicable to borehole permeability tests by replacing the borehole with the lower half of a spheroid of equal volume and of the same axial ratio as the water filled length of the borehole (Figure 4.6). By making this substitution, Philip was able to develop a solution with which to estimate the hydraulic conductivity from vertical borehole permeability tests. The derivation of the adapted Philip solution is initiated by replacing the borehole of interest by a prolate spheroid. A prolate spheroid (i.e., an ellipsoid in which there is one long axis and two smaller axes which are equal in length) is chosen to replace the borehole due to the similarities between their basic geometries. In order for the half spheroid to have the same volume and axial ratio as that of the borehole, the major semiaxis of the spheroid must equal $(3/2)^{1/3}c$ while the minor semiaxis becomes $(3/2)^{1/3}a$. The cartesian coordinate system on which the derivation is based is oriented parallel to the major semiaxis of the half spheroid (Figure 4.7).

Recall that the equation for an ellipsoid is

$$\frac{x^2}{a^2} + \frac{y^2}{b^2} + \frac{z^2}{c^2} = 1 \qquad (4.34)$$

From equation 4.34, the radius of the half spheroid may be determined at different locations along the length of its major semiaxis. For a prolate spheroid, b = a

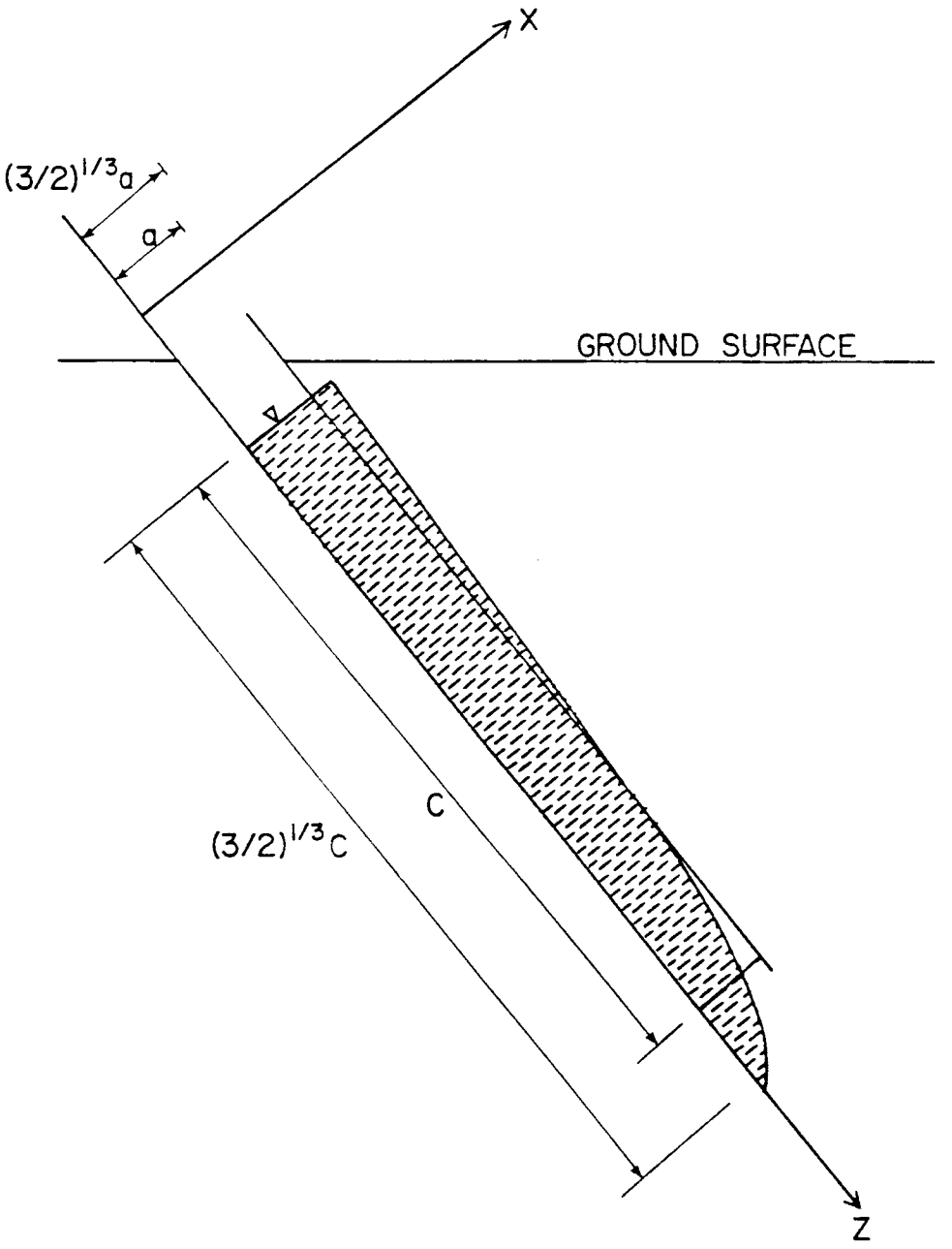

Figure 4.6. Replacement of borehole with a half spheroid.

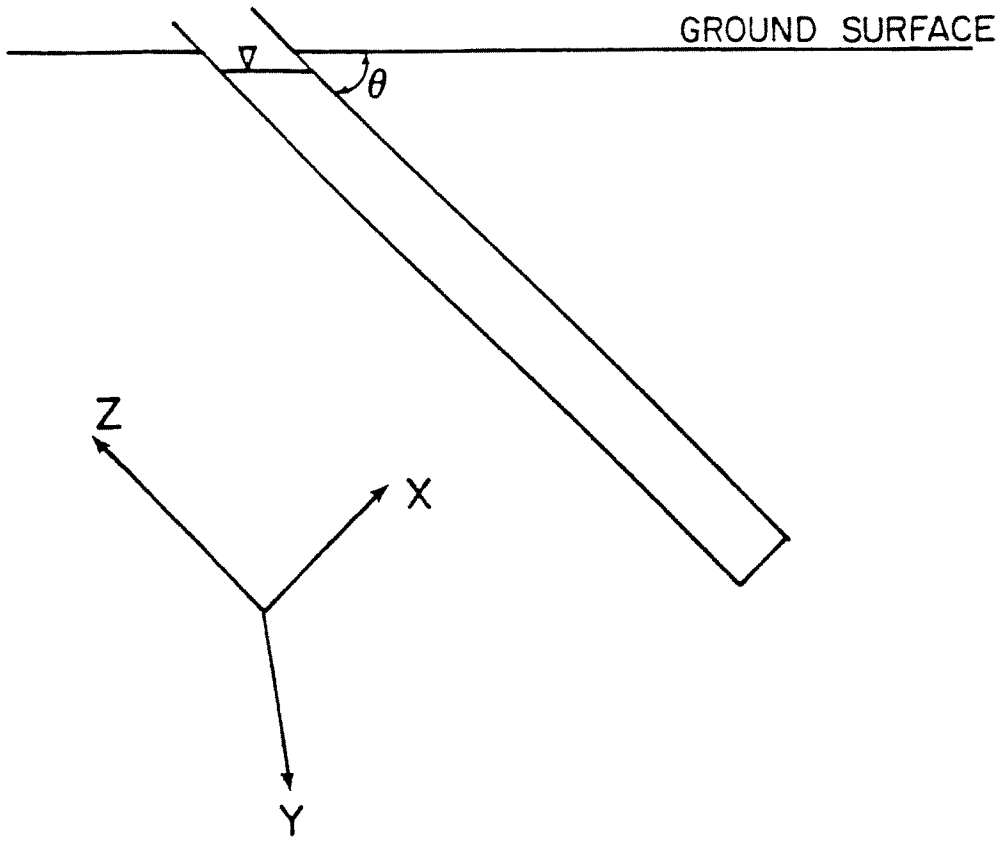

Figure 4.7. Orientation of the cartesian coordinate system utilized in the derivation of the adapted Philip solution.

$$\frac{x^2}{a^2} + \frac{y^2}{a^2} + \frac{z^2}{c^2} = 1$$

(4.35) $$x^2 + y^2 = a^2 \left[1 - (z^2/c^2)\right]$$

Since $r^2 = x^2 + y^2$, equation 4.35 becomes

(4.36) $$r^2 = a^2 \left[1 - (z^2/c^2)\right]$$

The parameters a, c and z must be corrected so as to reflect the lengths of the axes of the half spheroid rather than that of the borehole.

(4.37) $$r^2 = (3/2)^{2/3}\, a^2 \left[1 - (z^2/c^2)\right]$$

Where r is the radius of the spheroid in the xy plane at the location of interest, a is the radius of the borehole, z is the location of the point at which the radius is of interest as measured from the top of the half spheroid, and c is the water filled length of borehole. The need for an expression defining the radius of the half spheroid at different locations along the z axis will become apparent later.

Consider the fact that the potential at large distances from the half spheroid tends to the value

(4.38) $$H = x\frac{dH_x}{dx} + y\frac{dH_y}{dy} + z\frac{dH_z}{dz}$$

Within the saturated region surrounding the half spheroid, the gradient at a great distance from the spheroid is due only to gravitational forces. Therefore, the gradient is equal to unity and directed in a

vertical direction. For the case of an inclined borehole, the gradient at great distance is

$$\begin{aligned} dH_x / dx &= \cos \theta \\ dH_y / dy &= 0 \\ dH_z / dz &= \sin \theta \end{aligned} \tag{4.39}$$

Now considering the effect of the source, from Carslaw and Jaeger the potential inside, H_i, and outside, H_o, the spheroid is

$$H_i = \frac{x\, dH_x/dx}{1 + Ao(\alpha - 1)} + \frac{y\, dH_y/dy}{1 + B_o(\alpha - 1)} + \frac{z\, dH_z/dz}{1 + C_o(\alpha - 1)} \tag{4.40}$$

$$H_o = x\frac{dH_x}{dx} + y\frac{dH_y}{dy} + z\frac{dH_z}{dz} - \frac{(\alpha - 1)\, dH_x/dx\, A_\lambda x}{1 + A_o(\alpha - 1)} \frac{(\alpha - 1)\, dH_y/dy\, B_\lambda y}{1 + B_o(\alpha - 1)} - \frac{(\alpha - 1)\, dH_z/dz\, C_\lambda z}{1 + C_o(\alpha - 1)} \tag{4.41}$$

wnere $\alpha = K'/K$ and λ is the positive root of

$$\frac{x^2}{a^2 + \lambda} + \frac{y^2}{b^2 + \lambda} + \frac{z^2}{c^2 + \lambda} = 1 \tag{4.42}$$

For the particular case of a prolate spheroid where $c > a = b$

$$C_\lambda = \frac{(1 - e^2)}{e^3} \left\{ \frac{1}{2} \ln \frac{1 + e'}{1 - e'} - e' \right\} \tag{4.43}$$

$$A_\lambda = B_\lambda = \frac{(1 - e^2)}{2e^3} \left\{ \frac{e'}{1 - e'^2} - \frac{1}{2} \ln \frac{1 + e'}{1 - e'} \right\} \tag{4.44}$$

Where $e' = [(c^2 - a^2) / (c^2 + \lambda)]^{1/2}$

e' being the eccentricity of the confocal ellipse through the external point considered. To evaluate e, λ is simply set equal to zero. Similarly A_0, B_0 and C_0 are computed from A_λ, B_λ and C_λ by setting e' equal to e. In reality c and a should be replaced by the lengths of the semiaxes of the half spheroid, however, because both are a product of the same constant, $(3/2)^{1/3}$, the constant will cancel when introduced into the equation for the eccentricity.

Substituting the expressions for the gradient at a great distance, equation 4.39, into equation 4.40 yields the potential at any point inside the spheroid.

$$(4.45) \quad H_i = \frac{x \cos \theta}{1 + A_0(\alpha - 1)} + \frac{z \sin \theta}{1 + C_0(\alpha - 1)}$$

Taking the partial derivative of equation 4.45 with respect to each of the coordinate axis yields the gradient inside the spheroid

$$(4.46) \quad H_i = \frac{\cos \theta}{1 + A_0(\alpha - 1)} + \frac{\sin \theta}{1 + C_0(\alpha - 1)}$$

Knowing the gradient and outflow rate from the borehole, one can estimate the equivalent saturated hydraulic conductivity by use of Darcy's law

$$(4.47) \quad Q = K' A \nabla H_i$$

Where Q is the flow rate, K' is the hydraulic conductivity inside the spheroid, A is the area normal to the outflow, and ∇H is defined in

equation 4.46. Due to continuity considerations, the total flux leaving the spheroid is equal to that which is entering the spheroid. The flow entering the half spheroid is replenished via the circular cross-sectional area at the top of the ellipsoid. Equation 4.47 can be recast in a fashion so as to consider the flow crossing the top of the half spheroid;

$$(4.48) \quad Q = K'\pi r^2 \, dH/dz$$

where the flow rate is the same as that which is monitored in the field. Recall from Chapter 3, that the outflow rate from the borehole is considered equal to the flow rate through the packer, or in other words, the flow rate moving down the long axis of the borehole. Note also that the flow produced by the gradient in the y direction is implicitly considered in equation 4.48. For this reason, the gradient in the y direction may be neglected. Substituting the gradient in the z direction, the second term in equation 4.46, into equation 4.48 yields

$$(4.49) \quad Q = K'\pi r^2 \quad \frac{\sin \theta}{1 + C_0(\alpha - 1)}$$

Substituting in the term for α yields

$$(4.50) \quad Q = K'\pi r^2 \quad \frac{\sin \theta}{1 + C_0(K' + K \,/\, K)}$$

Multiplying by K'/ K' gives

$$(4.51) \quad Q = \pi r^2 \frac{\sin \theta}{\frac{1}{K'} + \frac{C_o}{K} - \frac{C_o}{K'}}$$

Because the permeability within the borehole is large (i.e., allow K' to approach infinity) and C_o never exceeds 1 for the range over which the eccentricity may exist, equation 4.51 becomes

$$(4.52) \quad Q = K\pi r^2 \, (\sin \theta / C_o)$$

For the case where θ is set equal to 90°, equation 4.52 will match that given by Philip. However in Philip's derivation two mistakes are made. The reason that Philip's solution matches the solution given in equation 4.52 is because the effects of the two mistakes tend to cancel each other.

Philip's first mistake is made when he claims that the constant heat flux density inside the spheroid, as taken from Carslaw and Jaeger, is

$$(4.53) \quad \frac{K'}{K + C_o(K' - K)}$$

He allows K' to approach infinity which yields

$$(4.54) \quad 1 / C_o$$

However in reality equation 4.53 is

$$(4.55) \qquad \frac{K}{K + C_o(K' - K)}$$

Philip also makes the mistake of assuming the flow across the equatorial plane of the spheroid is a function of the hydraulic conductivity outside the spheroid, as shown in equation 44 of his paper.

$$(4.56) \qquad Q = \pi r^2 K \, dH/dz$$

where $dh/dz = 1/C_o$

$$(4.57) \qquad Q = \pi r^2 \, K \, / \, C_o$$

Equation 4.57 being the same as that given in equation 4.52.

For the case of single-hole packer tests, the conductivity is measured over intervals shorter than the length of the borehole. To adapt the solution in equation 4.52 for packer test analysis, the solution must be modified to consider the length of the test interval and its location along the length of the spheroid. Noting that the outflow over any test interval is equal to the difference in the flux, oriented down the borehole, at the top and bottom of the test interval (Figure 4.8), or

$$(4.58) \qquad \Delta Q = Q_1 - Q_2$$

Substituting equation 4.52 into equation 4.58 yields

$$(4.59) \qquad \Delta Q = \frac{\pi K \sin \theta \, (r_1^2 - r_2^2)}{C_o}$$

Substitution in the expression for the radius, equation 4.37, yields

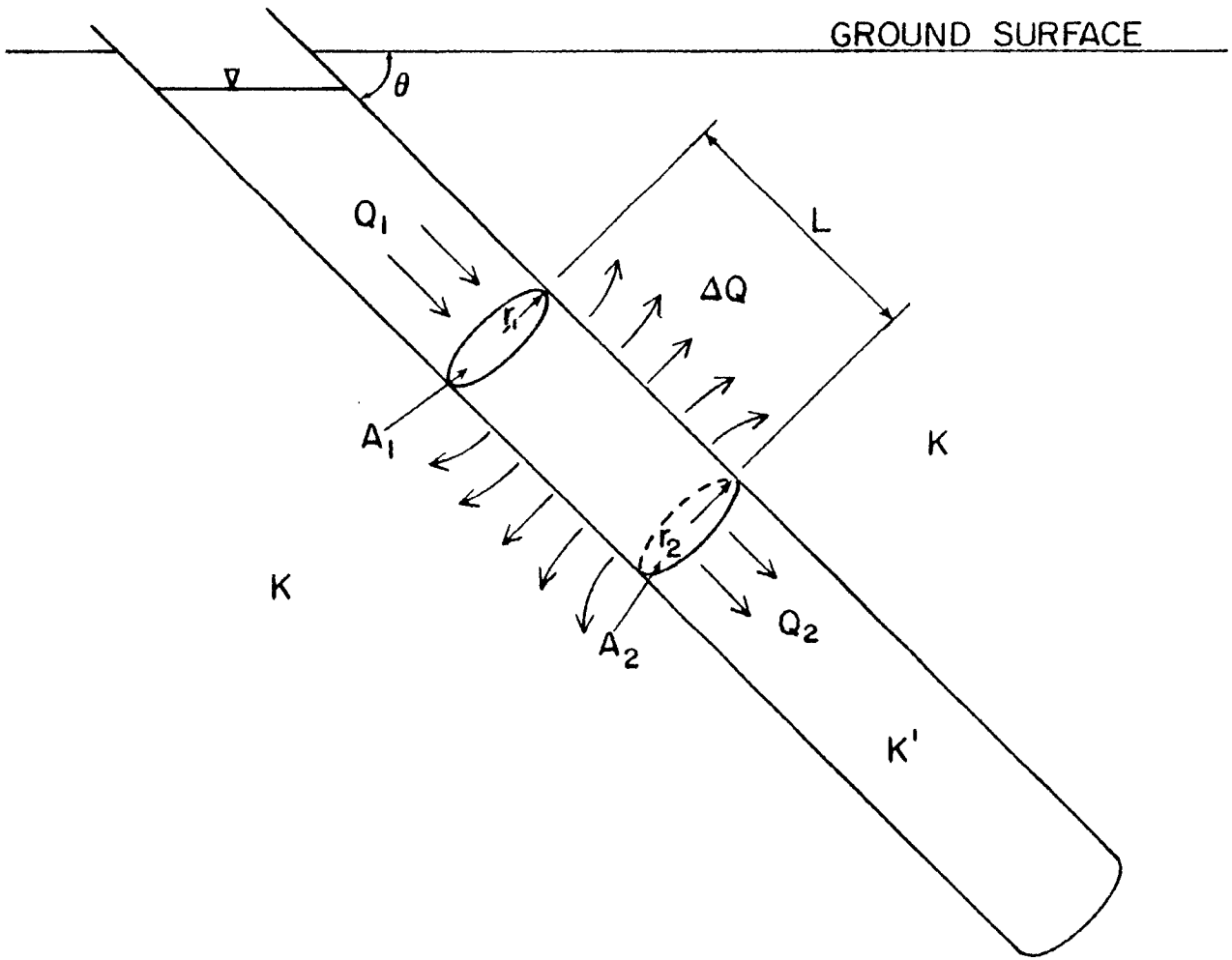

Figure 4.8. Schematic diagram depicting the interval outflow rate as applied in the adapted Philip solution.

$$(4.60) \quad \Delta Q = \frac{\pi K \sin \theta \, (3/2)^{2/3} a^2 \, (z_2^2 - z_1^2)}{C_o \, c^2}$$

Solving for K gives

$$(4.61) \quad K = \frac{c^2 \, \Delta Q \, C_o}{(3/2)^{2/3} a^2 \, \pi \sin \theta \, (z_2^2 - z_1^2)}$$

Equation 4.61 provides an estimate of the equivalent saturated hydraulic conductivity using data from single-hole packer tests conducted in slanting boreholes. The conductivity is shown to be a function of the outflow rate, the pressure head on the system, the geometry and inclination of the borehole, and the length and location of the test interval.

A point worthy of consideration is the method by which the increase in pressure head with depth is treated. The fact is considered by allowing the strength of the source to increase with depth. The strength of the source is increased by reducing the cross-sectional area over which the outflow occurs. As is indicated in equation 4.60 and 4.61, it is the difference in the radius at the top and bottom of the test interval which is of importance. Figure 4.9 shows the rate of change of the radius with a change in location along the z axis of the half spheroid. The gradient, on the other hand, remains constant throughout the borehole, as is indicated by equation 4.46. It is evident that this solution considers both the elevation and pressure head acting on the system. The elevation head being considered as the gradient at a great distance, and the pressure head considered through

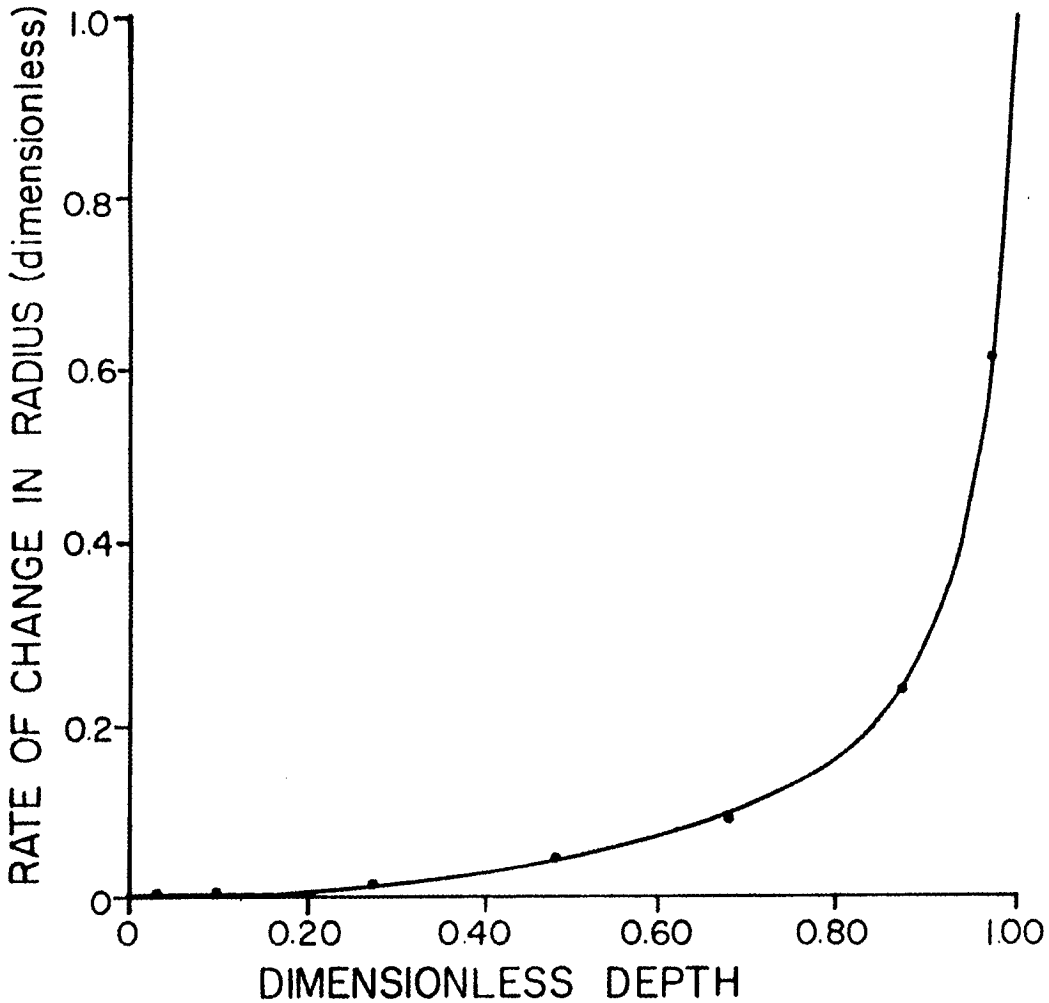

Figure 4.9. Dimensionless rate of change in radius with dimensionless depth along the major semiaxis of a prolate spheroid.

the increase in source strength along the length of the borehole.

To develop the potential field as generated by the source, both equations 4.40 and 4.41 must be consulted. Equation 4.40 provides the potential at any point inside the spheroid, while equation 4.41 yields the potential at any point outside the source.

As with the adapted Glover solution, when the spheroid is in a horizontal position the gradient is zero. Unfortunately the Philip solution cannot easily be adapted so as to describe outflow from a horizontal borehole. The major problem being that the elliptical shape is not conducive to the analysis in a horizontal orientation, and there is no way in which to consider pressure flow from the borehole. As with the adapted Glover solution, the adapted Philip solution will suffer from error associated with differences in the orientation of the water surface within the borehole relative to that assumed in the derivation of the solution when θ approaches 0°. However, as before the error is alleviated when packers which maintain saturated conditions in the test interval are used. Therefore this error will not adversely effect the accuracy of the results obtained in this investigation.

4.5 VALIDITY OF MODELS

Now that two solutions have been developed with which to estimate the equivalent saturated hydraulic conductivity, the validity of each model must be assessed. In order to properly evaluate these solutions, consideration of the physical properties and assumptions on which the solutions are based is necessary. Of primary concern is the ability of the analytical solutions to emulate the associated flow field and the

consequences of neglecting capillary forces and assuming homogeneous, isotropic conditions within the investigated media. To assist in this matter, a dissertation by Stephens (1979), which compares analytical solutions for borehole permeability tests to results obtained by means of numerical simulation, will be consulted.

In actuality the adapted solutions are still very similar to their classical counterparts. In both cases the adapted solution is predicated on the same set of physical conditions and the same general assumptions as were used in the derivation of the original solution. In addition the modifications, which are made to allow for slanting boreholes and multiple test intervals, are consistent with the physical properties and assumptions made by the classical models as well. For this reason, the classical and adapted solutions are expected to behave in much the same fashion. Due to the similarity, the investigation preformed by Stephens will help shed light on the validity to the two modified models.

Stephens (1979) compared the Cornwell, Glover, and Nasberg-Terletskaya solutions to numerical simulations involving saturated flow with a free surface and saturated/unsaturated flow. The Philip solution was obviously not tested since it was not developed until after the publication of Stephens work. However, Philip compares his solution for flow within the saturated region surrounding the borehole with the work done by Stephens. Stephens bases his investigation on the comparison of the dimensionless quantities

$$(4.62) \quad C_u = Q / KrH$$

(4.63) $H_D = H / r$

The four analytical solutions for constant head borehole permeability tests conducted for deep water table conditions become

(4.64) $C_u = 2\pi H_D / \ln(H_D)$ (Cornwell)

(4.65) $C_u = 2\pi H_D / \sinh^{-1}(H_D) - 1$ (Glover)

(4.66) $C_u = 2.364\ H_D / \log(2H_D)$ (Nasberg-Terletskaya)

(4.67) $C_u = 4.117\ H_D / \ln(2\ H_D) - 1$ For $H_D >> 1$ (Philip)

Values for C_u are evaluated by each of the analytical solutions as well as by numerical simulation for a host of H_D values. Numerical simulations involving saturated flow with a free surface were preformed using a finite element computer program entitled FREESURF (Neuman and Witherspoon, 1970). A series of numerical simulations were also preformed for four soils of differing unsaturated hydraulic properties using the saturated/unsaturated computer models FLUMP (Neuman and Narasimhan, 1977) and TRUST (Narasimhan and Witherspoon, 1977).

Since both adapted solutions neglect capillary forces, Stephens simulations involving saturated flow with a free surface are of primary concern. Results obtained by the numerical simulations indicate that the Nasberg-Terletskaya solutions underestimates values for C_u by 5-10% of those predicated by FREESURF when $H_D > 50$, and by 25% or more when $H_D < 30$. Numerical simulations also indicate that the Cornwell and Glover solutions, as would be expected, do not differ significantly from each other, and they exceed those computed with FREESURF by 35-40% when $H_D > 50$ but approach the FREESURF results as H_D decreases. Stephens

concludes that the Nasberg-Terletskaya formula reflects FREESURF results closely for $H_D > 50$ because the formula accounts explicitly for the existence of a free surface. The Glover solution, on the other hand, fits FREESURF results when $H_D < 50$ because the increase in source strength with depth along the borehole is considered. Philip compared C_u values determined by means of his solution to those obtained by the Nasberg-Terletskaya and Glover solutions for equivalent H_D values. What he found was that his solution behaves in much the same manner as the Nasberg-Terletskaya solution.

Comparison of the analytical solutions with FREESURF basically relate how accurately each analytical solution solves the Laplace equation and the associated boundary condition. Assuming the Laplace equation accurately describes the flow field resulting from borehole permeability tests, then an exact solution would be expected to fall somewhere between the results obtained from the Glover and Philip solutions. However, for the sake of this investigation the Philip solution is expected to offer a more accurate estimate of the hydraulic conductivity than that predicted by the Glover solution. This assumption is predicated on similarities between C_u values obtained from the Philip solution and FREESURF for high H_D values. It is at this range of H_D values for which all data from the field site are collected. As a result, estimates of the equivalent saturated hydraulic conductivity evaluated by means of the adapted Philip solution will be adopted as the primary data set for analysis.

All four classical solutions and the subsequent adapted solutions are predicated on the Laplace equation and the associated boundary

conditions. However, the Laplace equation neglects the effects of capillary forces and assumes homogenous, isotropic conditions. The validity of these assumptions must be assessed in light of the conditions encountered when dealing with fractured, unsaturated media.

Unsaturated fracture flow is not envisioned as contributing significantly to the overall transport of water from flooded boreholes. This is in contrast to cases involving fine sands and other fine grained materials which, under steady-state conditions, are able to transport significant quantities of water through partially saturated pores. Under such conditions, Stephens recognized from computer simulations that saturated conditions do not extend from the borehole to a depth at which only gravitational forces drive the flow, but is confined to a bulb shaped area surrounding the borehole. It follows that a significant portion of the water emanating from the borehole is subsequently transported by means of capillary forces as it moves further from the borehole. On the other hand, fractures generally tend to desaturate quickly under slight negative pressures which, in turn, greatly reduces the hydraulic conductivity of the fracture.

Wang and Narasimhan (1985) studied the hydrologic mechanism governing fluid flow in a partially saturated, fractured, porous media. They found that in contrast to saturated conditions in which fluid moves rapidly along fractures, fractures will usually desaturate first during the drainage process, and the bulk of fluid flow will be through interconnected pores in the matrix. Fractures desaturate first due to their large size as compared to the size of the pores in the matrix. Within a partially drained fracture, the presence of a relatively

continuous air phase will produce an infinite resistance to liquid flow in the direction parallel to the fracture. Since fractures remain desaturated under most negative pressures, unsaturated flow occurs predominantly in the rock matrix crossing fracture surfaces only in areas in which residual water is held. Residual water being held by capillary forces in the regions around fracture contact area when the apertures are small.

It makes sense that the reverse of this process, known as rewetting will have the same effect in that the fracture will remain relatively dry until a pressure threshold, dependent on the fracture aperture, is exceeded. Therefore fractures will remain dry, except for isolated pockets of water associated with fracture contact areas, for all except a small range of very low negative pressures. This implies that capillary forces will have little effect on the flow field developed by borehole permeability tests conducted in fractured rock.

Saturated/unsaturated numerical analysis preformed by Stephens also suggests that capillary forces are minimal in cases involving soils in which conductivity drops off significantly with decreasing water content. One of the four soils used in the analysis was a coarse sand, which like fractured rock, desaturates quickly under relatively small suctions. Actually, coarse sand in most cases will have a higher propensity to resist desaturation than do fractures when subject to negative pressure. Stephens found only slight differences between unsaturated/saturated numerical simulation involving coarse sand and the FREESURF model. He also found that the saturated/unsaturated solutions include a free surface similar to that predicted in section 4.1. It is

concluded therefore, that neglecting capillary forces will not introduce significant error into the estimates of the equivalent saturated hydraulic conductivity.

The other assumption used in the development of the two analytical solutions is the treatment of the fractured media as homogeneous and isotropic. It is reasonable to treat each test interval as homogeneous and isotropic as long as the scope of the investigation is of a larger scale than the test interval, as is the case here. However, the analytical solutions assume that the media, in all directions to infinity, is homogeneous and isotropic. In other words, when calculating the equivalent saturated hydraulic conductivity for a particular test interval, the result is predicated on the assumption that the media outside the cylinder of rock surrounding the borehole test interval is the same as that found in the cylinder of rock associated with the test interval. This creates biasing of estimated conductivity values due to possible interference between neighboring test intervals. For the case of a highly permeable zone located next to one of low permeability — flow from the low permeable zone tends to cross the boundary to the neighboring zone which creates unrepresentatively high outflow rates in the low permeability zone. On the other hand, outflow rates measured in zones of high permeability will be reduced due to extraneous flow from neighboring low permeability zones. The primary means of interference in fractured media will be through intersecting fractures. Recall that an important factor governing network conductivity is the interconnectiveness of the fractures. Therefore, any estimate of the equivalent saturated

hydraulic conductivity for a particular test interval needs to consider the interaction between fractures cutting the test interval and those lying outside the test interval. For this reason, the interaction of the outflow along fractures cutting different test intervals is considered a measure of the interconnectiveness of the fractures and not a means of interference of the outflow.

CHAPTER FIVE

ANALYSIS OF DATA

The equivalent saturated hydraulic conductivity has been estimated by the aforementioned procedure for nine slanting boreholes at the Apache Leap test site. Field data were collected over a period of time beginning on June 16, 1987 and ending July 21, 1987. The field data were subsequently used to estimate the hydraulic conductivity through the application of the adapted Philip and Glover solutions, equations 4.26 and 4.61 respectively. A statistical analysis of the data has also been preformed to determine the reliability of the collected data and in turn the quality of the hydraulic conductivity estimates. Finally, the spatial distribution of the hydraulic conductivity was investigated to provide a better understanding of the conductivity characteristics of the tuff on a larger scale.

5.1 PRESENTATION OF FIELD DATA

Eighty-five test intervals, each with a length of approximately three meters, were monitored for associated outflow rates given a constant hydraulic head at the Apache Leap test site. The measured outflow rates are presented in Appendix B in units of m^3/sec while the associated constant hydraulic head under which each borehole was subjected during testing may be found in Appendix C. Measured outflow

rates span five orders of magnitude from 1.6×10^{-8} to a maximum of 1.2×10^{-3} (m^3/sec); however, all but three of the test intervals exhibit outflow rates below 2.6×10^{-5} m^3/sec. The measured interval outflow rates are positively skewed as displayed by a coefficient of skew of 5.98. As a result of the skewness of the distribution, the median value, 6.3×10^{-7} m^3/sec, provides the best indication of the average outflow rate since the median value lies closest to the peak associated with skewed distributions. The outflow data also exhibit a relatively significant degree of variability about the mean. Supportive of this fact is the coefficient of variation associated with the data which was measured to be 2.09.

Of special interest are two test intervals which exhibit outflow rates which are two orders of magnitude greater than that found in all but one other test interval which is located 9.34 m from the lip of the casing in borehole Z1. As a result of their disproportionate size, these two outflow rates are neglected when evaluating the statistical properties of the data. The reason being that by neglecting these outflow rates, statistical properties are obtained which are more representative of the majority of the data. The core logs associated with these zones indicate the presence of only a single major fracture in each. In fact, due to the location and orientation of the fractures, it is possible that this is actually a single fracture cutting both boreholes.

Total borehole outflow rates, as measured along the entire length of borehole, also exhibit a large degree of variability. Total outflow rates range from 6.1×10^{-7} to a maximum of 1.2×10^{-3} (m^3/sec).

Measurements indicate that the Z series of boreholes have the overall largest outflow rates while borehole X1 and Y1 yield the least outflow.

5.2 PRECISION AND SENSITIVITY OF THE FIELD TECHNIQUE

The ultimate value of the methodology presented in this investigation is basically dependent on the sensitivity and precision of the falling-head flowmeter and its associated field procedure. If stringent standards are not set to assure the collection of quality data, little reliability can be placed on the results obtained, or in this case, estimates of the equivalent saturated hydraulic conductivity. To assure the collection of quality data, field techniques must be able to detect subtle changes in outflow rates and yield similar results when tests are repeated. At this time the quality of the gathered field data will be investigated to determine the confidence with which hydraulic conductivity values may be estimated from these data.

As described in Chapter 3, six readings are taken at each test interval with the mean value being reported as the outflow rate associated with that interval. In most cases a slight degree of variability exists between the six measurements which indicates that some degree of error is inherent in the monitoring technique. This measurement error is blamed primarily on the lack of precise timing involved with monitoring the outflow rate. Recall that the outflow rate is determined by noting the time, by means of a hand held stopwatch, necessary for a specified volume of water to empty from one of the three falling-head flowmeter cylinders. By taking six readings, a means is provided with which to monitor the measurement error associated with the

data. The error is monitored by setting a confidence interval within which the sample mean, as determined from the six measurements at each test interval, must fall. The confidence interval is defined by means of the T distribution which requires knowledge of the sample mean and variance associated with the six outflow rate measurements. The T distribution is chosen due to its properties which allow the use of variances calculated from small samples. The confidence interval developed from the T distribution takes on the form

$$(5.1) \quad T\,S/\sqrt{n} < \bar{x} - E[x] < T\,S/\sqrt{n}$$

where $\bar{x}$ is the sample mean, E[x] is the expected mean, S is the sample standard deviation and n is the sample size. Equation 5.1 takes on the following form when a 95% confidence interval with 5 degrees of freedom is chosen

$$(5.2) \quad \bar{x}\beta = \pm 2.57\,S/\sqrt{n}$$

where β is the percent error between the expected and sample mean. For purposes of this investigation, the sample mean is required to be within 1% of the expected mean for a 95% confidence interval. If this criteria is not met, more measurements must be taken until an acceptable error is reached. However, six readings were found to be sufficient for all test intervals since the overall mean percent error associated with each sample was only 0.3% with only one sample having a percent error as high as 1%.

In order to fully assess the precision and sensitivity of this field technique, one must also determine how well the data repeats

itself when subjected to similar tests. Repeating of the data requires the reoccupation of a test interval at some time after its initial testing and the taking of six new measurements which are averaged to determine the outflow rate for the repeated interval. For tests repeated at the Apache Leap test site, differences were found to exist between the initial outflow rate measurements and the repeated measurements for the same test interval. The greatest difference being 1.8×10^{-7} m^3/sec while the average difference was only 6.3×10^{-8} m^3/sec. The differences are attributed to three factors: 1) difficulty in exact relocation of the packer, 2) inability to attain true steady-state flow conditions and 3) change in water temperature during testing.

Changing water volume as a result of variations in water temperature is not anticipated to have an appreciable influence on the precision of the field technique. The primary reason for this assumption is that water temperatures were maintained within a five degree range during testing. The change in water volume for temperature variations of this magnitude only amount to 0.15% of the measured water volume. This 0.15% degree of error is envisioned as being of an insignificant nature.

Exact repositioning of the packer, on the other hand, is critical to the collection of repeatable data. Positioning of the packer dictates the total open length of borehole, as well as, which fractures will intersect a particular test interval. Difficulties in positioning of the packer, in part, stem out of problems with accurately measuring the distance between the packer and the lip of the casing. Also, drag between the packer and the walls of the borehole prevent the packer from

moving freely within the borehole which makes positioning of the packer a tedious task.

Likewise, problems were encountered due to difficulties in reaching true steady-state outflow conditions with the flooded boreholes. Figure 3.4 indicates that outflow rates decreased exponentially for about the first two hours after flooding and thereafter reached a relatively constant outflow rate. However, for test intervals which were repeated at different times during the same day, the initial measured outflow rate was always slightly greater than the repeated measurement. This indicates that outflow rates did not reach a steady-state. Total borehole outflow rates were monitored for 22 days in boreholes X1, X2, Y1 and Y2 to determine, in part, the behavior of the outflow rate as the saturated region associated with the borehole increases. What was found was that the outflow rates, after the first couple of hours, decreased on the average of 7.02×10^{-3} m^3/day and was highly variable after this time. The initial sharp drop in outflow rate may be attributed to "wetting up" of the rock in close proximity to the borehole, while the continued slow decline in outflow rate is a result of lower hydraulic conductivity of the tuff on a larger scale. Since conditions well outside the vicinity of the borehole influence outflow rates very slowly, measurements taken relatively soon after the initial steep drop in the outflow rate will accurately represent steady-state saturated conditions near the borehole. However, the initial outflow rate is preferred over a repeated measurement for estimation of the hydraulic conductivity mainly out of convention since less time has elapsed for

conditions outside the vicinity of the borehole to influence the outflow rate.

Of primary importance to the quality of the estimated conductivity values, is the measured interval outflow rate which is the difference between the outflow rate measured at either end of the test interval. In order to evaluate the reliability of the interval outflow rate measurements, fourteen intervals were repeated during the period of time over which testing was preformed. These repeated intervals represent 16% of the total test intervals at the Apache Leap test site and sample flow rates ranging from 1.6×10^{-8} to 2.6×10^{-5} (m^3/sec). Analysis of the pairs of repeated interval outflow rates will ultimately provide a means with which to determine the precision and sensitivity of the field technique. The repeated interval outflow rates (Table 5.1) provide a set of data to determine a confidence interval in which the expected mean interval outflow rate will be confined. As in the previous case the T distribution is utilized which requires knowledge of the variance inherent in measuring the interval outflow rate. This variance is primarily a result of measurement error and difficulties in occupying an exact location in the borehole with the packer. The difference between repeated outflow rates provides a direct indication of this variance because the difference is independent of the outflow rate as shown in Figure 5.1. The variance inherent in measuring the interval outflow rate is determined from the variance, as calculated in equation 5.3, between the fourteen values representing the difference between repeated interval outflow rates.

$$(5.3) \quad S^2 = 1/n \, \Sigma \, (x_i - \bar{x})^2$$

Table 5.1. Compilation of repeated interval outflow rate data and associated error.

Borehole	Depth (m)	Initial Measurement (m^3/sec)	Repeated Measurement (m^3/sec)	Difference (m^3/sec)
X1	3.80	1.0×10^{-7}	8.3×10^{-8}	1.7×10^{-8}
X1	6.84	1.7×10^{-8}	1.7×10^{-8}	0
X2	3.81	1.5×10^{-6}	1.4×10^{-6}	1.8x10-7
X2	6.78	3.0×10^{-7}	2.5×10^{-7}	5.0×10^{-8}
X2	9.78	2.6×10^{-7}	2.6×10^{-7}	0
X2	12.78	2.1×10^{-6}	2.0×10^{-6}	8.3×10^{-8}
X2	15.78	1.8×10^{-6}	1.6×10^{-6}	1.5×10^{-7}
X2	18.78	9.6×10^{-7}	9.5×10^{-7}	1.7×10^{-8}
X2	21.78	1.6×10^{-6}	1.5×10^{-6}	1.0×10^{-7}
X2	24.78	2.8×10^{-7}	2.3×10^{-7}	5.0×10^{-8}
Z1	9.34	2.6×10^{-5}	2.6×10^{-5}	1.2×10^{-7}
Z2	21.83	6.6×10^{-6}	6.5×10^{-6}	5.0×10^{-8}
Z2	24.83	2.5×10^{-6}	2.4×10^{-6}	1.6×10^{-8}
Z2	27.55	1.1×10^{-6}	1.0×10^{-6}	6.6×10^{-8}
Mean				6.3×10^{-8}
Variance				1.7×10^{-10}

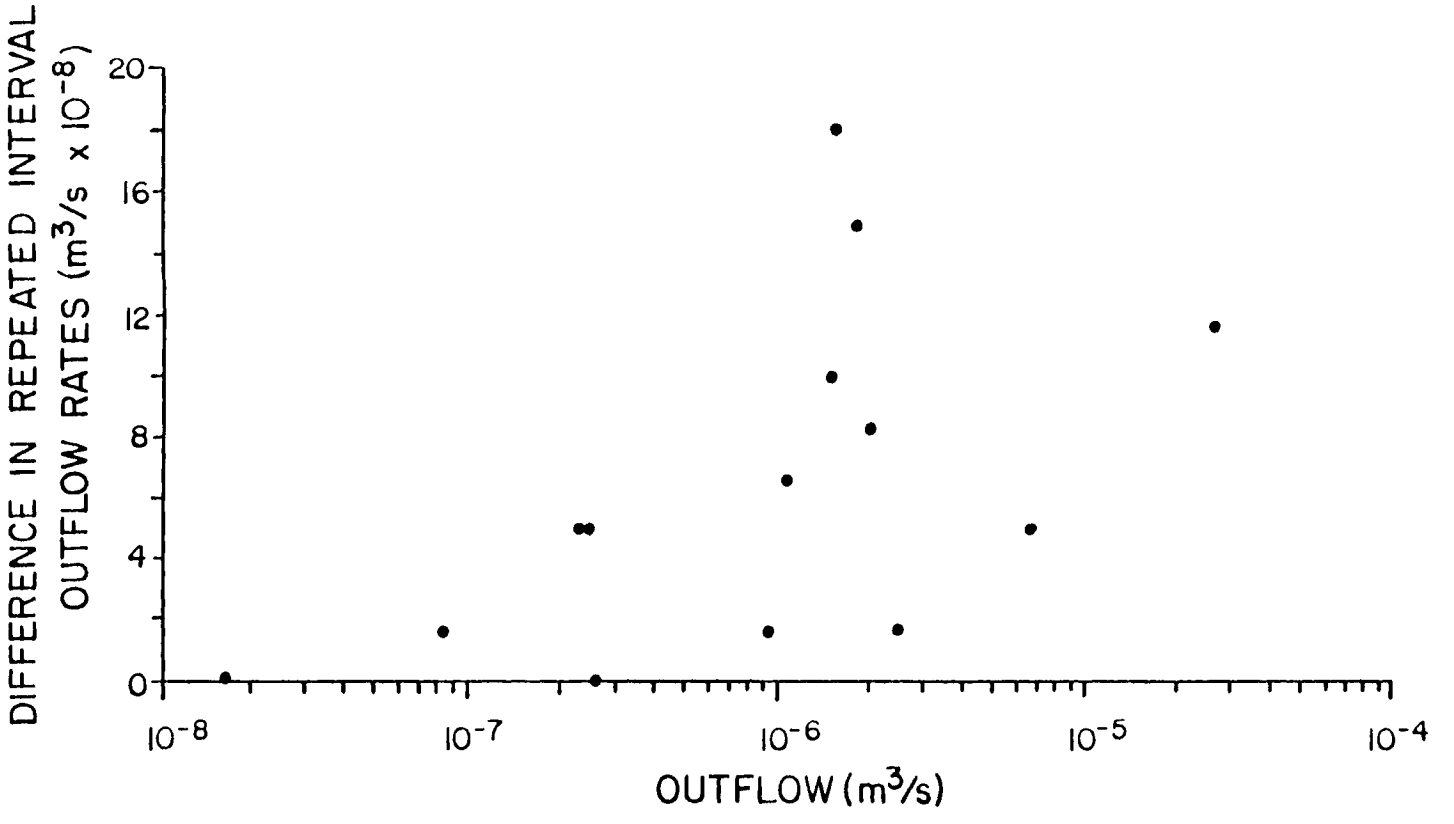

Figure 5.1. Error in repeated interval outflow rate against the associated outflow rate. Error is shown to be independent of the outflow rate.

where x_i represents the difference between each repeated pair of measurements. Equation 5.3 yields the variance associated with the error between repeated interval outflow rates to be $S^2 = 1.1x10^{-5}$. The variance computed in equation 5.3, represents the variance inherent in measuring both the initial and repeated interval outflow rate. However, it is the variance associated with measuring only a single interval outflow rate which is of interest. Recalling that the variance of two random variables is equal to the following

(5.4) $\mathrm{Var}[A + B] = \mathrm{Var}[A] + \mathrm{Var}[B] + 2\mathrm{Cov}[AB]$

The variance inherent in measuring the outflow rate is the same for both the initial measurement and repeated measurements since both are subject to the same likelihood that measurement error or inaccurate positioning to the packer may cause the measured outflow rate to be different from that in actuality. It follows that the interval outflow rate measured initially in no way effects measurements at a later time; therefore, the two measurements are independent and the covariance is zero. With these facts in mind equation 5.4 becomes

(5.5) $\mathrm{Var}[A] = (\mathrm{Var}[A] + \mathrm{Var}[B]) / 2$

From equation 5.5, the variance inherent in measuring the interval outflow rate is found to equal $S^2 = 5.3x10^{-6}$. Note that the variance calculated in equation 5.5 is the result, in part, of the lack of steady-state conditions. This non-equilibrium state creates a slight biasing of the variance. Due to the variable nature at which the outflow rate changes with time, it is not realistic to remove the bias

from the data. Therefore, the bias is neglected which provides a conservative estimate of the outflow rate, because the bias tends to increase the variance associated with the outflow measurements.

A confidence interval which predicts how well a measured interval outflow rate represents the actual outflow rate can now easily be defined with the variance known. Using the T distribution

(5.6) $\beta = \pm T\ S$

where β represents the error between the measured outflow rate and the actual outflow rate. Adopting a 95% confidence interval with 13 degrees of freedom, equation 5.6 becomes

(5.7) $\beta = \pm 2.16\ S$

From equation 5.7 and the variance calculated in equation 5.5, a confidence of 95% is placed on the fact that the measured interval outflow rate will be within $\pm 8.3 \times 10^{-8}$ m^3/sec of the actual outflow rate. With knowledge of the precision involved in measuring interval outflow rates, the precision of the estimated equivalent saturated hydraulic conductivity value may also be assessed. Both equation 4.26 and 4.61, the adapted Glover and Philip solutions respectively, may be represented as

(5.8) $K = Q \cdot D$

where D is a proportionality constant including all terms on the right side of each of the respective equations, except for the measured outflow rate. Since K is directly proportional to Q, the estimate of

the conductivity will likewise be directly affected by measurement error associated with the interval outflow rate. Therefore, the precision of the estimated conductivity values are directly proportional to the size of the measurement error, $\pm 8.3 \times 10^{-8}$ m^3/sec, as determined in equation 5.7, relative to the total outflow rate. In other words, estimates of the conductivity will suffer from a lower degree of precision at lower outflow rates, while being effected very little at higher outflow rates. Whether precision of this degree is acceptable or not must be determined on an individual investigation basis depending on the detail required. Sensitivity of the field technique, on the other hand, is relatively good. Data collected from the Apache Leap test site indicate that the field technique is capable of identifying differences in outflow rates spanning four orders of magnitude. However, due to the lack of precision at lower outflow rates only relative statements, as opposed to absolute, may be made concerning the variability of outflow rates in the lower range.

5.3 EVALUATION OF THE EQUIVALENT SATURATED HYDRAULIC CONDUCTIVITY AND ITS ASSOCIATED SPATIAL DISTRIBUTION

Estimation of the equivalent saturated hydraulic conductivity is made possible by equations 4.26 and 4.61, which are the adapted Glover and Philip solutions respectively. The estimated conductivity values may be found in Appendix B in units of m/sec along with their associated depth and outflow rates. As discussed in section 4.5 the Philip approach is expected to provide the most accurate estimate of the hydraulic conductivity. So for this reason only estimates made by the

adapted Philip solution will be utilized in characterizing the spatial variability of the hydraulic conductivity at the Apache Leap test site. Noting that the adapted Philip solution consistently yields results twice as large as that predicted by the adapted Glover solution, one would expect that the conductivity values estimated from the adapted Glover solution would follow similar trends concerning the spatial distribution of the hydraulic conductivity as that predicted by the adapted Philip solution, but with overall lower conductivity values.

Estimates of the equivalent saturated hydraulic conductivity behave in much the same fashion as the associated outflow rates. Conductivities values were found to span five orders of magnitude from 4.8×10^{-10} to 3.9×10^{-5} (m/sec) while the overall distribution remains positively skewed. As a result of the skewness of the distribution, the median value, 1.2×10^{-8} m/sec, is shifted well toward the lower range of conductivity values. Likewise, a relatively large coefficient of variation of 2.41 provides evidence that the conductivity values exhibit a reasonable degree of spread about the mean value. Once again the conductivities of the two "super" conducting zones have been neglected in the calculation of the sample statistics in order to obtain statistical properties which are most representative of the majority of the data.

Analysis of the data indicates that the hydraulic conductivity is very nearly log normally distributed (Figure 5.2). The data deviates from a log normal distribution only in the large conductivity range as a result of the two highly permeable zones. The log normal nature of the data is consistent with the fact that hydraulic conductivity

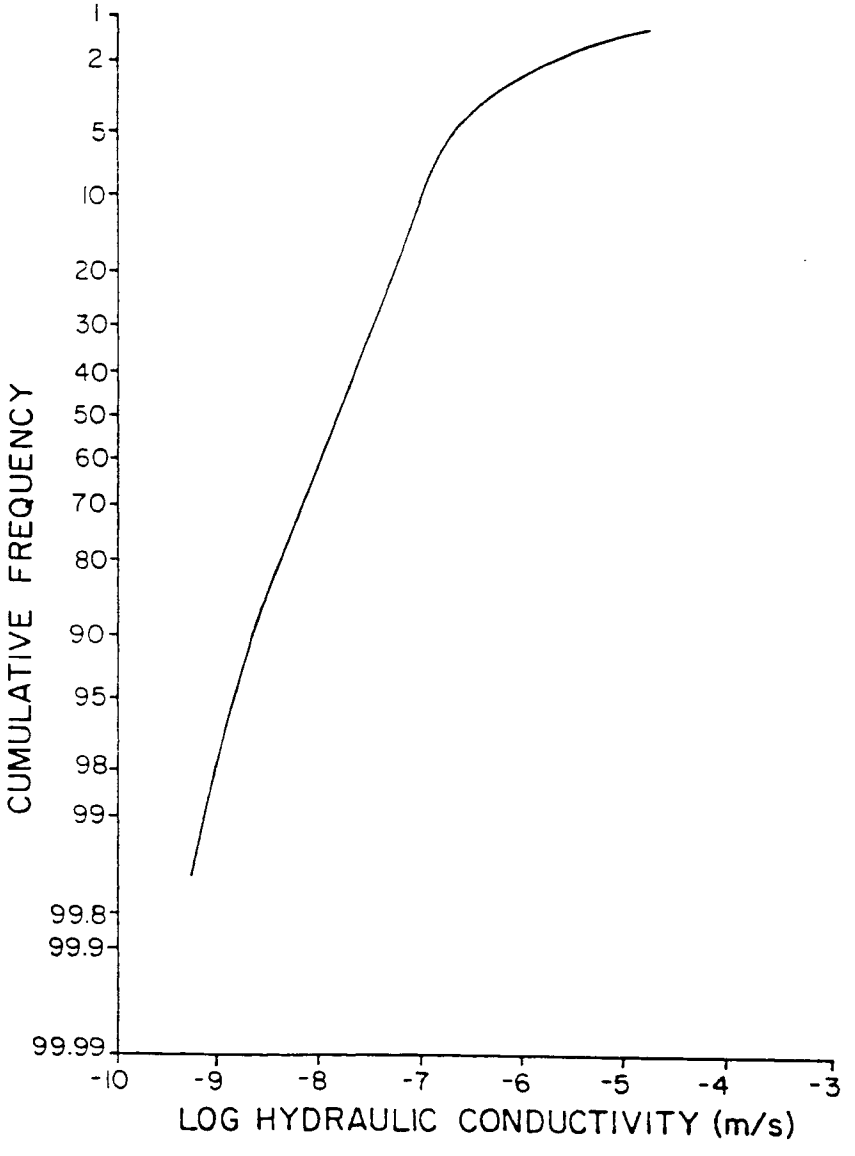

Figure 5.2. Cumulative frequency distribution of the log hydraulic conductivity.

distributions and fracture aperture distributions are generally characterized by a log normal behavior.

The hydraulic conductivity distribution as measured along each of the nine boreholes monitored at the Apache Leap test site is presented in Figures 5.3 - 5.5. The most notable feature of the graphs is the high degree of variability exhibited by the conductivity. In many cases conductivity values vary one to two orders of magnitude between adjacent test intervals. Likewise, conductivity values may vary in a single borehole from less than one to over three orders of magnitude. The overall hydraulic conductivity of the nine boreholes also display a great deal of variability. On the average the Z series of boreholes exhibit the largest conductivity values while X1 and Y1 exhibit the smallest.

In order to evaluate the spatial variability of the hydraulic conductivity at the Apache Leap test site, consideration is given to the behavior of the hydraulic conductivity in each of the principal coordinate directions. The principal coordinate directions being oriented parallel and normal to the strike of the boreholes and in the direction of depth.

Figures 5.6 - 5.8 have been developed to aid in the recognition of any trends which may exist between conductivity and depth. Conductivity is plotted on a logarithmic scale simply to facilitate graphing of the large range of conductivities which are encountered. Figure 5.6 presents the variation in conductivity with depth as measured in the block of tuff containing boreholes X1 and Y1, the bottom 18 m of boreholes X2 and Y2, and the bottom 18 m of boreholes X3 and Y3. The

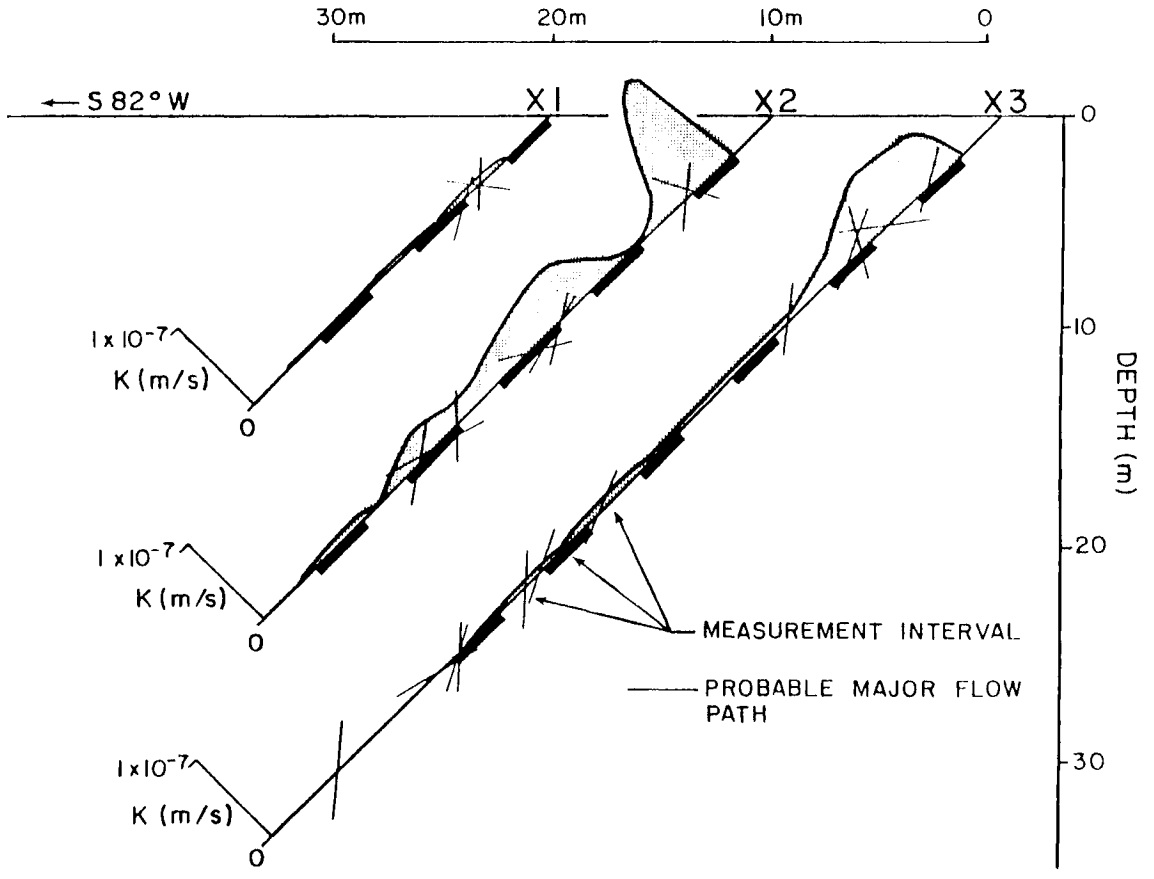

Figure 5.3. Equivalent saturated hydraulic conductivity distribution along the X series boreholes at the Apache Leap test site. Positions at which major probable flow paths cut the respective boreholes are also represented.

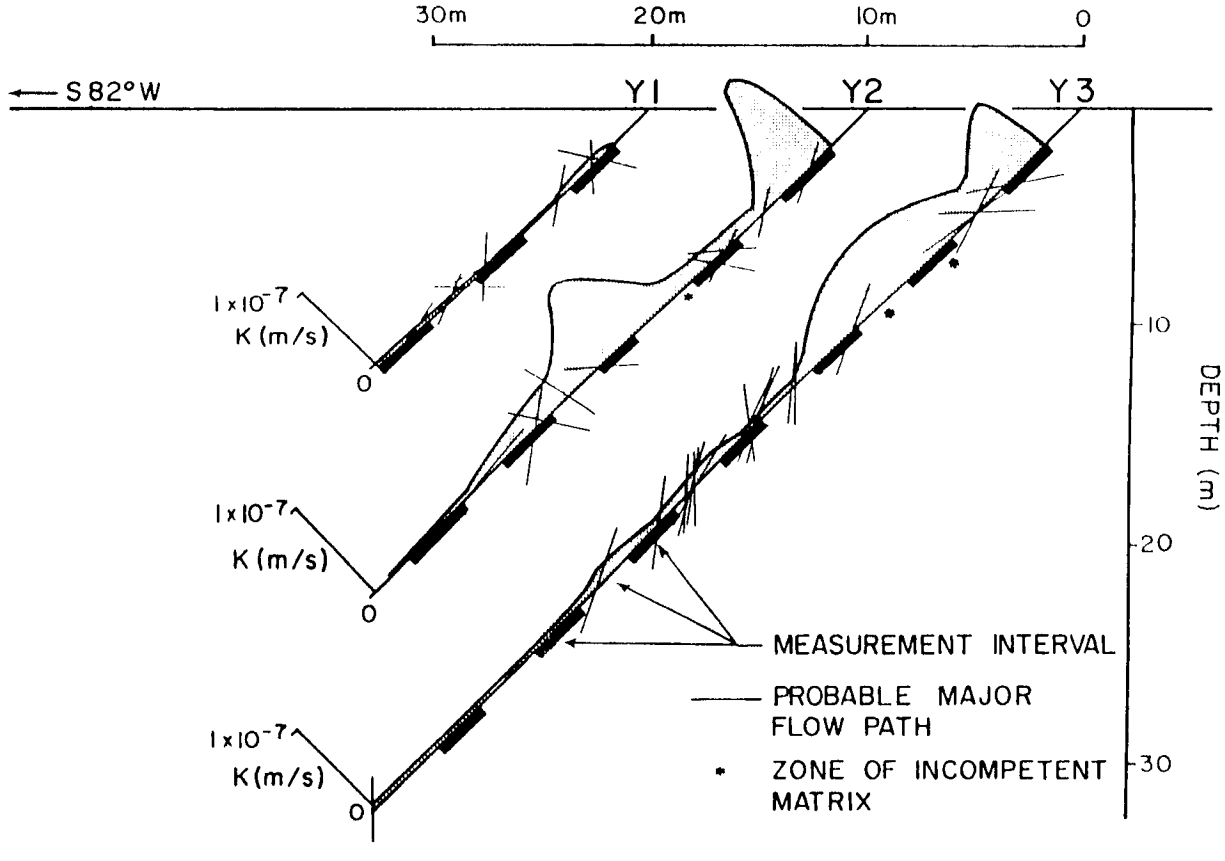

Figure 5.4. Equivalent saturated hydraulic conductivity distribution along the Y series boreholes at the Apache Leap test site. Positions at which major probable flow paths cut the respective boreholes are also represented.

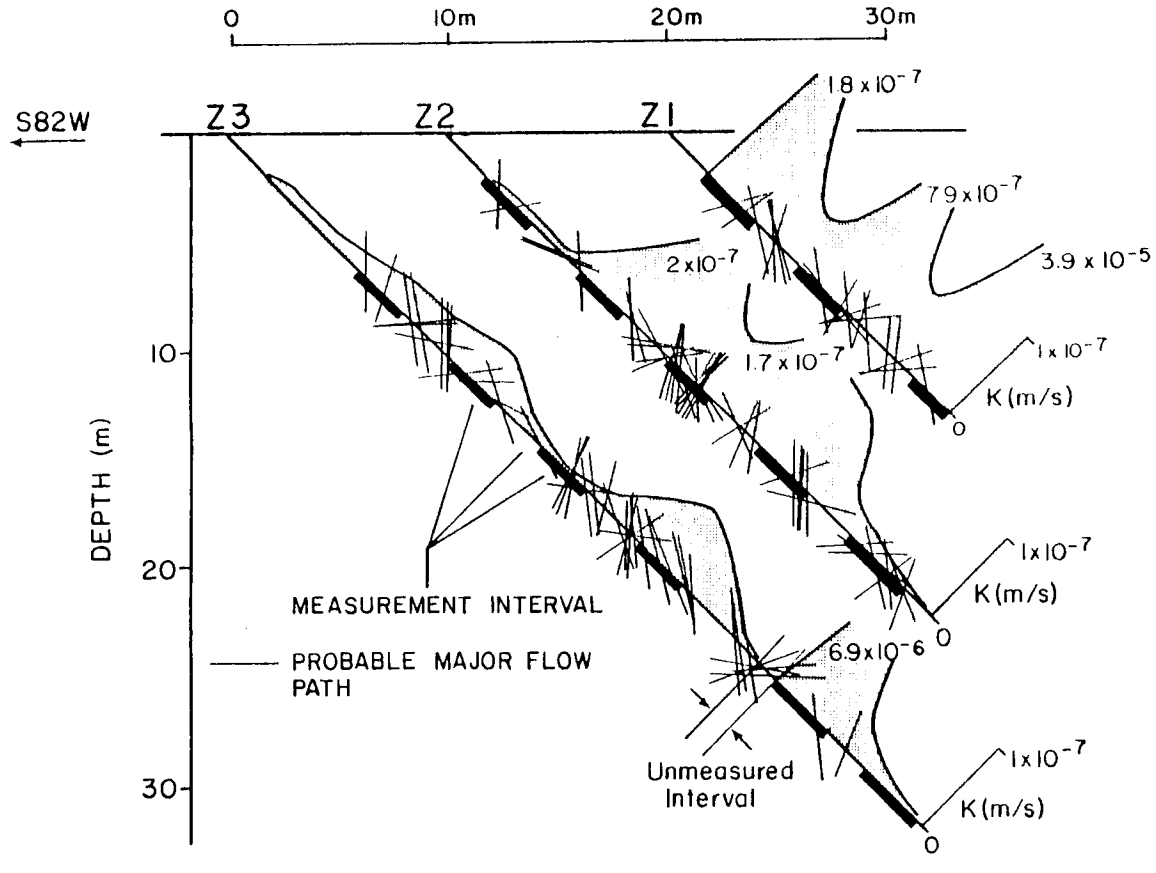

Figure 5.5. Equivalent saturated hydraulic conductivity distribution along the Z series boreholes at the Apache Leap test site. Positions at which major probable flow paths cut the respective boreholes are also represented.

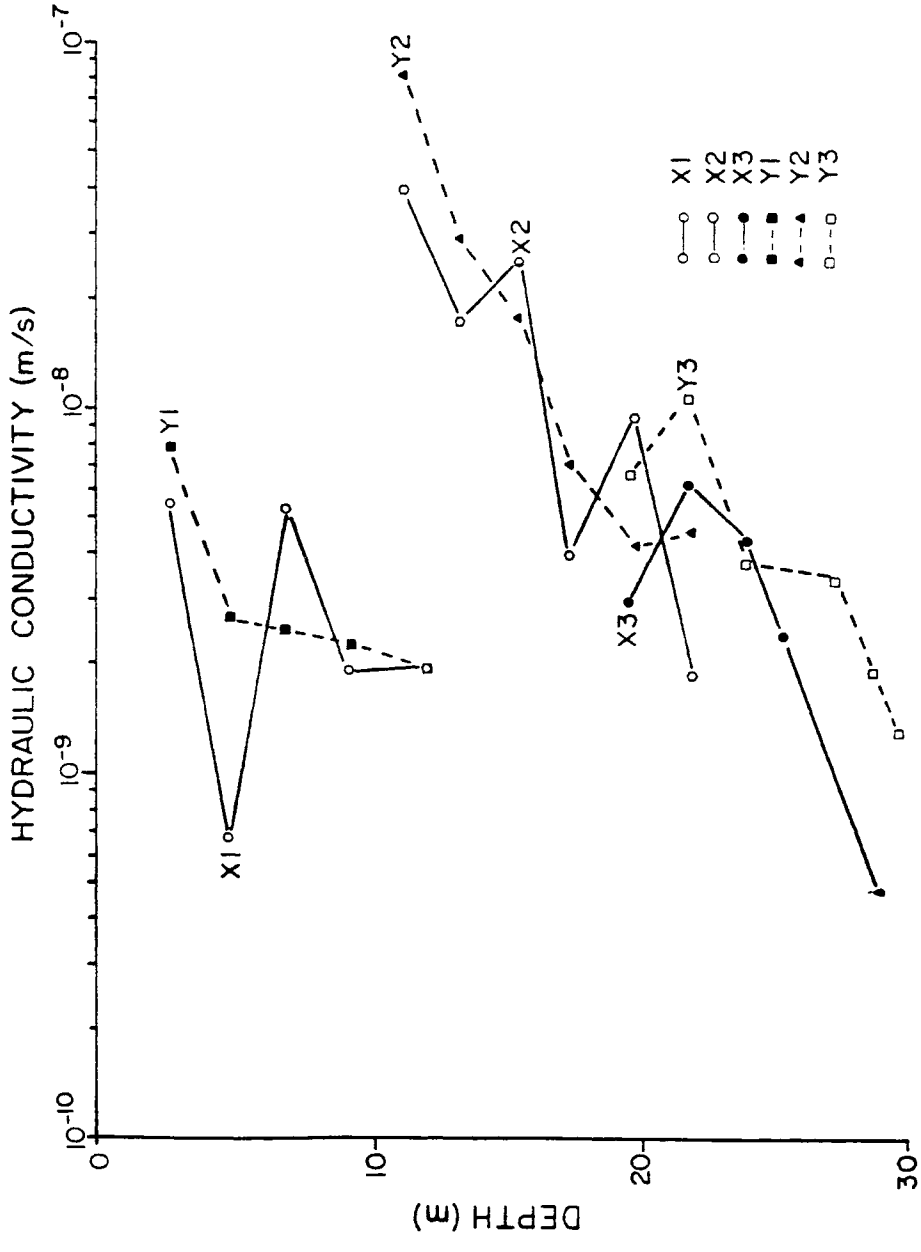

Figure 5.6. Hydraulic conductivity showing variation with depth as measured in a block of tuff containing boreholes X1 and Y1, the bottom 18 m of boreholes X2 and Y2, and the bottom 18 m of boreholes X3 and Y3.

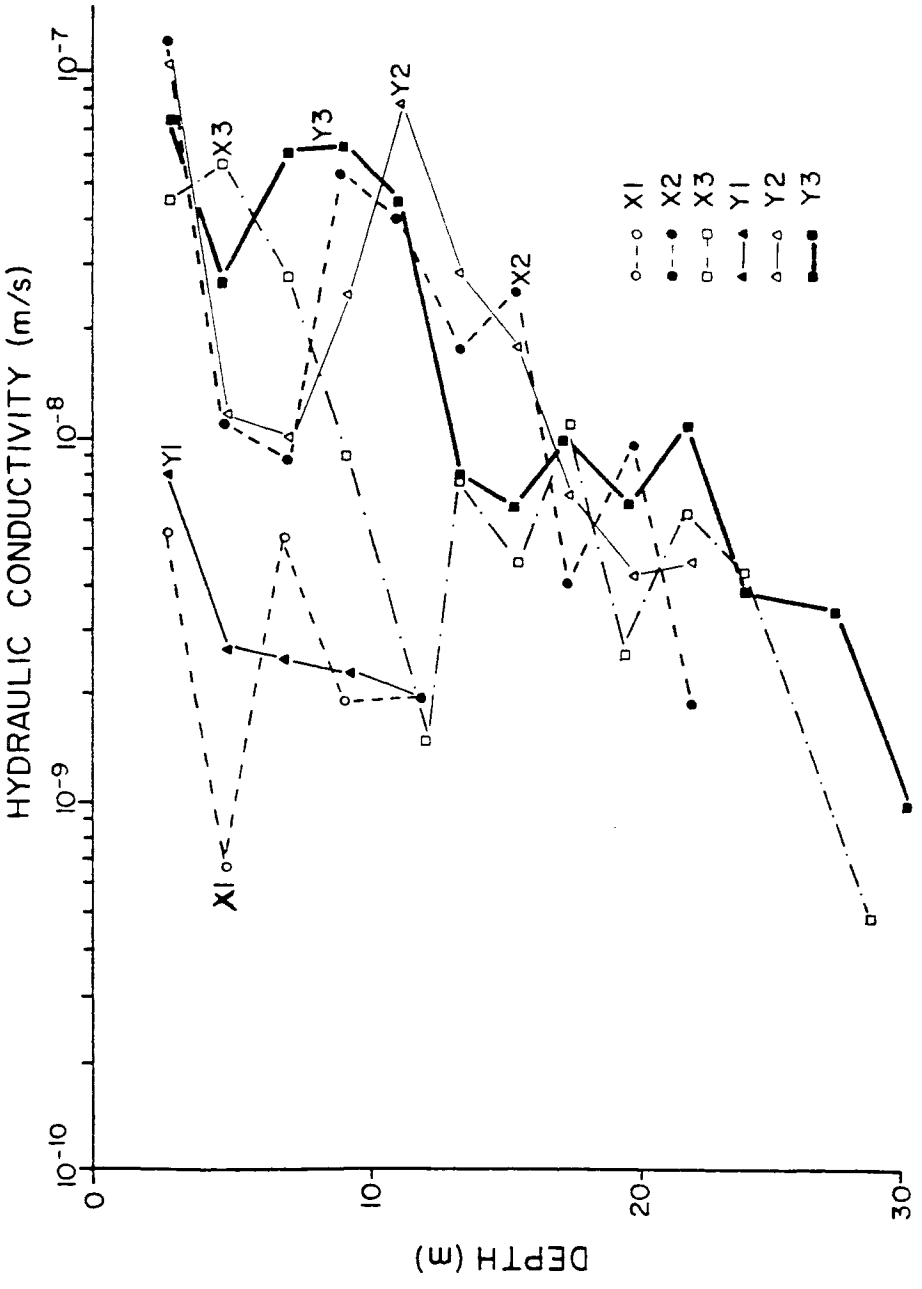

Figure 5.7. Hydraulic conductivity showing variation with depth as measured along each of the X and Y series boreholes.

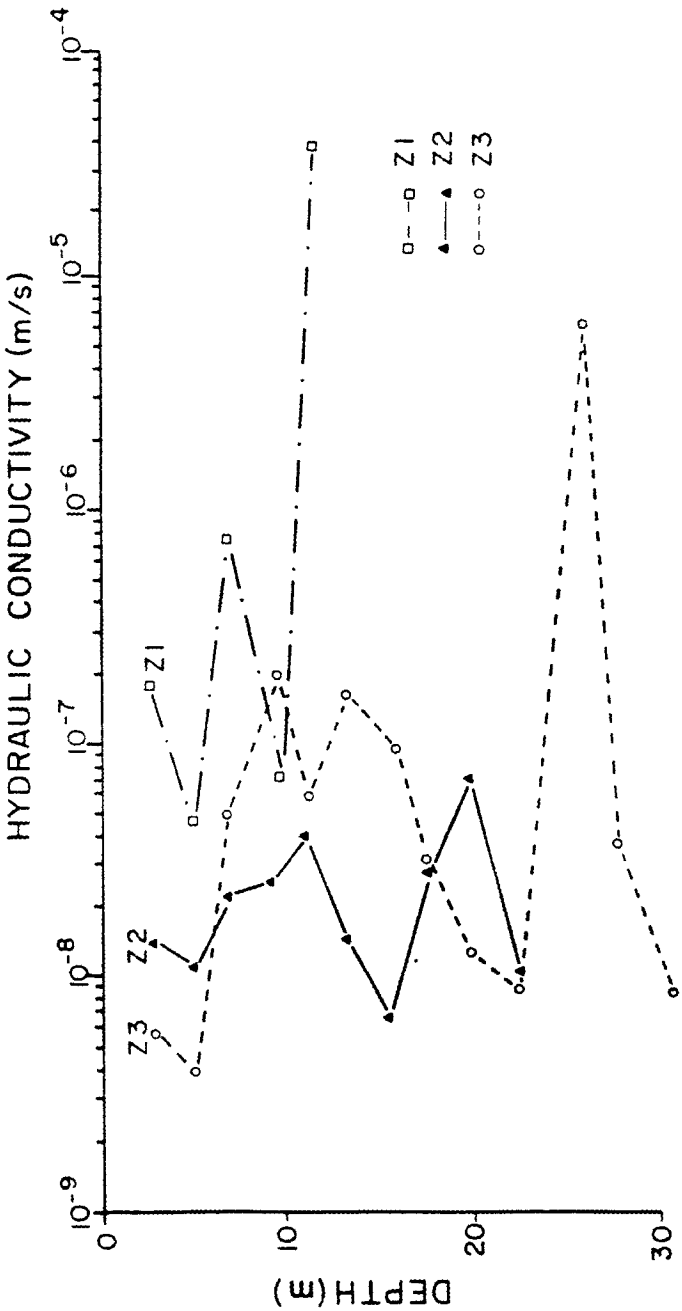

Figure 5.8. Hydraulic conductivity showing variation with depth as measured along the Z series boreholes.

conductivity distributions along the X and Y series of boreholes in this block of tuff show relatively good correlation. Figure 5.6 also indicates that the conductivity of this block of tuff is greatest from 10 to 20 meters below ground surface with a definite trend toward decreasing conductivity with depth. However, when the entire length of borehole for both the X and Y series is considered, Figure 5.7, much different trends are encountered. At the slightly larger scale, correlation between the boreholes of the two series drops off significantly, the trend of decreasing conductivity with depth becomes much more vague, and the larger conductivity values in each borehole are spread throughout the entire upper 20 m of tuff. By further expanding the scale of the analysis to include the Z series of boreholes (Figure 5.8), it becomes apparent that there is a definite lack of continuity between depth and conductivity.

Also of concern is the spatial variability of the conductivity in the direction parallel to the dip of the boreholes. Figure 5.9 indicates that a distinct trend toward increasing conductivity from west to east across the test site is exhibited by all nine boreholes. Figure 5.10, on the other hand suggests that conductivity increases in a north to south direction across the test site as well. These trends are no doubt attributable to a greater degree of fracturing associated with a more connected fracture system toward the north and east boundary of the test site. One possible explanation for the increased incidence of fracturing is the development of en echelon fractures associated with a major fault. En echelon fractures are tension fractures which form parallel to the principal stress axis of the stress ellipsoid associated

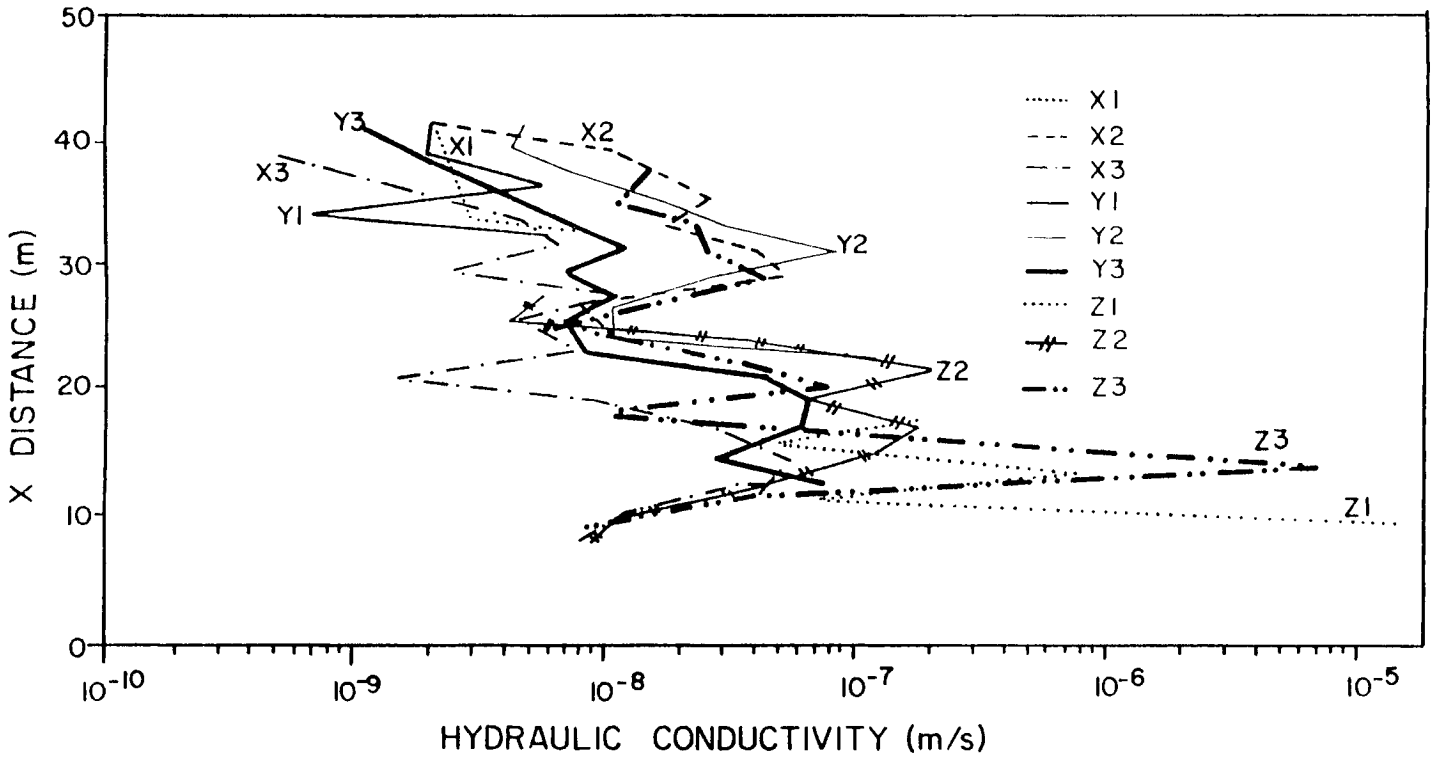

Figure 5.9. Hydraulic conductivity showing spatial variation parallel to the dip of the boreholes. Distance measured from an arbitrary point located 10 m east of the upper lip of borehole X-3.

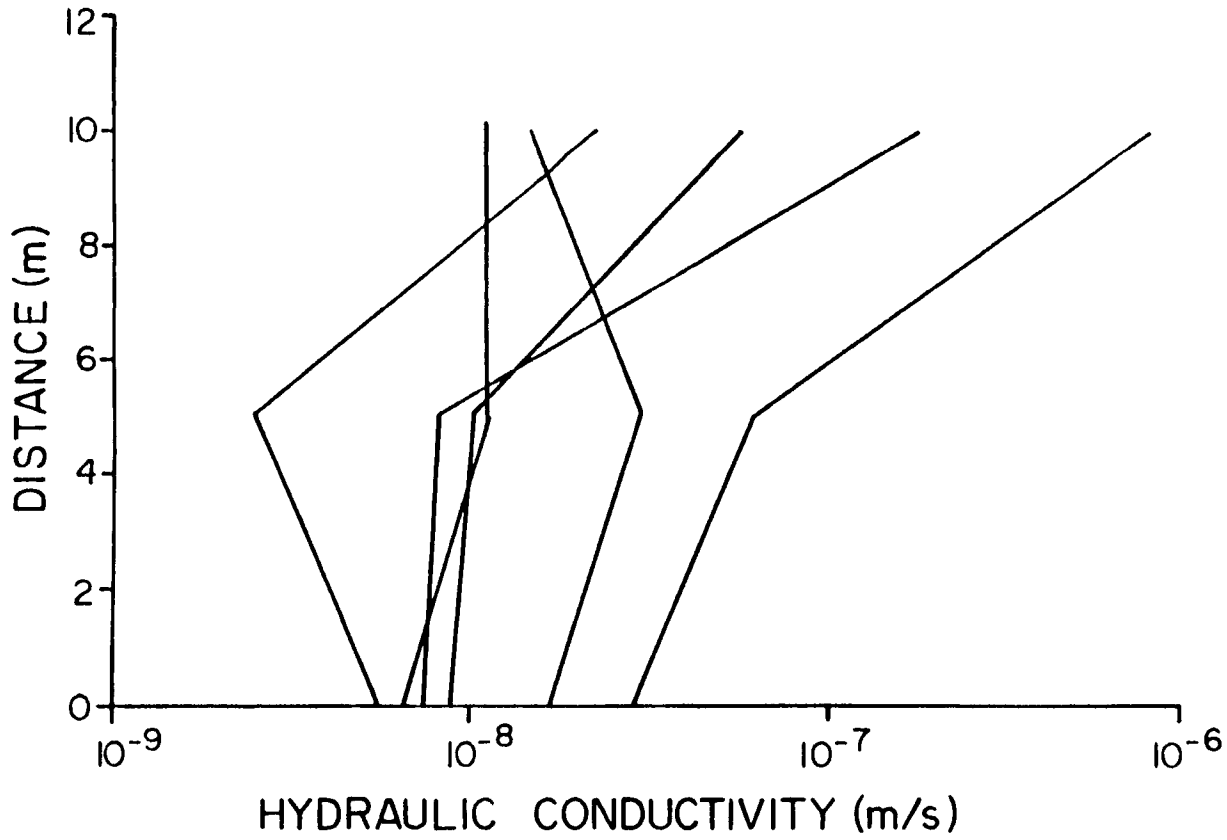

Figure 5.10. Hydraulic conductivity showing spatial variation normal to the dip of the boreholes. Distance measured from X series boreholes.

with a major fault. In addition to the en echelon fractures accounting for increased fracturing, due to their intimate association with a major fault, it is expected that such fracturing would also produce a well connected fracture network. It may be further be postulated that the fault responsible for the en echelon fractures may be the same fault which is associated with the "super" conducting zones.

Consideration of figures 5.3 - 5.5 indicate the presence of differing trends at different scales. Over a small scale, Figure 5.3, decreasing conductivity with depth is noted. However, as the scale is increased the trend disappears and is replaced by another. These trends no doubt are a direct result of the geologic nature of the test site. Since the investigation involves fractured media, it is the fractures, which are the result of a complex stress field induced by tectonic activity, that dictate the spatial conductivity distribution. In addition, several episodes of tectonic activity are responsible for the geologic complexion of the field site. For this reason, it is no wonder that such a range of variability is exhibited by the conductivity.

Since fractures generally act as the major transporting agent in a saturated fractured media, the relationship between fractures and the equivalent saturated hydraulic conductivity is of interest. Along with the conductivity distribution, the major borehole flow paths have also been included in Figures 5.3 - 5.5. The major probable flow paths are identified by fractures cutting the rock cores which were removed during the drilling of the nine boreholes at the Apache Leap test site. The degree with which a fracture is capable of conducting water is estimated from the presence of precipitated minerals and clays along the fracture

plane. The mechanism by which these constituents are precipitated being dependent on the passage of water through the fracture. Inspection of Figures 5.3 - 5.5 suggest that relationships are lacking which relate conductivity and the number of fractures intersecting the associated test interval. Analysis by means of linear regression was preformed to determine if a relationship associating fracture density, the number of fracture per meter of borehole, and the equivalent saturated hydraulic conductivity exists (Figure 5.11). A correlation coefficient of -0.037 was obtained from the analysis which indicates the total lack of any relationship between the two parameters. This lack of correlation is not surprising if one recalls the work by Long (1985) where she points out that fracture connnectivity is more critical to fracture network conductivity than fracture density. It follows that fracture density, when used alone, is of little help in estimating the equivalent saturated hydraulic conductivity of a fractured medium. It must also be realized that the fracture aperture exerts a great deal of influence on the fracture conductivity. Therefore, test intervals cut by fractures with relatively small apertures will exhibit conductivities which are similar to that of the matrix alone.

Although conductivity is not correlated with fracture density, the hydraulic conductivity of a test interval is dependent on the presence of fractures. Note that at least one fracture or zone of incompetent matrix is associated with each test interval which registered a conductivity greater than 1.4×10^{-8} m/sec. This indicates that the conductivity of the fractured tuff results from a dual porosity system-- one involving the porosity of the matrix and the other the porosity

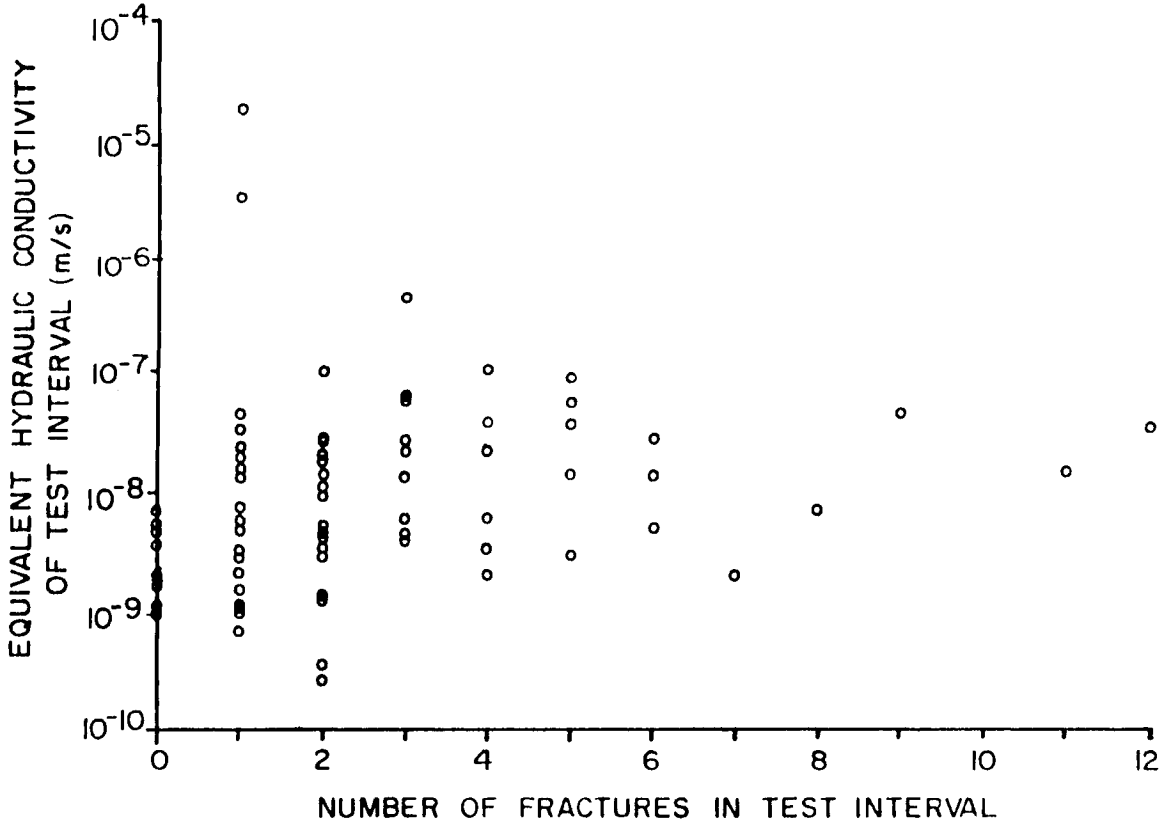

Figure 5.11. Fracture density against conductivity as measured at the Apache Leap test site. Linear regression indicates the lack of correlation between the two parameters.

associated with the fractures. Therefore test intervals which exhibit relatively low outflow rates are dominated by matrix flow while larger outflow rates are consistently more dependent on fracture flow. In some cases outflow rates as well as conductivities due to fractures may be five orders of magnitude greater than that contributed by the matrix alone.

In test intervals which are totally void of fractures, any conductivity which is attributed to such zones must be due only to the matrix. In particular there are eleven such intervals identified at the Apache Leap test site, all of which displaying conductivities less than 1.4×10^{-8} m/sec. At similarly spaced test intervals, unfractured cores measuring 5 cm in length and 6 cm in diameter were tested by mean of the Tempe-cell pressure method to determine the saturated hydraulic conductivity of the matrix (Evans, 1988). Laboratory results obtained from cores associated with test intervals lacking fractures compare well with the related field measured conductivity values (Table 5.2). A correlation coefficient of .67 was yielded upon correlation of the two sets of data (Figure 5.12). The related mean saturated matrix conductivity for the eleven field measured intervals was found to be 4.39×10^{-8} m/sec. It follows that conductivities measured in this range may be assumed to be dominated by matrix flow. Also of interest is the fact that conductivity values attributed to matrix flow exhibit a reasonable degree of heterogeneity but span a much smaller range of values than that experienced with conductivities dominated by fracture flow.

Table 5.2. Comparison of field and laboratory measured saturated matrix hydraulic conductivity.

Borehole	Depth (m)	Saturated Matrix Hydraulic Conductivity Lab (m/sec x 10^{-9})	Field
X1	12.84	1.38	1.94
X1	15.84	1.47	1.99
X2	24.78	6.61	3.98
Y2	24.37	4.25	7.11
Y2	27.37	3.54	4.31
Y2	30.37	4.66	4.64
Y3	33.39	2.06	3.88
Y3	36.39	3.42	3.41
Y3	39.39	3.96	1.96
Y3	42.39	1.44	1.03
Z1	3.52	6.55	14.11
Mean		3.62	4.39
Variance		11.97	3.27

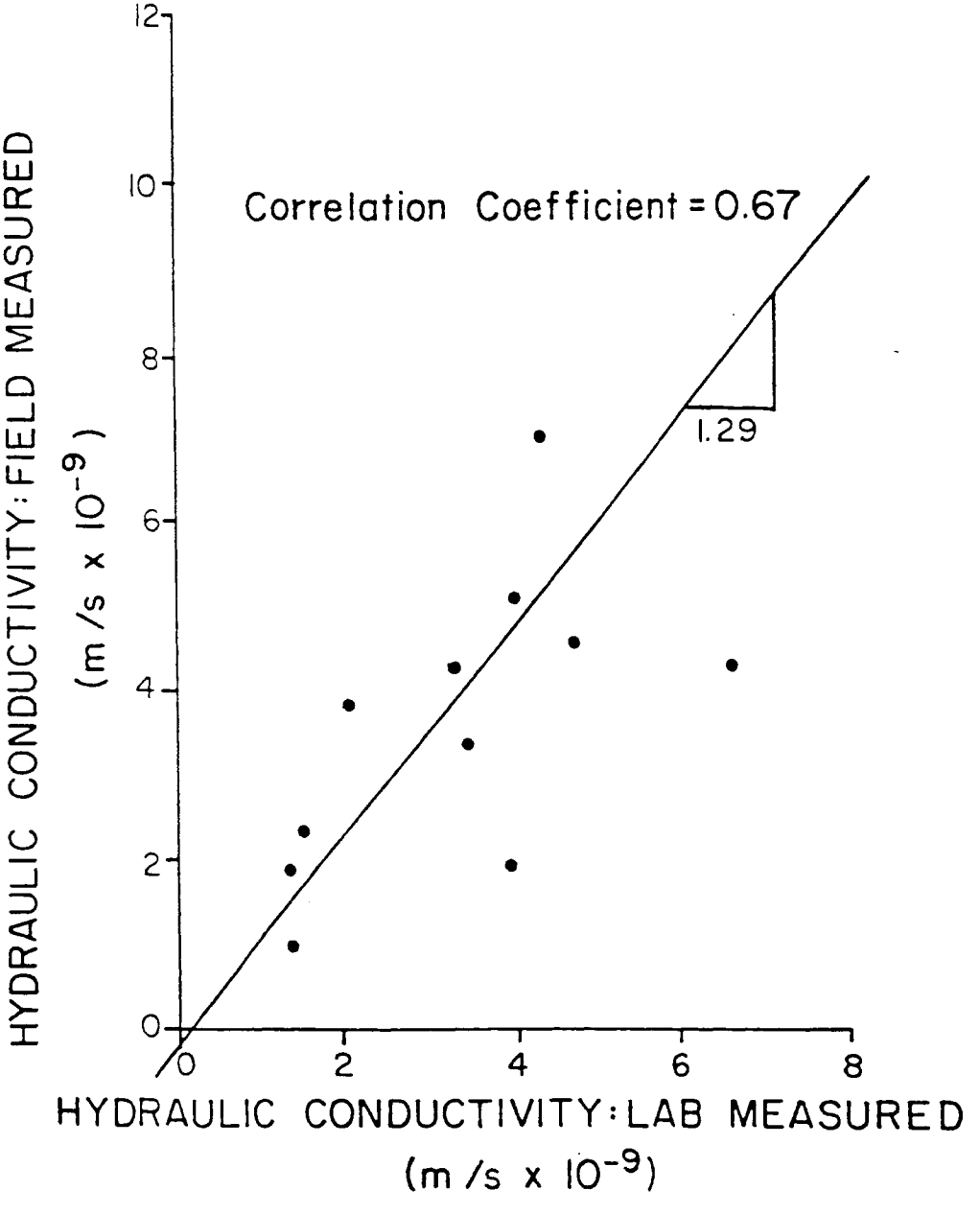

Figure 5.12. Correlation between field and laboratory measured saturated matrix hydraulic conductivity.

The reasonably good correlation between matrix saturated conductivity values, as measured by different means, indicates that the sensitivity of the field technique may be better than that predicted by the statistical analysis. Comparison of these data indicated that the falling-head flowmeter is able to measure conductivities attributable wholely to matrix flow. However, it is realized that a high degree of precision is still lacking at such small outflow rates. For this reason the falling-head flowmeter is best utilized for identification of low permeability zones and to provide a good first estimate of the conductivity, while more exact measurements such as laboratory techniques are necessary for detailed work.

Inspection of the data presented in this investigation reveals the presence of one characteristic which is applicable in any fractured media setting. This characteristic being the dominating presence of fractures on the equivalent saturated hydraulic conductivity. In areas void of fractures, the conductivity of a media is dependent only on the matrix which may be several orders of magnitude less than similar cases involving a well connected fracture. However, the presence of a fracture or a number of fractures does not assure substantially higher flow rates. Also, born out in this investigation is the importance of the role that the scale of the investigation and the geological nature of the test site play in the spatial distribution of the equivalent saturated hydraulic conductivity which is obtained.

CHAPTER SIX

CONCLUSIONS AND RECOMMENDATIONS

A method for determining the equivalent saturated hydraulic conductivity and its associated spatial variability in fractured, low permeability rock situated within the vadose zone has been developed. The methodology is applicable to any consolidated material located above the water table in which capillary forces induced by partially saturated media are minimal. The method also allows flexibility in the orientation of the borehole in which test are conducted, number and location of test intervals along a borehole and the magnitude of the constant head applied during testing. The primary value of this procedure is the development of a method to characterize the conductivity properties of fractured rock for calibrating and validating flow and transport models associated with fractured material.

The method and instrumentation utilized in obtaining field data from which conductivity values are estimated has been improved over the falling-head borehole permeability tests described by the U.S. Bureau of Reclamation (1977). Monitoring of outflow rates has been improved by the design of a falling-head flowmeter which allows the measurement of a large range of outflow rates while maintaining a small drop in head during testing. Precautions in this investigation are also taken to assure that near steady-state outflow conditions are maintained by the

flooded boreholes during testing. Furthermore, attention is paid to developing a comprehensive sampling scheme which will provide data that is representative of the media of interest. This involves orienting boreholes in a manner so as to intersect the major fracture sets or geologic structure of a particular test site.

Confidence in the reliability of the data obtained by the field technique is gained through the precision and sensitivity analysis conducted on data acquired from the Apache Leap test site. From the analysis, measured interval outflow rates are expected to be within $\pm 8.3 \times 10^{-8}$ m^3/sec of the actual outflow rate, while sensitivity of the instrumentation is capable of discriminating between outflow rates on the order of 1.6×10^{-8} m^3/sec. The precision of the technique can be increased by developing a better means of locating the packer along the length of the borehole. This involves incorporating a steel measuring tape or something of similar nature which is not prone to stretching or wearing off with time. Utilization of a straddle-packer system will also increase the precision by requiring the packer to be positioned only once in order to measure interval outflow rates. However, use of a straddle-packer system will also require development of a means with which to dissipate pressure built up in the test interval during the inflation of the packers.

Accompanying the developed field technique are two analytical solutions with which to estimate the equivalent saturated hydraulic conductivity from collected field data. Since most classical methods for estimating the saturated conductivity from borehole permeability tests involve the use of vertical boreholes in which the borehole acts

as the entire measurement interval, the associated classical analytical solutions reflect these restrictions. For this reason, classical solutions were adapted to meet the special needs of this investigation. The solutions are based on Laplace's equation which assumes homogeneous, isotropic conditions and neglects the effect of capillary forces. By making these assumptions, one is provided with only an approximate solution to the problem. However, an exact solution would require consideration of capillary forces, the dual porosity existing between the matrix and fractures, and the geometry of the fracture network. At this time techniques are lacking with which to determine fracture network geometries or to evaluate relationships between water content and hydraulic conductivity in fractured rock. Therefore, the solutions presented in this investigation provide as accurate an estimation of the saturated hydraulic conductivity as possible, given the degree of information available in most field situations. Even if such information was available, models which take capillarity and fracture geometry into consideration would require very exhaustive analysis. For this reason, the given solutions will still provide a reliable means of estimating the conductivity when detailed analysis is not necessary.

In addition to developing a methodology for collecting conductivity data, a primary concern of this investigation is to provide a data set of saturated conductivity values for fractured, partially-welded tuff. As a result the developed field technique is utilized to determine the equivalent saturated hydraulic conductivity and its associated spatial distribution at the Apache Leap test site. The most notable feature of the collected data is the large degree of variability exhibited by the

conductivity measurements and the presence of two "super" conducting fractures. For the most part, measured conductivities range over three orders of magnitude while the two "super" conducting fractures display conductivities two orders of magnitude larger than the rest of the data. Estimates of the saturated matrix conductivity were also determined from test intervals lacking fractures. Matrix conductivities measured in the field were found to compare closely with laboratory tests preformed on cores associated with the test interval. The only definable trends exhibited by the data is that of increasing conductivity to the east and south boundary of the field site. This trend is most likely the result of a higher incidence of fracturing and a better connected fracture system at the southeast end of the field site. The fracturing being the result of en echelon fractures associated with a major fault such as the one related to the "super" conducting zones located at the southeast end of the field site.

Several features inherent to the nature of fractured rock were also noted by the investigation. Of primary importance is the dominant role fractures play in determining the conductivity. If fractures are lacking, flow occurs by means of the rock matrix only, while the presence of a single well connected fracture way raise conductivity rates by five orders of magnitude over that due to the matrix only. However, the presence of a fracture does not guarantee higher associated conductivities, nor does conductivity correlate with fracture density. Basically this indicates that fracture connectivity is the governing factor motivating fracture network flow. Finally, well defined trends associated with the spatial distribution of the hydraulic conductivity

of fractured media are simply the expression of the random nature with which fractures are induced by complex stress fields.

APPENDIX A

NOTATION

A	area normal to flow, L^2
a	radius of borehole, L
b	fracture aperture, L
C	fracture proportionality factor equal to the fracture density multiplied by the fracture roughness, 1/L
C_u	dimensionless flow rate
c	saturated length of borehole, L
$E[x]$	expected mean
e	eccentricity of a confocal ellipse
$f(b)$	normalized aperture fracture frequency distribution
g	acceleration of gravity, L/T^2
H	saturated length of borehole, L
H_D	dimensionless height of water
H_i	potential inside half ellipsoid, L
H_o	potential at any point outside the half spheroid, L
H^*	location of source above base of borehole as measured along the length of borehole, L
h'	difference in assumed saturated length of borehole and actual saturated length for an inclined borehole, L
K	saturated hydraulic conductivity, L/T
K'	saturated hydraulic conductivity inside ellipsoid, L/T
L	length of borehole open to formation, L

n	sample size
P	pressure head, L
Q	total flow rate, L^3/T
q	specific flux, L/T
R	radial distance from source to point of interest, L
r	radial distance from borehole axis, L
r_{fs}	radius of free surface at distance where flow is due only to gravitational forces, L
r_w	radius of borehole
S^2	sample variance
S	sample standard deviation
T	Critical value for the T distribution
$\bar{x}$	sample mean
x_i	data points where i=1,N
Z	length from bottom of borehole to bottom of test interval as measured along the length of the borehole, L
α	ratio of saturated hydraulic conductivity inside the ellipsoid to the saturated conductivity outside the ellipsoid
β	error measurement
∇	gradient operator, 1/L
λ	normal distance between an inscribed ellipsoid and its associated outer ellipsoid
θ	dip of borehole, degrees
μ	dynamic viscosity, $M\ L^{-1}T^{-1}$
ρ	density of water, M/L^3
Cov	covariance between random variables
ln	natural logarithm

$\sinh^{-1}$ inverse hyperbolic sin function

Var variance of a random variable

APPENDIX B

DATA TABLE

BOREHOLE	DEPTH* (m)	FLOW RATE (m^3/s E-7)	SATURATED CONDUCTIVITY K(GLOVER) (m/s E-9)	K(PHILIP) (m/s E-9)
X1	3.80	0.83	2.94	5.50
	6.84	0.16	0.36	0.68
	9.84	1.83	2.91	5.45
	12.84	0.83	1.04	1.94
	15.84	1.67	1.14	1.99
X2	3.81	15.67	57.92	120.31
	6.78	2.50	5.62	11.63
	9.78	2.67	4.33	8.96
	12.78	20.16	25.65	53.04
	15.78	18.16	18.98	39.25
	18.78	9.67	8.57	17.73
	21.78	16.16	12.45	25.74
	24.78	2.83	1.92	3.98
	27.78	7.83	4.77	9.87
	30.78	2.16	0.96	1.89
X3	3.84	5.67	20.23	45.66
	6.84	11.17	24.82	56.04
	9.84	8.00	12.91	29.14
	12.84	31.67	4.01	9.06
	15.84	0.67	0.69	1.57
	18.84	3.83	3.39	7.66
	21.84	2.67	2.05	4.64
	24.84	7.16	4.88	11.02
	27.84	1.83	1.12	2.53
	30.84	5.16	2.86	6.45
	33.84	3.83	1.94	4.37
	40.84	2.00	0.27	0.48
Maximum		31.67	20.23	120.31
Minimum		0.16	0.27	0.48
Mean		6.92	8.47	18.02
Median		3.83	3.39	7.66
Coefficient of Variation		1.07	1.51	1.49

BOREHOLE	DEPTH (m)	FLOW RATE (m^3/s E-7)	SATURATED CONDUCTIVITY K(GLOVER) (m/s E-9)	K(PHILIP) (m/s E-9)
Y1	3.81	1.16	4.31	8.02
	6.77	0.66	1.48	2.76
	9.77	0.83	1.34	2.49
	12.77	1.00	1.26	2.33
	15.77	1.00	1.06	1.97
Y2	3.61	12.16	51.44	106.52
	6.37	2.50	5.83	11.68
	9.37	3.00	5.00	10.02
	12.37	9.67	12.55	25.12
	15.37	39.33	41.78	83.63
	18.37	16.16	14.53	29.08
	21.37	11.50	8.96	17.94
	24.37	5.16	3.55	7.11
	27.37	3.50	2.15	4.31
	30.37	2.83	2.15	4.64
Y3	3.52	8.16	34.09	73.17
	6.39	5.67	13.16	27.32
	9.39	17.50	29.15	60.49
	12.39	23.50	30.51	63.31
	15.39	4.00	21.80	45.25
	18.39	4.33	3.90	8.10
	21.39	4.16	3.26	6.76
	24.39	7.00	4.83	10.02
	27.39	5.16	3.19	6.62
	30.39	10.16	5.68	11.78
	33.39	3.67	1.87	3.88
	36.39	3.50	1.64	3.41
	39.39	2.16	0.94	1.96
	42.39	1.67	0.53	1.03
Maximum		39.33	51.44	106.52
Minimum		0.66	0.53	1.03
Mean		7.28	10.76	22.09
Median		4.16	4.31	8.10
Coefficient of Variation		1.12	1.44	1.43

BOREHOLE	DEPTH (m)	FLOW RATE (m^3/s E-7)	SATURATED CONDUCTIVITY K(GLOVER) (m/s E-9)	K(PHILIP) (m/s E-9)
Z1	3.52	22.16	95.90	182.53
	6.34	11.00	25.75	47.37
	9.34	260.50	433.59	797.56
	12.34	47.16	41.51	71.45
	15.34	12320.00	19126.00	39224.00
Z2	3.70	0.67	2.76	5.74
	6.55	0.83	1.96	4.00
	9.55	16.00	26.85	54.81
	12.55	75.16	98.01	200.09
	15.55	28.67	30.57	62.41
	18.55	94.16	84.93	173.38
	21.55	65.83	51.45	105.03
	24.55	24.83	17.12	34.95
	27.55	10.67	6.58	13.43
	30.55	6.33	4.19	8.91
Z3	3.83	1.83	6.75	14.11
	6.82	2.50	5.64	11.78
	9.82	6.50	10.59	22.11
	12.82	9.66	12.32	25.73
	15.82	19.50	20.42	42.63
	18.82	8.00	7.11	14.84
	21.82	4.16	3.21	6.71
	24.82	20.16	13.74	28.69
	27.82	58.00	35.42	73.95
	31.78	15.83	5.67	10.82
	36.97	8340.00	3435.80	6947.90
	39.80	36.16	17.88	38.56
	42.82	13.83	4.46	8.38
Maximum		12320.00	19126.00	39224.00
Minimum		0.67	13.74	29.08
Mean		33.08	52.46	79.23
Median		16.00	17.12	34.95
Coefficient of Variation		1.56	1.52	1.94
For all Boreholes:				
Maximum		12320.00	19126.00	39224.00
Minimum		0.16	0.27	0.48
Mean		15.34	19.57	38.87
Median		6.33	5.64	11.63
Coefficient of Variation		2.09	2.57	2.41

* All depths are measured to center of test interval along the length of the borehole.

APPENDIX C

CONSTANT HYDRAULIC HEAD MAINTAINED ON BOREHOLES

Borehole	Saturated Length of Borehole (m)	Total Hydraulic Head (m)
X1	19.51	13.79
X2	33.65	23.79
X3	47.75	33.76
Y1	18.15	12.83
Y2	32.09	22.69
Y3	46.12	32.61
Z1	18.08	12.78
Z2	32.41	22.91
Z3	46.18	32.65

REFERENCES

Abelin, H., J. Gidlund, and I. Neretnieks, 1983, Migration Experiments in a Single Fracture in the Stripa Granite: Preliminary Results, in Proceedings of the Workshop on Geological Disposal of Radioactive Waste in Situ Experiments in Granite, Stockholm, Sweden, p.154-163, Organization for Economic Co-Operation and Development, Paris.

Bear, J., 1979, Hydraulics of Groundwater, McGraw-Hill, New York, 569p.

Billaux, D., B. Feuga and S. Gentier, 1984, Etude Theorique et en Laboratoire du Comportment d'und Fracture Rocheuse Sous Contrainte Normale, Revue Francaise Geotechnique, in press.

Carslaw, H.S., and J.C. Jaeger, 1959, Conduction of Heat in Solids, 2nd ed., Clarendon, Oxford.

Cornwell, F.E., 1953, Flow from a Short Section of Test-Hole Below Groundwater Level, in Theory and Problems of Water Percolation, C.N. Zanger, U.S. Bureau of Reclamation Engineering Monograph No.8, p.66-71.

Englman, R., Y. Gur, and Z. Jaeger, 1985, Fluid Flow Through a Crack Network in Rocks, Journal of Applied Mechanics, Vol.50, p.707-711.

Evans, D.D., 1988, Unsaturated Flow and Transport Through Fractured Rock Related to High-Level Waste Repositories, NRC 04-86-114 Progress Report, 52p.

Glover, R.E., 1953, Flow from a Test-Hole Located Above Groundwater Level, in Theory and Problems of Water Percolation, U.S. Bureau of Reclamation Engineering Monograph No.8, p.66-71.

Hsieh, P.A., S.P. Neuman, G.K. Stiles, and E.S. Simpson, 1985, Field Determination of the Three-Dimensional Hydraulic Conductivity Tensor of Anisotropic Media, 2, Methodology and Application to Fractured Rocks, Water Resour. Res., Vol.21, No.11, p.1667-1676.

Huitt, J.L., 1956, Fluid Flow in Simulated Fractures, Journal of the American Institute of Chemical Engineers, Vol.2, p.259.

Kozminski, G., 1973, Contribution a l'Etude de Projects de Puits d'Injection en Milieu non Sature, Bureau de Recherches Geolegiques et Minieres, 73 SGN 358 AME, 23p.

Kranz, R.L., A.D. Frankel, T. Engelder, and C.H. Scholz, 1979, The Permeability of Whole and Jointed Barre Granite, International Journal of Rock Mechanics and Mineral Science, Vol.16, p.225-234.

Long, J.C.S., and P.A. Witherspoon, 1985, The Relationship of the Degree of Interconnection to Permeability in Fracture Networks, Journal of Geophysical Res., Vol.90, No.B4, p.3087-3098.

Long, J.C.S., H.K. Endo, K. Karasaki, L. Pyrak, P. Maclean, and P.A. Witherspoon, 1985a, Hydrologic Behavior of Fracture Networks, in Proceedings, Memoirs of the 17th International Congress of International Association of Hydrologists, Vol.XVII, p.449-462, International Association of Hydrogeologists, Tucson, Arizona.

Messer, A.A., 1986, Fracture Permeability Investigation Using Heat-Pulse a Flowmeter, Masters Thesis, Department of Hydrology and Water Resources, University of Arizona, Tucson, 72p.

Narasimhan, T.N. and P.A Witherspoon, 1977, Numerical Model for Saturated-Unsaturated Flow in Deformable Porous Media, part I: Theory, Water Resour. Res., Vol.13, No.3, p.657-664.

Nasberg, V.M., 1951, The Problem of Flow in an Unsaturated Soil for Injection Under Pressure, Inzvestja Akademia Nauk, SSSR odt tekh Nauk, No.9, Translated by Mr. Reliant, 1973, B.R.G.M., France.

Neuman, S.P., and P.A. Witherspoon, 1970, Finite Element Method of Analyzing Steady Seepage with a Free Surface, Water Resour. Res., Vol.6, No.3, p.689-697.

Neuman, S.P., and T.N. Narasimhan, 1977, Mixed Explicit-Implicit Finite Element Scheme for Diffusion Type Problems: I. theory, International Journal for Numerical Methods in Engineering, Vol.11, p.309-323.

Neuman, S.P., 1987, Stochastic Continuum Representation of Fractured Rock Permeability as an Alterative to the REV and Fracture Network, Rock Mechanics: Proceedings of the 28th U.S. Symposium on Rock Mechanics, Tucson, p.533-561.

Neuzil, C.E., and J.V. Tracy, 1981, Flow Through Fractures, Water Resour. Res., Vol.17, No.1, p.191-199.

Peterson, D.W., 1961, Dacitic Ash-Flow Sheet near Superior and Globe, Arizona: Stanford University, Stanford, California, Ph.D. thesis, 130p.; U.S. Geological Survey open-file report, April 3, 1961, 130p.

Peterson, D.W., 1968, Zoned Ash-Flow Sheet in the Region Around Superior, Arizona: in S. Titley (ed.), Arizona Geological Society, Southern Arizona Guidebook, III, April 11-13, 1968, Tucson, Arizona, p.215-222.

Philip, J.R., 1985, Approximate Analysis of the Borehole Permeameter in Unsaturated Soil, Water Resour. Res., Vol.21, No.7, p.1025-1033.

Rasmussen, T.C. and D.D. Evans, 1987, Unsaturated Flow and Transport Through Fractured Rock Related to High-Level Waste Repositories, NUREG/CR-4655, 474p.

Schrauf, T.W. and D.D. Evans, 1986, Laboratory Studies of Gas Flow Through a Single Natural Fracture, Water Resour. Res., Vol.22, No.7, p.1038-1050.

Sharp, J.C., 1970, Fluid Flow Through Fissured Media, Ph.D. thesis, Imperial College of Science and Technology, London.

Snow, D.T., 1969, Anisotropic Permeability of Fractured Media, Water Resour. Res., Vol.5, No.6, p.1273-1289.

Snow, D.T., 1970, The Frequency and Apertures of Fractures in Rock, International Journal of Rock Mechanics and Mineral Science, Vol.7, p.23-40.

Stephens, D.B., 1979, Analysis of Constant Head Borehole Infiltration Tests in the Vadose Zone, Ph.D. Thesis, Department of Hydrology and Water Resources, University of Arizona, Tucson, 366p.

Terletskaya, N.M., 1954, Determination of Permeability in Dry Soils, Hydroelectric Waterworks No.2, February, Moscow.

Trautz, R.C., 1984, Rock Fracture Aperture and Gas Conductivity Measurements In Situ, Masters Thesis, Department of Hydrology and Water Resources, University of Arizona, Tucson, 141p.

Tsang, Y.W., 1984, The Effect of Tortuosity on Fluid Flow Through a Single Fracture, Water Resour. Res., Vol.20, No.9, p.1209-1215.

Tsang, Y.W., and P.A. Witherspoon, 1985, Effects of Fracture Roughness on Fluid Flow Through a Single Deformable Fracture, in Proceedings, Memoirs of the 17th International Congress of International Association of Hydrologists, Vol.XVII, p.683-694, International Association of Hydrogeologists, Tucson, Arizona.

U.S. Bureau of Reclamation, 1974, Earth Manual, 2nd. edition, U.S. Government Printing Office, Washington, D.C., 810p.

U.S. Bureau of Reclamation, 1977, Ground Water Manual, U.S. Government Printing Office, Washington, D.C., 480p.

Wang, J.S.Y., and T.N. Narasimhan, 1985, Hydrologic Mechanisms Governing Fluid Flow in a Partially Saturated, Fractured, Porous Medium, Water Resour. Res., Vol.21, No.12, p.1861-1874.

Weber, D., 1986, Mineralogic, Isotopic and Spatial Properties of Fractures in an Unsaturated Partially-Welded Tuff near Superior, Arizona, Masters Thesis, Department of Hydrology and Water Resources, University of Arizona, Tucson, 128p.

Witherspoon, P.A., J.S.Y. Wang, K. Iwai, and J. Gale, 1979b, Validity of Cubic Law for Fluid Flow in a Deformable Rock Fracture, Technical Report 23, Lawrence Berkeley Laboratory, University of California, Berkeley.

Yeh, T.C.J., T.C. Rasmussen and D.D. Evans, 1988, Simulation of Liquid and Vapor Movement in Unsaturated Fractured Rock at the Apache Leap Tuff Site: Models and Strategies, NUREG/CR-5097, 73p.

Zanger, C.N., 1953, Theory and Problems of Water Percolation, U.S. Bureau of Reclamation Engineering Monograph No.8, 76p.